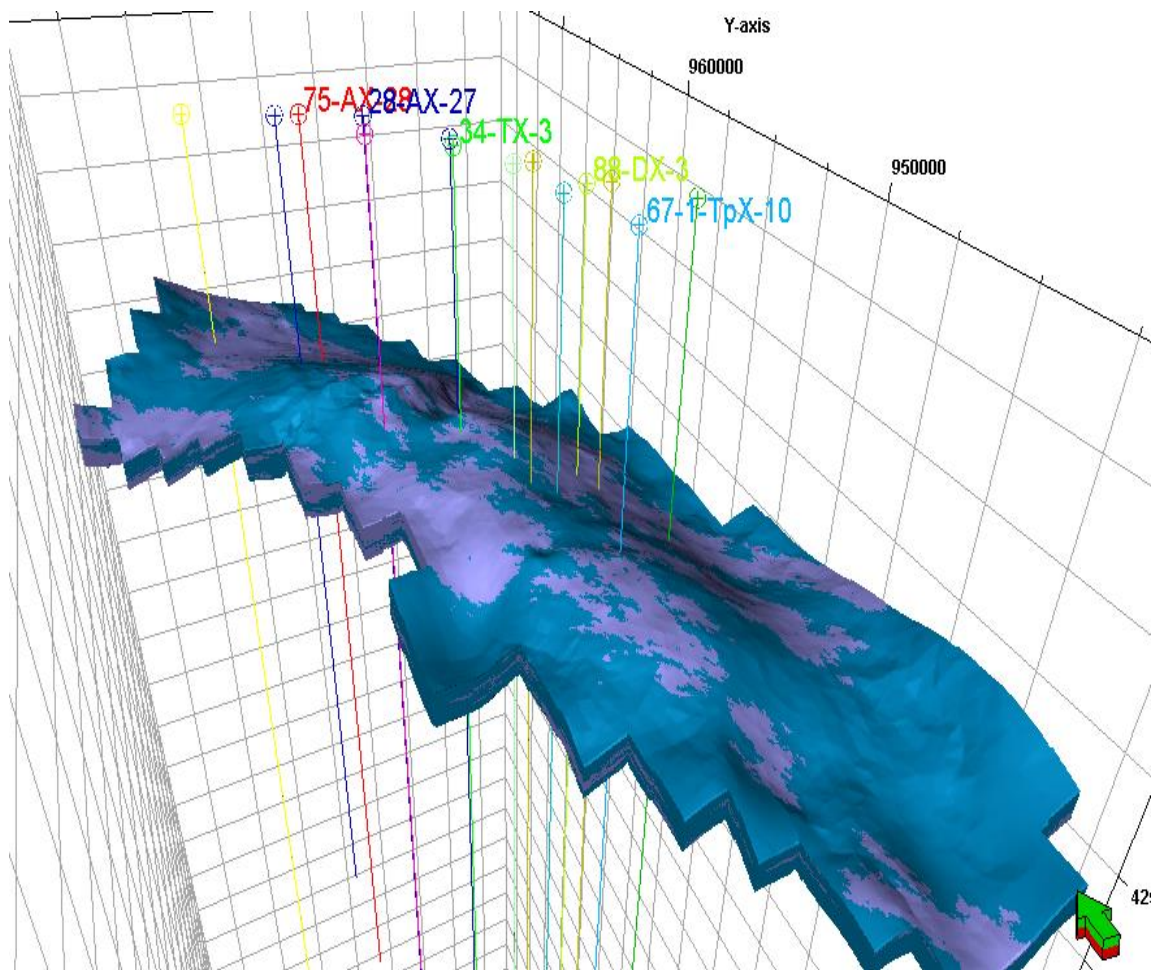


CAPROCK INTEGRITY STUDY OF THE 2nd WALL CREEK RESERVOIR: A CASE STUDY FROM TEAPOT DOME, WYOMING



Supervisors: Ismaila Adetunji Jimoh
Wolfgang Weinzierl
Erik Gydesen Sjøgaard

Authors: Jacquelin Cobos
Jhony Quintal



AALBORG UNIVERSITY
DENMARK

CAPROCK INTEGRITY STUDY OF THE 2nd WALL CREEK RESERVOIR: A CASE STUDY FROM TEAPOT DOME, WYOMING

Project Period: 01/02/2017 to 08/06/2017

Date of submission: 08/06/2017

Place of study: Aalborg University Esbjerg

Supervisor: Ismaila Adetunji Jimoh, Wolfgang Weinzierl (Schlumberger Oilfield Services, Denmark) & Erik Gydesen Søggaard

Authors:

Jacquelin Cobos

Jhony Cesar Quintal Nunes

ABSTRACT

Over the last few years, the study of caprocks for geologic CO₂ storage has been increased due to the significant risk regarding safety and environment if the containment is not ensured.

In this work, a multi-disciplinary approach that integrates geology, petrophysics, rockphysics, and geomechanics concepts are used to characterize the caprock of the 2nd Creek Wall reservoir, Teapot Dome, Wyoming regarding its tensile strength. This field was chosen due to the information availability and the numerous sequestration pilot projects carried out in the site.

The first part of this study was done in Techlog©, wellbore platform from Schlumberger and comprises the computation of the petrophysical and mechanical characteristics of the caprock based on the available wireline logging data for 18 wells. The integration of that information is then used to calculate the brittleness index which is related to the tensile strength of the caprock. A neuronal analysis in IPSOM was considered to classify the caprock regarding its ductility and brittleness.

The final results of this study show that 2nd Wall Creek reservoir can be seen as a good candidate for a CO₂ sequestration project. Finally, those properties are loaded in Petrel, integrated subsurface platform, to create a 3-D grid map the brittleness and ductility of the caprock. The map indicates the possible drilling locations for CO₂ storage.

ACKNOWLEDGEMENT

First and foremost, we wish to thank our project supervisor and Techlog© trainer Ismaila Adetunji Jimoh. We express our appreciation to Wolfgang Weinzierl who was our Petrel instructor and also for his help in the 3-D modeling. Last but not least, we thank Erik Gydesen Søgaaard who has been our supervisor in the university.

We would like to extend our gratitude to Schlumberger Software Integrate Solutions in Denmark for providing the software grant of Techlog© and Petrel and also for the training received in their office in Copenhagen.

Sincere thanks to Aalborg University-Esbjerg for their support, equipment, and installations and the IT department.

At last, we would like to acknowledge the US Geological Survey Site (USGS) and Rocky Mountain Oilfield Testing Center (RMOTC), for the public data source we used for the present study.

CONTENTS

CHAPTER I. INTRODUCTION	1
1.1. Problem Statement	2
1.2. Data and Methods	2
1.3. Area of Investigation	5
1.4. Carbon Sequestration	6
1.5. Project Limitations	6
1.6. Project Outline	7
CHAPTER II. LITERATURE REVIEW	8
2.1. Caprock in CO ₂ Sequestration	8
2.2. Seal Potential	9
2.2.1. Seal Capacity	9
2.2.2. Seal Geometry	10
2.2.3. Caprock Integrity	10
2.3. Caprock Effectiveness	11
2.3.1. Lithology	11
2.3.2. Ductility	11
2.3.3. Thickness	13
2.3.4. Burial Depth	13
CHAPTER III. GEOLOGICAL BACKGROUND	14
3.1. Geology of Teapot Dome	14
3.2. Stratigraphy	16
3.3. Lithology	19
CHAPTER IV. PETROPHYSICAL EVALUATION	21
4.1. Data Analysis	21
4.2. Well Correlation Study	23
4.3. Petrophysical Analysis	25
4.3.1. Volume of shale	26
4.3.2. Porosity calculation	30
4.3.3. Fluid Saturation	35

4.3.4.	Lithology estimation	36
CHAPTER V. GEOPHYSICS.....		41
5.1.	Overview	41
5.2.	Acoustic properties	42
5.3.	Dynamic Elastic Properties.....	45
CHAPTER V. GEOMECHANICS		49
6.1.	Overview	49
6.2.	In-Situ Stress	51
6.2.1.	Overburden Stress	51
6.2.2.	Pore Pressure	53
6.3.	Rock Strength.....	56
6.3.1.	Unconfined Compressive Strength	57
6.3.2.	Tensile Strength	60
CHAPTER VII. CAPROCK INTEGRITY		62
7.1.	Dynamic elastic properties analysis.....	62
7.2.	IPSOM Classification	65
7.3.	Brittleness Index	69
7.3.1.	Evaluation of Brittleness Index	72
CHAPTER VIII. CAPROCK MODELING		75
8.1.	Data and Methods	75
8.2.	Surface Model.....	77
8.3.	Facies Modeling	79
8.4.	Petrophysical Modeling	82
8.5.	Modeling Results.....	87
8.6.	Drilling locations for the CO ₂ injection wells	89

LIST OF FIGURES

Figure 1 – Caprock Integrity Flowchart.....	4
Figure 2 – General location of Wyoming and Teapot Dome Field (4)	5
Figure 3 – Upward migration of CO ₂ due to buoyancy (8).....	10
Figure 4 – Relative ductility and compressibility vs strength/sonic velocity	12
Figure 5 – Map of the Teapot Dome (14)	14
Figure 6 – Structural map of the reservoir (17)	15
Figure 7 – Depth-structure map of the 2 nd wall creek sandstone (17)	16
Figure 8 – Teapot Dome stratigraphic column (3)	17
Figure 9 – Frontier formation cross section (18)	18
Figure 10 – Location of the wells in the Teapot Dome field	22
Figure 11 – Well correlation in the 2 nd Wall Creek formation	24
Figure 12 – Determination of GR_Matrix and GR_Shale	27
Figure 13 – Computation of shale volume (V _{sh}) for the wells: 28-AX-27, 36-MX-10, 67-1-TpX-10, 11-DX-26, 12-AX-33.....	28
Figure 14 – Shale Volume histogram for all the wells	29
Figure 15 – Calculation of porosity by neutron-density logs for the wells: 28-AX-27, 36-MX-10, 67-1-TpX-10.....	31
Figure 16 – Histogram of total porosity	33
Figure 17 – Matrix histogram for effective porosity	34
Figure 18 – Distribution of water saturation across the wells in the caprock.....	36
Figure 19 -Cross-plot RH _{maa} vs U _{maa} for mineralogy identification	38
Figure 20 -Cross-plot RH _{maa} vs DT _{maa} for mineralogy identification.....	39
Figure 21 - Mineralogy log for well 67-1-TpX-1	40
Figure 22 - Acoustic properties for well 67-1-TpX-10.....	43
Figure 23 – Shear velocity for the well 67-1-TpX-10.....	44
Figure 24 – Compressional to shear velocity ratio and dynamic Poisson’s ratio for the well 67-1-TpX-10.....	46
Figure 25 – Type of stresses (31)	49
Figure 26– Stress-strain curve (32)	50
Figure 27 – Stress-strain curve for ductile and brittle rocks.....	50
Figure 28 – Overburden stress.....	52
Figure 29 – Overburden stress histogram.....	53
Figure 30 – Pore pressure calculation by using the Eaton’s method.....	55
Figure 31 – Pore pressure histogram	56
Figure 32 – Unconfined compressive strength	58
Figure 33 – Unconfined compressive strength crossplots.....	59
Figure 34 – Unconfined compressive strength histogram.....	59

Figure 35 –Tensile strength histogram	60
Figure 36 –Box plots for UCS and TS	61
Figure 37 –Young’s modulus vs Poison’s ratio crossplot colored by gamma ray	63
Figure 38 - Mineral content of the caprock in the well 67-1-TpX-10.....	64
Figure 39 – Correlation of variables used for IPSOM classification	65
Figure 40 – IPSOM classification using an indexation of 2.....	66
Figure 41 - IPSOM classification results using an indexation of 2.....	67
Figure 42 – a) Young’s modulus vs Poison’s ratio crossplot colored by IPSOM classification and b) Young’s modulus vs Poison’s ratio crossplot colored by gamma ray	68
Figure 43 – IPSOM classification pie chart for the well 67-TpX-10.....	68
Figure 44 – IPSOM classification pie chart for all the wells	69
Figure 45 – Brittleness index comparison for the well 67-1-TpX-10	71
Figure 46 – Brittleness index vs volume of shale for all the wells	73
Figure 47 – Final result of brittleness index.....	74
Figure 48 – Modeling flowchart for the simulation	76
Figure 49 – Conformal gridding example.....	77
Figure 50 – Available seismic data for Teapot Dome field.....	77
Figure 51 – Available seismic data for Teapot Dome field.....	78
Figure 52 – Conformal 3D grid	79
Figure 53 – Estimated facies proportions percentage	80
Figure 54 – Proportion curves for each facie (ductile and brittle).....	81
Figure 55 – IPSOM variogram	81
Figure 56 – Facies volume height map	82
Figure 57 – Vertical, Major and minor direction for group 1.....	84
Figure 58 – Vertical, Major and minor direction for group 2.....	84
Figure 59 –Distribution of the modeled Brittleness index.....	85
Figure 60 –Brittleness index volume height maps filtered with IPSOM classification	86
Figure 61 – BI average thickness map.....	86
Figure 62 – Ductility proportional thickness map.....	87
Figure 63 –Brittleness proportional thickness map	88
Figure 64 –Possible drilling locations for CO ₂ storage	90

LIST OF TABLES

Table 1 – Ductility of different caprock lithologies (11).....	12
Table 2 – Well logs summary	21
Table 3 – Thickness summary for the 2 nd Wall Creek formation	25
Table 4 – Mechanical parameters.....	41
Table 5 – Statistical parameters of dynamic properties for the caprock of the 2 nd Wall Creek reservoir and histograms made for Young modulus, shear modulus, bulk modulus and Poisson’s ratio	48
Table 6 – Variable correlation and contribution.....	66
Table 7 – IPSOM classification statistics	67

LIST OF APPENDIX

APPENDIX 1 – WELL LOGGING TOOLS AND PRINCIPLES

Figure 1. 1 – Well logging setup (47)	99
Figure 1. 2 – Gamma Ray response (47)	100
Figure 1. 3 – Bulk Density log (22).....	101
Figure 1. 4 – Photoelectric Factor log (22).....	102
Figure 1. 5 – Neutron log (22)	103
Figure 1. 6 – Resistivity logs (22).....	104
Figure 1. 7 –Compressional Slowness log (22).....	105

APPENDIX 2 – WELL CORRELATION

Figure 2. 1 – Correlation across the 18 wells that penetrates the 2 nd Wall Creek Reservoir	107
--	-----

APPENDIX 3 – SHALE VOLUME

Figure 3. 1 - Shale volume calculation for the wells from left to right: 28-AX-27, 36-MX-10, 67-1-TPX-10, 11-DX-26, 12-AX-33, 14-LX-28-WD, 28-AX-34, 34-TX-3, 36-11-SX-2	108
Figure 3. 2 - Shale volume calculation for the wells from left to right: 41-2-X-3, 41-AX-3, 53-LX-3, 62-TPX-10, 64-JX-15, 71-1-X-4, 75-AX-28, 88-AX-28, 88-DX-3	109

APPENDIX 4 – TOTAL AND EFFECTIVE POROSITY

Figure 4. 1- Total and effective porosity for the wells from left to right: 28-AX-27, 36-MX-10, 67-1-TPX-10, 11-DX-26, 12-AX-33, 14-LX-28-WD, 28-AX-34, 34-TX-3, 36-11-SX-.....	110
Figure 4. 2 - Total and effective porosity for the wells from left to right: 41-2-X-3, 41-AX-3, 53-LX-3, 62-TPX-10, 64-JX-15, 71-1-X-4, 75-AX-28, 88-AX-28, 88-DX-3	111

APPENDIX 5 – WATER SATURATION

Figure 5. 1 - Water saturation for the wells from left to right: 28-AX-27, 36-MX-10, 67-1-TPX-10, 11-DX-26, 12-AX-33, 14-LX-28-WD, 28-AX-34, 34-TX-3, 36-11-SX-2.....	112
Figure 5. 2 - Water saturation for the wells from left to right: 41-2-X-3, 41-AX-3, 53-LX-3, 62-TPX-10, 64-JX-15, 71-1-X-4, 75-AX-28, 88-AX-28, 88-DX-3	113

APPENDIX 6 – MINERALOGY

Figure 6. 1 - Mineralogy for the wells from left to right: 28-AX-27, 36-MX-10, 67-1-TPX-10, 11-DX-26, 12-AX-33, 14-LX-28-WD, 28-AX-34, 34-TX-3, 36-11-SX-2.....	114
Figure 6. 2 - Mineralogy for the wells from left to right: 41-2-X-3, 41-AX-3, 53-LX-3, 62-TPX-10, 64-JX-15, 71-1-X-4, 75-AX-28, 88-AX-28, 88-DX-3	115

APPENDIX 7 – ACOUSTIC PROPERTIES

Figure 7. 1 - Acoustic Properties for the wells from left to right: 28-AX-27, 36-MX-10, 67-1-TPX-10, 11-DX-26, 12-AX-33, 14-LX-28-WD, 28-AX-34, 34-TX-3, 36-11-SX-2	116
Figure 7. 2 - Acoustic Properties for the wells from left to right: 41-2-X-3, 41-AX-3, 53-LX-3, 62-TPX-10, 64-JX-15, 71-1-X-4, 75-AX-28, 88-AX-28, 88-DX-3	117

APPENDIX 8 – SHEAR VELOCITY

Figure 8. 1 - Shear velocity for the wells from left to right: 28-AX-27, 36-MX-10, 67-1-TPX-10, 11-DX-26, 12-AX-33, 14-LX-28-WD, 28-AX-34, 34-TX-3, 36-11-SX-2	118
Figure 8. 2 – Shear velocity for the wells from left to right: 41-2-X-3, 41-AX-3, 53-LX-3, 62-TPX-10, 64-JX-15, 71-1-X-4, 75-AX-28, 88-AX-28, 88-DX-3	119

APPENDIX 10 – IPSOM RESULTS AND DYNAMIC ELASTIC PROPERTIES

Figure 9. 1 - Pore pressure for the wells from left to right: 11-DX-26, 12-AX-33,14-LX-28-WD, 28-AX-27,28-AX,34-TX-3	120
Figure 9. 2 - Pore pressure for the wells from left to right: 36-11-SX-2, 36-MX-10,41-2-X-3,41-AX-3,53-LX-3,62-TpX-10.....	121
Figure 9. 3 - Pore pressure for the wells from left to right: 64-JX-15, 67-1-TpX-10,71-1-X-4,75,AX-28,88-AX-28,88-DX-3	122

APPENDIX 11 – IPSOM PIE-CHARTS

Figure 10. 1 - IPSOM results and dynamic elastic properties for the wells from left to right: 28-AX-27, 36-MX-10, 67-1-TPX-10, 11-DX-26, 12-AX-33	123
Figure 10. 2 - IPSOM results and dynamic elastic properties for the wells from left to right: 14-LX-28-WD,28-AX-27,28-AX,34-TX-3, 41-2-X-3, 41-AX-3, 53-LX-3.....	124
Figure 10. 3 - IPSOM results and dynamic elastic properties for the wells from left to right: 62-TPX-10, 64-JX-15, 71-1-X-4, 75-AX-28, 88-AX-28, 88-DX-3	125

APPENDIX 9 – PORE PRESSURE

Figure 11. 1 - Pie-charts for the wells from left to right: 11-DX-26, 12-AX-33, 14-LX-28-WD, 28-AX-27, 28-AX, 34-TX-3.....	126
Figure 11. 2 - Pie-charts for the wells from left to right: 36-11-SX-2, 36-MX-10, 41-2-X-3,41-AX-3,53-LX-3,62-TpX-10.....	127
Figure 11. 3 - Pie-charts for the wells from left to right: 64-JX-15, 67-1-TpX-10,71-1-X-4,75-AX-28,88-AX-28,88-DX-3	128

APPENDIX 12 – BRITTLE INDEX

Figure 12. 1 – Brittle index for the wells from left to right: 28-AX-27, 28-AX-34, 11-DX-26	129
Figure 12. 2 – Brittle index for the wells from left to right: 36-MX-10, 67-1-TpX-10, 12-AX-33	130
Figure 12. 3 – Brittle index for the wells from left to right: 14-LX-28-WD, 34-TX-3, 36-11-SX-2	131
Figure 12. 4 – Brittle index for the wells from left to right:41-2-X-3,41-AX-3,53-LX-3.....	132
Figure 12. 5 – Brittle index for the wells from left to right: 62-TpX-10, 64-JX-15, 71-1-X-4.	133
Figure 12. 6 – Brittle index for the wells from left to right: 75-AX-28,88-AX-28,88-DX-3	134

NOMENCLATURE

σ	Stress
\emptyset	Porosity
3-D	Three dimensional
a	Tortuosity factor
AI	Acoustic impedance
BI	Brittle index
BI _H	Ingram and Urai brittle index
BI _M	Wang and Gale's brittle index
BI _R	Rickman's brittle index
BI _R	Brittleness index evaluation
CALR	Caliper
CCS	Carbon Capture and Storage
C _{dyn}	Dynamic bulk compressibility
CO ₂	Carbon dioxide
DEN_EXTRAPOLATED	Extrapolated bulk density
DT	Compressional slowness
DT _{maa}	Matrix apparent compressional slowness
DT _{norm}	Normal Compressional slowness
DT _o	Initial travel time
Ductile	Caprock ductility percentage
E	Young's modulus
E _{dyn}	Dynamic young's modulus
EOR	Enhanced oil recovery
G	Shear modulus
G _{dyn}	Dynamic shear modulus
GHG	Greenhouse emission
GR	Gamma ray
GRFS	Gaussian random function simulation
HighThickness_LowBI	High Thickness and Low BI
IF	Integrity factor
IPSOM	Index and Probability Generating a Self-Organizing Map
ITF	Interfacial tension
K	Bulk modulus
K _{dyn}	Dynamic bulk modulus
L	Number of monomineralic lithology constituent
m	Cementation
M	Compressional modulus
MICP	Mercury injection capillary pressure

n	Saturation exponent
NPHI	Neutron porosity
NPR3	Naval petroleum reserve
OBMW_EXT	Vertical stress gradient equivalent
P _c	Threshold pressure
P _e	Photoelectric absorption
PE	Photoelectric factor
PHIE_ND	Effective porosity
P _p	Pore pressure
P _{p_DT}	Pore pressure Eaton sonic
P _{p_R}	Pore pressure Eaton resistivity
P _{pnorm}	Normal pore pressure
P-waves	Principal compressional waves
r	Pore radius
R	Resistivity
RDEP	Deep resistivity
RFOC	Shallow resistivity
RHOB	Bulk density
RHomaa	Apparent grain density
RILM	Medium resistivity
RMOTC	Rocky mountain oilfield testing center
R _{norm}	Normal resistivity
R _o	Sediment resistivity
R _t	Formation resistivity
R _w	Formation water resistivity
scf	Standard cubic feet
SIS	Sequential indicator simulation
SP	Spontaneous potential
SPR	Slowness time projection
SVERTIVAL_EXT	Overburden stress
S _w	Water saturation
S-waves	Secondary waves
T	Shear stress
TS	Tensile strength
TVD	Truth vertical depth
UCS	Unconfined compressive strength
UCS _{NC}	UCS of a consolidated rock
U _f	Apparent fluid volumetric cross section
Umaa	Matrix apparent volumetric photoelectric factor
v	Poisson ratio
v/v	Volume to volume ratio
VANH	Volume of anhydrite
VCLC	Volume of clay
VDOL	Volume of dolomite
V _{f_i}	Volume fractions of lithological constituents

V_o	Initial volume
VP	Compressional velocity
VPVS	Static Poisson's ratio
VQTZ	Volume of quartz
VS	Shear velocity
V_{sh}	Volume of shale
γ	Shear strain
z	Depth
ΔP	Pressure change
Δt	Wave transit time
Δt_{comp}	Bulk formation compressional slowness
Δt_f	Pore fluid transit time
Δt_{shear}	Bulk formation shear slowness
ΔV	Volume change
ϵ	Strain
ϵ_{axial}	Axial strain
ϵ_{trans}	Transverse strain
θ	Contact angle
ρ	Density
ρ_b	Bulk density
ρ_e	Electron density
$\rho_{Extrapolated}$	Extrapolated density
ρ_{fluid}	Fluid density
ρ_{matrix}	Matrix density
$\rho_{mudline}$	Mud density
σ_v	Vertical stress, overburden stress
γ	CO ₂ -water interfacial tension

CHAPTER I. INTRODUCTION

Carbon Capture and Storage is one of the most efficient alternatives to decrease the industrial greenhouse emissions (GHG), such as carbon dioxide (CO₂), into the atmosphere. Underground geological formations constitute a suitable storage for GHG because of its large storage capacity and the presence of an effective trap and sealing mechanisms. The ideal characteristics of the target reservoir are significant storage capacity, high leak-proof, effective sealing, and a non-faulted stratum. The stability of the sealing (caprock) during and after the CO₂ storage is associated with geophysical, geomechanical parameters and caprock-CO₂ and pore fluid interactions. The change in stress, chemical and physical alteration of the reservoir and caprock caused by carbonic acid (formed when CO₂ dissolves in the groundwater) can lead to strength reduction and failure of the caprock. Besides, the interaction of supercritical CO₂ with the brine in the reservoir and the changes in the stress field due to CO₂ injection can have an impact. Consequently, the caprock integrity is becoming more important in the reservoir characterization and especially for geo-sequestration projects.

This project covers the theory behind the caprock rock integrity, rock mechanics, and carbon sequestration. It is emphasized the quality check of conventional logs and computation of reference/index datasets for each well. The gamma ray and spontaneous potential logs are examined in the zone of interest for lithologic information to enable well correlation. The acoustic/rock physics properties are derived by using a combination of between bulk density, and compressional slowness log and the values of porosity and saturation are determined by neutron porosity and deep resistivity logs. Furthermore, the lithology and mineral composition of the rock is estimated by a four-point mineral model which uses the apparent matrix density (RH_{maa}), apparent matrix volumetric photoelectric factor (U_{maa}), and matrix apparent compressional slowness (Dt_{maa}) to interpolate between four end-point minerals. The 1D outputs from the petrophysical, geophysical and geomechanical calculations are modeled in 3D to show the variation in the rock properties.



1.1. Problem Statement

The success of any CO₂ sequestration operation depends on the sealing ability of the top layer (caprock) in the reservoir. The sealing is influenced by pre-existing fractures/faults or leakage pathways that are present and the ones that can occur due to interactions when the CO₂ is injected into the reservoir.

The aim of this project is to characterize the caprock of the 2nd Creek Wall reservoir, Teapot Dome, Wyoming based on the brittle index. This characterization can be done by integrating geology, petrophysics, rockphysics, and geomechanics concepts.

This project will use a multi-disciplinary approach through Techlog© which takes into consideration wireline logs including gamma ray (GR), spontaneous potential (SP), bulk density (RHOB), neutron (NPHI), deep resistivity (RDPE), compressional slowness (DT), and photoelectric effect (PE) logs and other available information to evaluate the seal rock. Subsequently, a 3-D grid model of the caprock lithofacies based on Petrel will be developed to identify the possible drilling locations for the CO₂ injection wells.

1.2. Data and Methods

The evaluation of the caprock in the 2nd Wall Creek reservoir, Teapot Dome field requires geophysical, geological data. This information was obtained from the US Geological Survey Site (USGS) and Rocky Mountain Oilfield Testing Center (RMOTC). The database includes the following well logs: gamma ray (GR), spontaneous potential (SP), bulk density (RHOB), neutron (NPHI), deep resistivity (RDPE), compressional slowness (DT), and photoelectric effect (PE) for the 18 wells. The research methodology of the present study is:

1. Geological background of the Teapot Dome field and 2nd Wall Creek reservoir
2. Well correlation of the caprock across the 18 wells
3. Computation of petrophysical parameters: volume of shale (VSH), porosity (\emptyset), water saturation (S_w)



4. Identification of the mineral content of the caprock
5. Determination of acoustic properties such as compressional velocity (VP), shear velocity (VS), acoustic impedance (AI) and compressional modulus (M).
6. Estimation of dynamic elastic properties: Poisson's ratio, Young's modulus, bulk modulus and shear modulus
7. Assessment of the geomechanical properties of the caprock
8. Evaluation of the caprock integrity through dynamic elastic properties, IPSOM neuronal analysis, and brittleness index
9. 3-D modeling of the caprock integrity

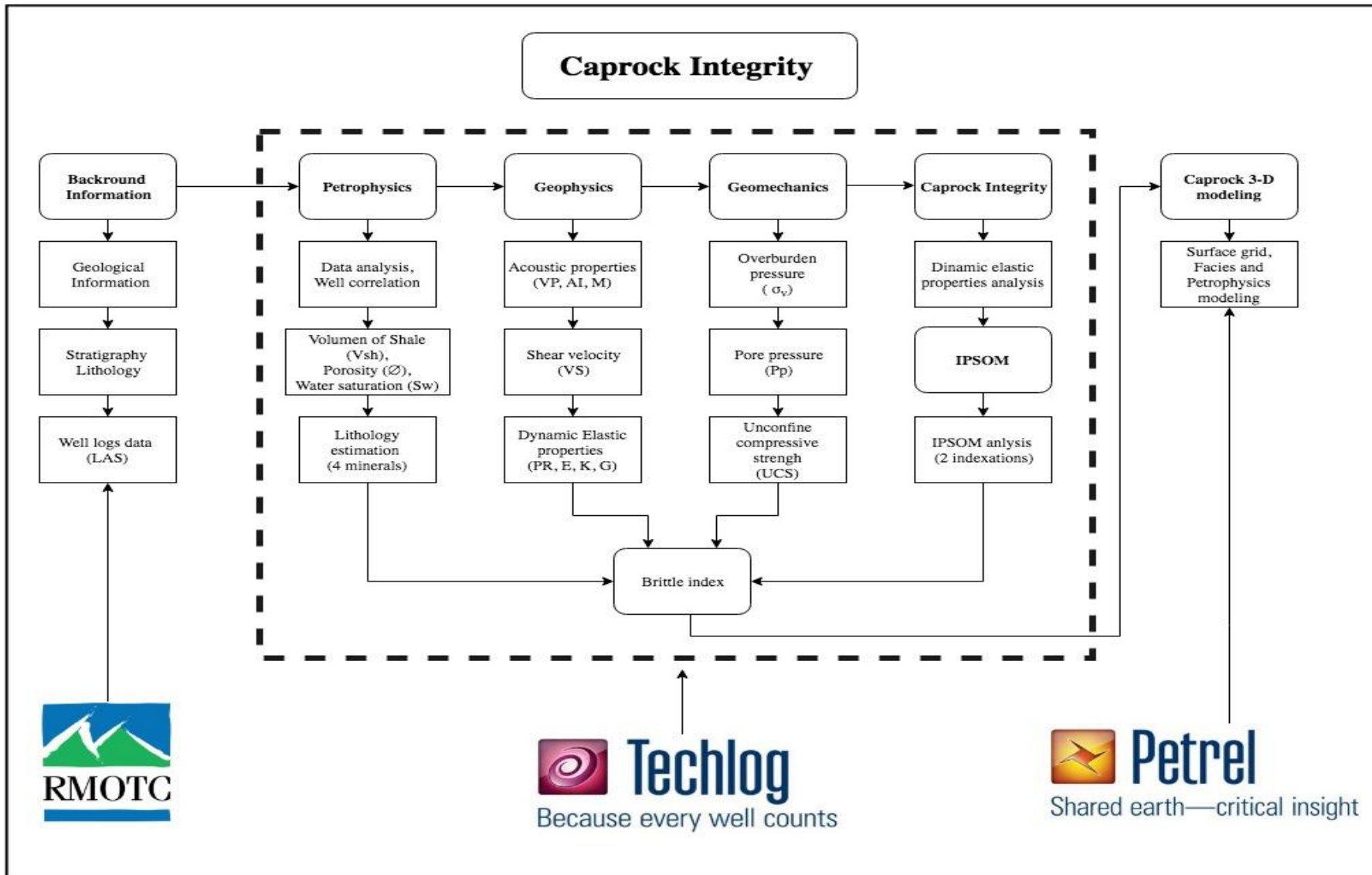


Figure 1 – Caprock Integrity Flowchart

1.3. Area of Investigation

The study area of the present project is the 2nd Wall Creek Reservoir in the Teapot Dome field, Wyoming, located at 48 km north of Casper in the Natrona County near the southwestern margin of the Powder River Basin (Figure 2). The area of the Teapot Dome field is approximately 40.5 km². It has more than 2200 wells around 1200 of those wells can be accessed, and 400 penetrates 11 formations situated at a depth at which the CO₂ is a supercritical fluid (31.1 °C, 73.9 bar) (1). It is necessary for an efficient CO₂ storage because at pressures higher than the critical point the CO₂ density can vary widely; approaching or exceeding the density of the water (2).

Teapot Dome field is considered as a Naval Petroleum Reserve (NPR3) where many experiments and research projects have been performed to get a scientific and technical insight into CO₂ - enhanced oil recovery (EOR) (3).

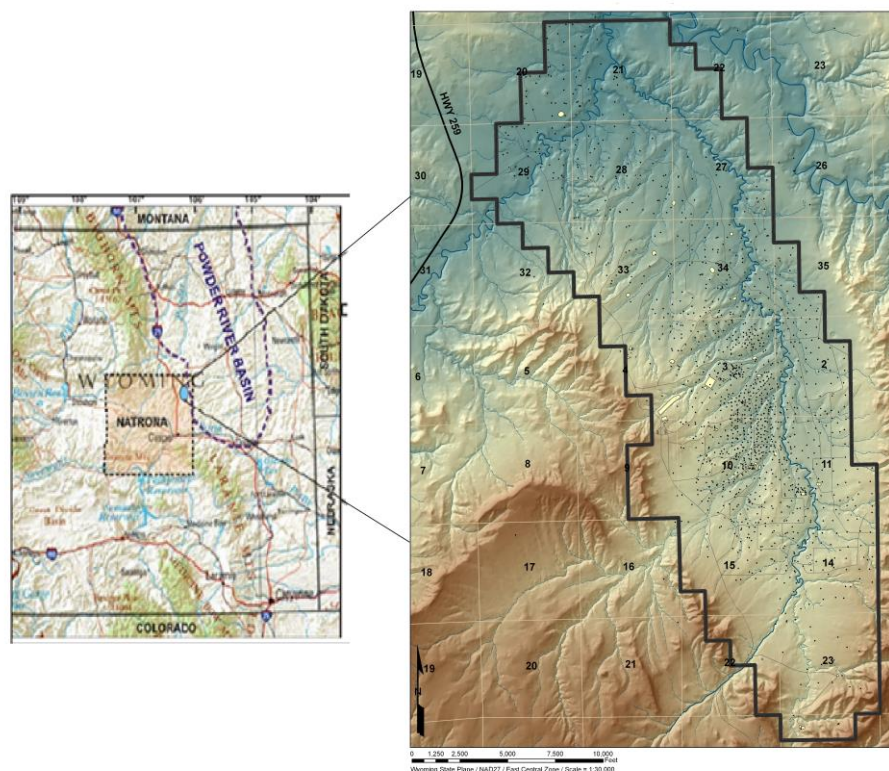


Figure 2 – General location of Wyoming and Teapot Dome Field (4)

1.4. Carbon Sequestration

Carbon sequestration or also called Carbon Capture and Storage (CCS) is a disposal option to reduce the greenhouse emissions into the atmosphere. There are two types of carbon sequestration: direct or indirect. In the direct sequestration, the CO₂ produced from industrial processes is captured in the generation place and then storage in the geological formation. On the contrary, the indirect sequestration captures the CO₂ that has been absorbed in the atmosphere (2).

The principal carbon sequestration techniques include the injection of CO₂ into mature reservoirs for enhanced oil recovery (EOR) purposes, low permeability coal bed to increase the methane recovery and deep saline formations (onshore or offshore) (2). Since the depleted oil and gas reservoirs have been already geologically characterized, the data from seismic and core analysis is available; making those reservoirs attractive targets for geological sequestration.

Many projects have been conducted worldwide in order to generate new knowledge that helps to understand the efficiency and risks of the geological carbon storage. One of the most significant concerns about the CO₂ storage is the possible leakage which can be gradual through undetected faults/fractures or abrupt through damaged injection wells (2). The presence of CO₂ in the subsurface contaminates the groundwater and has harmful effects on marine plants and animals because of the associated pH reduction (acidification).

The Teapot Dome oil field is considered as an ideal location for CO₂ studies because of geological, geophysical and geomechanical data availability (3). Some studies have been conducted in this field to understand fault relationships between deep and shallow reservoirs and how the seal capacity of the reservoir has been compromised by the presence of small faults.

1.5. Project Limitations

The lack of core data was one of the project limitations since it was not possible to confirm some of the results obtained in the study. Moreover, the absence of seismic data resolution at a depth of interest made impossible the calculation of seismic inversion properties that could be used to constrain the petrophysical model of the caprock.



1.6. Project Outline

Chapter 1 introduces the problem statement, data, and methods, area of investigation, overview of the carbon sequestration techniques and the major project limitations.

Chapter 2 presents a detailed literature review of the caprock characteristics for CO₂ geological storage; including the factors that control its integrity and effectiveness.

Chapter 3 gives a geological background of the investigation area. Also, it is described the geology of the Teapot Dome field, stratigraphy and lithology of the Frontier formation; being highlight the 2nd Wall Creek reservoir.

Chapter 4 is based on the caprock petrophysical evaluation in which petrophysical parameters such as the volume of shale, porosity and water saturation are computed through well logging analysis in Techlog®. The first part of this chapter includes quality check and data analysis of the available wells that penetrates the 2nd Wall Creek reservoir.

Chapter 5 involves the calculation of acoustic properties such as shear and compressional velocity which are determined through logging data in Techlog®. Those parameters are then used to calculate the dynamic elastic properties: Poisson's ratio, Young's modulus, bulk modulus and shear modulus.

Chapter 6 gives a general overview of the theory behind rock mechanics. The second part of this chapter comprises the computation of in-situ stress (overburden stress and pore pressure) and rock strength through unconfined compressive strength and tensile strength.

Chapter 7 presents the evaluation of the caprock integrity in which is combined the results from the petrophysical, geophysical and geomechanical analysis.

Chapter 8 address two types of modeling. The first one corresponds to the facies modeling in which the discrete attribute obtained from the IPSOM classification is populated into the grid cells. The second simulation corresponds to petrophysical modeling which is constrained to facies due to the lack of seismic data at the interest zone.



CHAPTER II. LITERATURE REVIEW

A long-term CO₂ storage requires a hermetic layer above the reservoir called caprock or seal which has a low permeability that varies between 10⁻³ mD to 10⁻¹⁸ mD. The caprock is the most critical feature of a reservoir because the effectiveness of the subsurface trapping system is determined by its physical characteristics.

In this chapter is provided an overview of the caprock characteristics and also the mechanisms that affect the sealing integrity.

2.1. Caprock in CO₂ Sequestration

For CO₂ storage purposes, the caprock needs to withstand the upward buoyancy-driven force of the injected supercritical CO₂ that is accumulated after a few years of injection (5). When the excessive pressure overcomes the critical stress and tensile strength of the rock, the caprock succumbs to hydraulic fracturing; being compromised its effectiveness. Another factor that needs to be considered for CO₂ storage is the migration mechanisms from the reservoir into the caprock. The major losses of CO₂ are: diffusion of the dissolved CO₂ in the interstitial water and flow through existing open fractures (5).

The CO₂ diffusion into the caprock occurs due to geochemical reactions between the CO₂ and the rock minerals. Those reactions take place when the CO₂ reaches the caprock bottom and dissolves into the interstitial water. The dissolution of the initial caprock minerals increases the porosity while the precipitation of the secondary minerals (reaction products) decreases its value (6). This weakens the rock skeleton and promotes the mechanical compaction of the rock. Many researchers have shown that this process has an insignificant relevance in the CO₂ leakage. Busch (2010) (7) shows that even considering the worst scenario (diffusion coefficient of 10⁻¹⁰ m²/s and a caprock with a thickness of 10 m) the diffusion will take 0.1 million of years. Therefore, it is considered negligible for CO₂ operations.



2.2. Seal Potential

The seal potential is described as the capacity, geometry, and integrity of the caprock to confine CO₂. It depends on the size of the interconnected pore throats, relative densities of CO₂/water and petrophysical properties such as wettability and interfacial tension (8).

2.2.1. Seal Capacity

The seal capacity is the column height of CO₂ that can be held back by the caprock before the capillary forces allow its migration. The CO₂ is driven into the pore throats by the buoyancy (product of the density difference between CO₂ and interstitial water multiplied by the column height and the pressure gradient of pure water). It is control by the capillary pressure or threshold pressure which is a function of the pore size, CO₂-water interfacial tension (IFT) and wettability of the rock as can be seen in Eq. 1. In this equation, P_c is the threshold pressure, γ is the CO₂-water interfacial tension, θ is the contact angle and r is the radius of the pore which is different from one type of rock to another (8).

$$P_c = \frac{2 \gamma \cos\theta}{r} \quad \text{Eq. 1}$$

The CO₂-brine interfacial tension (γ) is a crucial parameter for the caprock sealing capacity. It is a function of pressure, temperature, and CO₂ density. Under experimental conditions, the interfacial tension increases slightly as the temperature increases but decreases with an increase of pressure (8).

Usually to determine the contact angle (θ) is assumed that the wetting phase is water and CO₂ are the non-wetting phase; however, some experimental studies suggest that the wettability can change depending on the pressure and mineral content of the rock and can be affected by brine concentrations (8).

Figure 3 shows the migration of CO₂ through the pore space. It can be observed that the force that avoids the upward movement of CO₂ is the capillary pressure (8). When the buoyancy pressure of the CO₂ plus the injection pressure exceed the threshold pressure of the caprock, the CO₂ will migrate upwards (8).



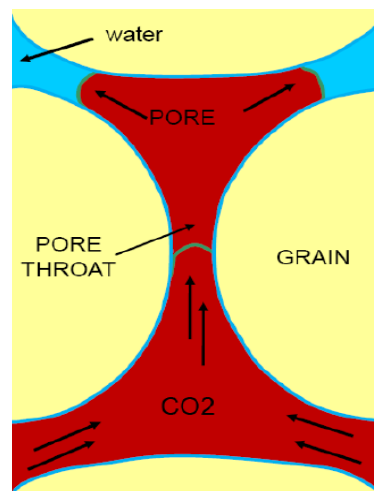


Figure 3 – Upward migration of CO₂ due to buoyancy (8).

2.2.2. Seal Geometry

The seal geometry depends on the thickness, area and structural position of the caprock. It is determined by an integral core data analysis, well logs, seismic data, sedimentological analyses, and analogs by making a comparison of the area between the estimated stratigraphic trap and the seal.

The caprock extension area needs to be sufficient, in other words, equal or greater than the reservoir area. It is desirable because the capillary of the caprock will be similar throughout the area.

2.2.3. Caprock Integrity

The caprock integrity is referred to the rock ductility and associated with the presence or absent of leakage pathways (fractures) and especially with the risk of creating new fractures or reactivating existing faults while the CO₂ is injected into the reservoir (8).

The main effects due to the CO₂ injection are (9):

1. Rock fatigue or irreversible deformation because of pressure cycling (injection and withdrawal of fluids)
2. Increasing of pore pressure that leads to micro shear fractures
3. Possibility of tensile stresses when the effective stresses decrease significantly
4. Failure of the rock when the shear strength is reduced

The principal objective of this project is to evaluate the caprock integrity of the 2nd Wall Creek Reservoir through the brittleness index

2.3. Caprock Effectiveness

The primary factors that control the effectiveness of the caprock are: lithology, ductility, thickness, lateral seal continuity and burial depth

2.3.1. Lithology

Theoretically, any lithology can be used, the minimum requirement is that the threshold pressure (displacement pressure) must be greater than the buoyancy pressure of the fluid inside of the pore spaces (10). Fine-grained siliciclastic (clay, shales), evaporites (anhydrite, halite) and organic-rich rocks constitute the most important caprocks. Shale caprocks comprise more than 60% of effective seals for hydrocarbon bearing reservoirs. This type of caprock seals more than 900 billion oil barrels and over 500 billion oil equivalent barrels. Evaporites are the next lithology in order of importance because they are the caprock for the majority of giant oilfields in the Middle East and North Africa. The organic-rich shale has limited potential due to substantial diffusive leakage via inherent microporosity (11). Since shale caprocks dominate over other lithologies in volume terms, they are the principal target for underground CO₂ storage.

2.3.2. Ductility

A caprock needs to be ductile (plastic behavior during the folding and flowage) to support all effective stresses applied on it. Ductile caprocks are less likely to faulting and fracturing than brittle lithologies. During periods of structural deformation, the caprocks are placed under substantial stress. This makes the ductility the most important requirement for seals in deformed areas like fold-thrust belts (11). *Table 1* shows the different caprock lithologies in terms of ductility. It can be noticed that evaporites are the most ductile and chert is the least ductile.



Table 1 – Ductility of different caprock lithologies (11)

Caprock Lithology	Ductility
Halite	Most ductile ↓ Least ductile
Anhydrite	
Organic-rich shales	
Shales	
Silty shales	
Calcareous mudstones	
Sandy shales	
Anhydrite plugged dolomite	
Carbonate cemented sandstones	
Chert	

Ductility and compressibility are inversely proportional to sonic velocity and rock strength. Some types of lithology are more ductile and compressible than others. *Figure 4* shows the relationship between ductility/compressibility and strength/sonic velocity of different lithologies and a relative Integrity Factor (IF) that ranges from 1.0 to 0. It can be appreciated that halite is more ductile and compressible than shales, but it has lower rock strength. The IF of this type of rock is almost 1 and is less likely to develop structural permeability (10). The shale, on the other hand, has an integrity factor between 0.5-0.75. In general, the shale ductility and compressibility are lower than the evaporites but its strength is higher.

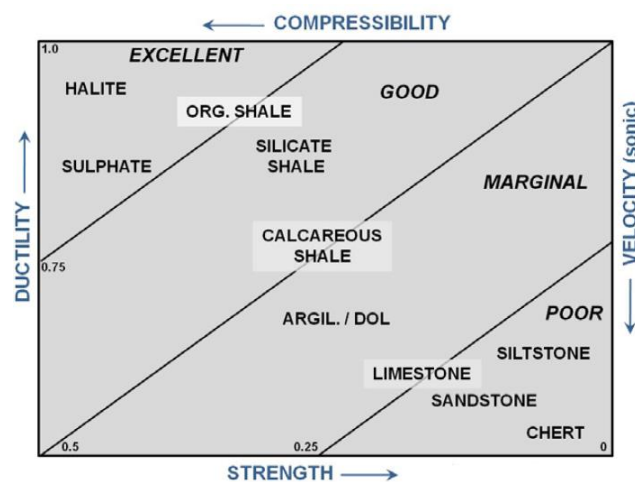


Figure 4 – Relative ductility and compressibility vs. strength/sonic velocity

2.3.3. Thickness

The caprock thickness is important because it provides several safety layers capable of covering the reservoir area. A thick caprock is required because it can prevent the horizontal leakage of the fluids; providing a lateral seal (10). It does not occur with thin caprocks since they are laterally no persistent over the entire prospect. Typically, the thickness of the caprock ranges from tens to hundreds of meters (11).

To determine the thickness of the caprock of the present study, different wells are correlated to find out the top and base of this unit by using GR.

2.3.4. Burial Depth

The sealing effectiveness of the caprock is influenced by the burial depth. As the burial depth increases, the pore pressure is increased and consequently the confining pressure decreases. This drop the effective minimum stresses which can cause failure along pre-existing fractures and hydraulic fracturing of the caprock (12).

CHAPTER III. GEOLOGICAL BACKGROUND

The Teapot Dome Field has plenty research information in the public domain such as well logs, seismic, production, and core data since it is an experimental facility designed to conduct carbon storage studies. This data can be used to characterize and interpret different stratigraphic units.

This chapter describes the geology and stratigraphy of the Teapot Dome and also the lithology of the Frontier formation; emphasizing the 2nd Wall Creek reservoir and its caprock.

3.1. Geology of Teapot Dome

The Teapot Dome is a Laramide-age anticline localized above a high angle thrust fault. It is part of the larger Salt Creek complex which is considered as a productive hydrocarbon structural trap because it provides an excellent four-way closure; entrapping significant amount of hydrocarbons (13). It can be seen in *Figure 5* that the Teapot Dome is surrounded by Sweetwater, Laramie and Bighorn uplifts and Wind River, Bighorn and Denver Basins.



Figure 5 – Map of the Teapot Dome (14)

The Teapot Dome is a basement-cored anticline which is asymmetrical, doubly plunging with a north-northwest axis with an approximated azimuth of 330° (15). It is characterized by steeper dips on the western flank, and shallow dips on the eastern flank where normal to oblique strike-slip faults strike almost perpendicular to the fold hinge (16). In the west side, there is a Laramide-style thrust fault propagating from north to south.

Figure 6 shows the faults at the Teapot Dome which are separated in two major blocks, S_1 Zone in the south and the S_2 Zone in the north in which there are four main faults, named S_1 to S_4 . The S_1 Zone is interpreted as a right lateral NE-SW oblique-slip fault. The S_2 Zone corresponds to NE-SW strike-slip faults which divide the field into several blocks. Those faults offset the basement and locally have steep dip angles which make the geometry of the field complex (17).

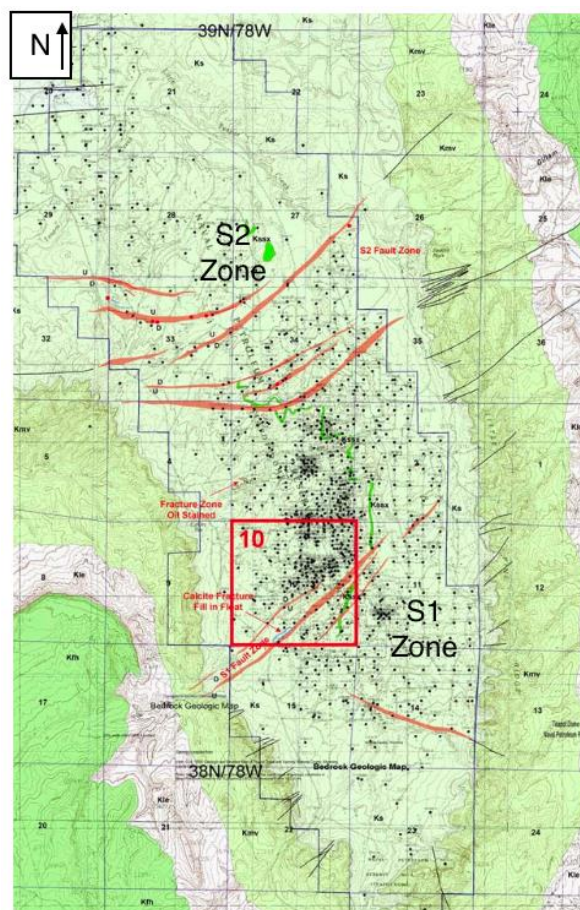


Figure 6 – Structural map of the reservoir (17)

Figure 7 shows the location of the seismic lines in a depth structure map of the 2nd Wall Creek reservoir for an NW-SE Cross-section of the Teapot Dome. As can be noticed, the S₂ fault network is highly complex both in geometry and azimuths.

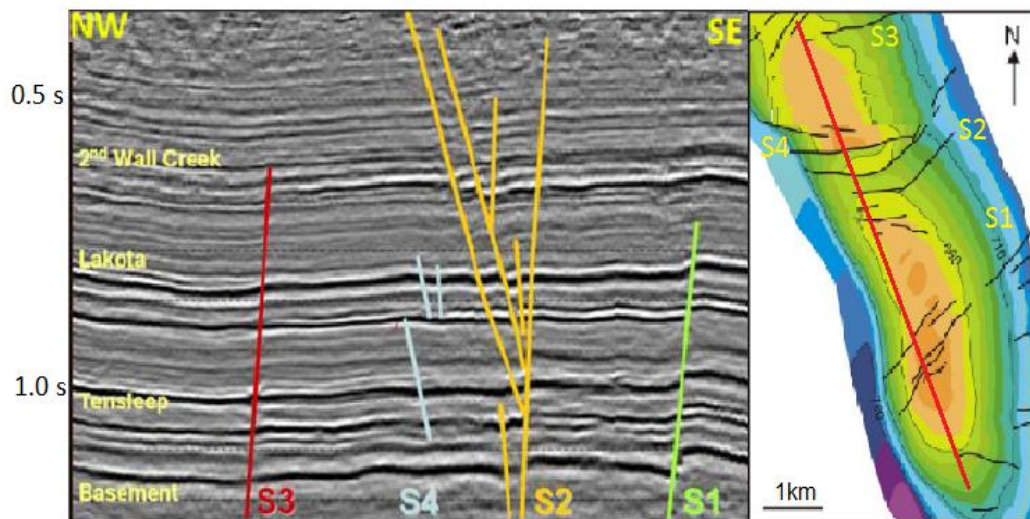


Figure 7 – Depth-structure map of the 2nd Wall Creek sandstone (17)

3.2. Stratigraphy

Teapot Dome comprises stratigraphic units from Devonian to Upper Cretaceous periods where there is an intercalation between permeable and porous formations with impermeable rocks. It can be seen in the

Figure 8 that the oil producing formations are: Shannon Ss, Niobrara Shale, 2nd Wall Creek, 3rd Wall Creek, Muddy Sandstone, Dakota, Lakota, and Tensleep. On the other hand, the water-bearing formations are Sussex Ss, Carlisle Shale, 1st Wall Creek, Upper Sundance, Crow Mountain, Madison and Undifferentiated. Those formations consist of marine lacustrine carbonates, sandstones, shallow shelf siliciclastic that overlay a granitic basement (17). The main productive zones are Shannon Formation, the 2nd Wall Creek, and the Tensleep Sandstone Formation.

PERIOD	FORMATION	LITHOLOGY	THICKNESS [m]	DEPTH [m]	PRODUCTIVE	
Upper Cretaceous	Steele Shale		59			
		Sussex Ss	9		○	
			88	69		
		Shannon Ss	37	157	●	
			413	194	●	
	Niobrara Shale		137		●	
	Carlisle Shale		73	744	○	
	Frontier	1st Wall Creek		49	817	○
				75	866	
		2nd Wall Creek		20	940	●
			53	960		
	3rd Wall Creek		2	1013	●	
			81	1015		
Lower Cretaceous	Mowry Shale		70	1096		
	Muddy Sandstone		5	1166	●	
	Thermopolis Shale		41	1170		
	Dakota		26	1212	●	
	Lakota		3	1237	●	
Jurassic	Morrison		82	1241		
	Sundance	Upper	29	1323	○	
		Lower	46	1352		
Triassic	Chungwater Group	Crow Mountain	24	1398	○	
		Alcova LS	6	1422		
		Red Peak	158	1428		
Permian	Goose Egg		98	1586		
Pennsylvanian	Tensleep		98	1684	●	
Mississippian	Amsden		49	1782		
Devonian	Madison		91	1830	○	
Cambrian	Undifferentiated		219		○	
Pre-Cambrian	Granite			2160		

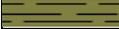
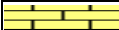
LITHOLOGY		POREFLUID	
	SHALE		OIL BEARING
	SANDSTONE		WATER
	LIMESTONE		
	GRANITE		

Figure 8 – Teapot Dome stratigraphic column (3)

The principal objective of this project is to characterize the caprock of the 2nd Wall Creek Reservoir. Therefore, it is important to know the stratigraphy of the frontier formation which is presented as follows.

The Frontier formation is an important oil-bearing zone in Wyoming. It has a series of sandstones, shales, sandy shales and several bentonite beds with a minimum amount of limestone. The total sandstone content varies from one place to another; being maximum (75-120 m) at the Teapot Dome Field (Powder River-Natrona area) (18).

The studies of Towse (1954) (18) divided the Frontier formation into four members: 1st, 2nd, and 3rd Wall Creek, and the Lower shale. Stratigraphic cross-sections were made to determine correlation criteria. For this purpose, rotary cuttings and electric logs of available wells were analyzed.

Figure 9 shows the cross section from Casper to Sage Spring Creek presented by Towse (1954) to exemplify the different units and lithology expected to be found in the Teapot Dome Field.

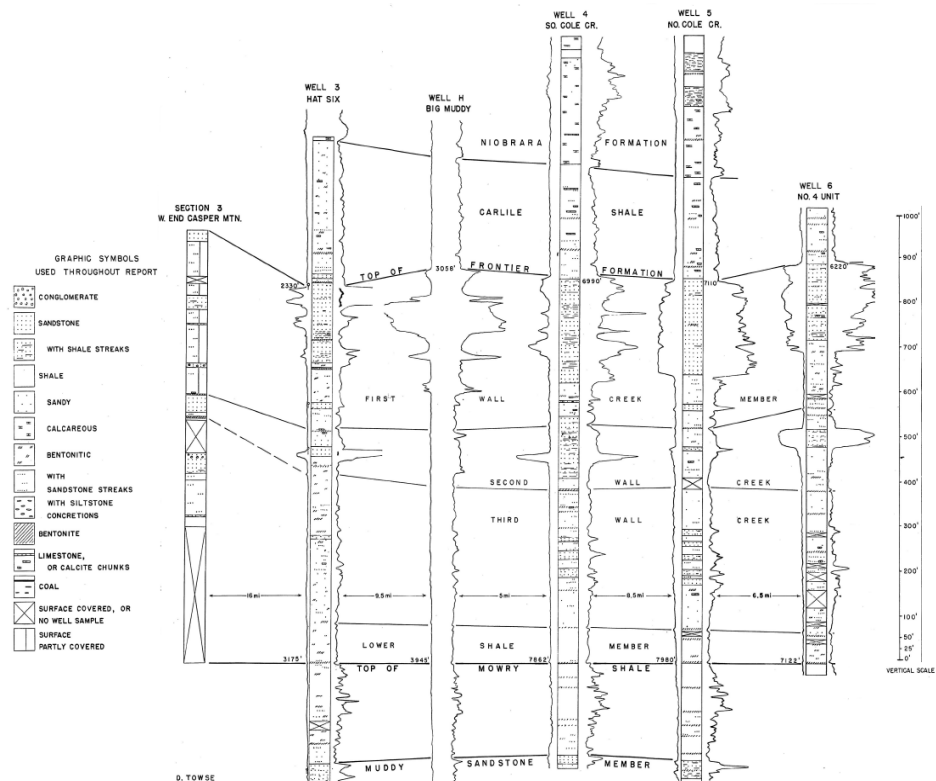


Figure 9 – Frontier formation cross section (18)

3.3. Lithology

Several studies show that the sandstones of the Frontier are relatively quartzose or cherty with minor amounts of other minerals (feldspar, biotite, and muscovite). The sand grains in the rock can be rounded or angular; being clay the cementing material. Concerning texture, the sandstones vary from fine to coarse and conglomeratic (18). Merewether (1917) (19) describes the sandstones in this formation as light-medium to brownish gray with grains that vary from the base to the top. In the base, the grains are very fine grained and horizontally bedded, and in the top, they are fine grained and crossbedded.

Towse (1954), describes the shales presented in the Frontier formation as soft, gray and sandy; being slightly calcareous or bentonitic in some parts of the formation. He also states that in the top of the formation, the sandy shales are thin bedded and better cemented than the ones in the lower shale unit. There are several beds of bentonite that contains siltstone concentrations, where the lowest part of the shale unit is the most bentonitic of the formation (18).

As follows it is described the lithological characteristics of the different units in the Frontier formation found by various authors (18) (19) (20).

The sand of the 1st Wall Creek is fine grained with diameters between 0.10 to 0.13 [mm]. The overall sorting is fair with coefficients between 1.2 to 1.4. There are important amounts of pink and crystalline quartz in the sand unit. The lower part contains limestone concentrations; being bentonite the bottom boundary of the member.

The 2nd Wall Creek in the Frontier Formation is the second largest hydrocarbon bearing zone at the Teapot Dome Field even though it is relatively thin (20 m). The sandstones are medium grained with average diameters of 0.09 to 0.22 mm (18). The sorting is usually poor with coefficients between 1.20 and 1.40. This sandstone unit is massively bedded, fairly quartzose and its composition is homogeneous (20). Besides, the sandstones are less shaley than in the 3rd Wall Creek. The overlying cap rock of this member is 75 m thick. It is considered as the primary regional seal within the Power River Basin; trapping more than 57 million oil barrels and 45 billion of standard cubic feet (scf) of natural gas at the Teapot Dome (3). It has similar characteristics to the Brent Group in the North Sea regarding connectivity, reservoir geometry and relative permeability (19). Since there is not a clear description for lithology and



mineralogy for the caprock of the 2nd Wall Creek due to the lack of information, it will be determined by using a four-point mineral model in the subsequent chapters.

The 3rd Wall Creek member is separated from the 2nd Wall Creek based on their sandstone mineralogy, where the top boundary has been placed at a bentonite and gypsum bed. It comprises a series of sandy shales and sandstones with few conglomerates.



CHAPTER IV. PETROPHYSICAL EVALUATION

The investigation of petrophysical parameters such as the volume of shale, porosity and water saturation is necessary in order to characterize the caprock of the 2nd Wall Creek reservoir. In this chapter, a comprehensive petrophysical approach was carried out over the zone of interest. Well logging analyses of the given wells were used to determine the petrophysical parameters by using Techlog© (wellbore platform).

4.1. Data Analysis

The available data for the 2nd Wall Creek reservoir consists of 18 wells. Most of the wells have the traditional well log data, caliper (CALR), gamma ray (GR), bulk density (RHOB), compressional slowness (DT), deep resistivity (RDEP), shallow resistivity (RFOC), medium resistivity (RILM), neutron porosity (NPHI) and photoelectric absorption (PE), which can be used in the petrophysical analysis. Those well logs passed through a quality check before any calculation in Techlog©. The primary logs used for the petrophysical analysis in this project are presented in *Table 2*. Not all the wells have the basic logs required for the study such as the well 12-AX-33. The

Table 2 – Well logs summary

Index	Well	DEPT	GR	RHOB	DT	RDEP	NPHI	PE
1	11-DX-26	X	X	X	X	X	X	
2	12-AX-33	X	X	X	X	X		
3	14-LX-28	X	X	X	X	X		
4	28-AX-27	X	X	X	X	X		
5	28-AX-34	X	X	X	X	X		
6	34-TX-3	X	X	X	X	X		
7	36-11-SX-2	X	X		X	X		
8	36-MX-10	X	X	X	X	X	X	
9	41-2-X-3	X	X	X	X	X		X
10	41-AX-3	X	X	X	X	X	X	
11	53-LX-3	X	X	X	X	X	X	
12	62-TpX-10	X	X	X	X	X		
13	64-JX-15	X	X	X	X	X		



Index	Well	DEPT	GR	RHOB	DT	RDEP	NPHI	PE
14	67-1-TpX-10	X	X	X	X	X	X	X
15	71-1-X-4	X	X		X	X		
16	75-AX-28	X	X	X	X	X	X	
17	88-AX-28	X	X		X	X	X	
18	88-DX-3	X	X	X	X	X	X	
	log Count	18	18	15	18	18	8	2

Considering that the Frontier formation properties do not change severely from one site to another within the Teapot Dome and the wells are relatively close to each other, the missing logs (bulk density (RHOB), neutron porosity (NPHI), photoelectric absorption (PE)) can be interpolated from the existed well logs. This procedure was done through well prediction tool in Techlog©.

Figure 10 shows the position of the wells in a field map. This map is based on the longitude and latitude of each well. It can be observed that the majority of the wells are concentrated in the center to the north of the study area while there is only one well in the southern part of the field.

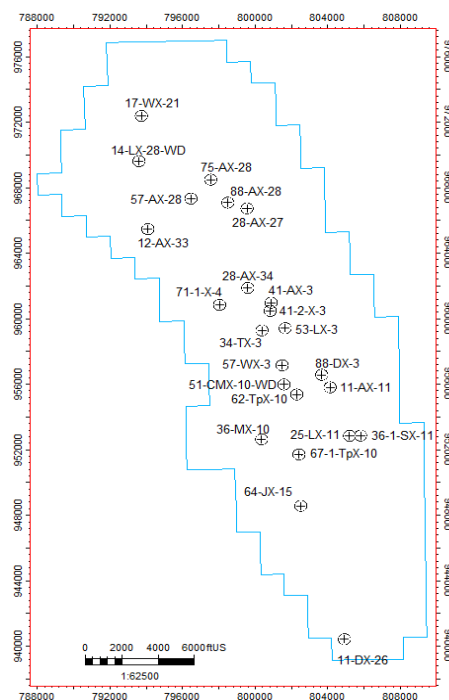


Figure 10 – Location of the wells in the Teapot Dome field

4.2. Well Correlation Study

Well correlation is a process where two or more geological formations spatially separated are equated. The main correlation methods are marker bed, pattern matching, and slice techniques. The marker bed is a reliable method where series of beds can be used as a marker although the lithology or origins are unknown. The pattern matching involves the recognition of distinctive log patterns that are correlated based on log shapes. It indicates lateral facies, thickness changes; making it useful for facies correlations. The slice technique, on the other hand, subdivides the interval arbitrarily which gives wrong relationship. It is only used when the other methods do not yield results (21).

The well correlation study in this project is done by using a market bed technique where gamma ray log indicates different marker beds within the 2nd Wall Creek. This is because every well without exception have a gamma ray log. The gamma ray log is used because it gives an indication of lithology. The amount of clay, minerals, carbonate and organic matter, vary slightly at the same stratigraphic level but changes abruptly through time which is ideal for well correlation because the gamma ray value is constant laterally but changes vertically (22).

The well correlation in the 2nd Wall Creek formation was done along with all the wells which can be found in APPENDIX 2. This correlation provides detailed information on the lateral extent of the units in the formation which is important both for the petrophysical analysis and caprock integrity assessment. It can be observed in *Figure 11*, the correlation of 5 wells from left to right (11-DX-26, 12-AX-33, 14-LX-28, 28-AX-27, 28-AX-34). In this example, there are two main units in the formation which are represented in blue (caprock) and yellow (reservoir). The 2nd Wall Creek formation in the first well (11-DX-26) is located approximately 221 m below the second well (12-AX-33). The position of the formation in the other wells does not change as it can be observed in *Figure 11*.



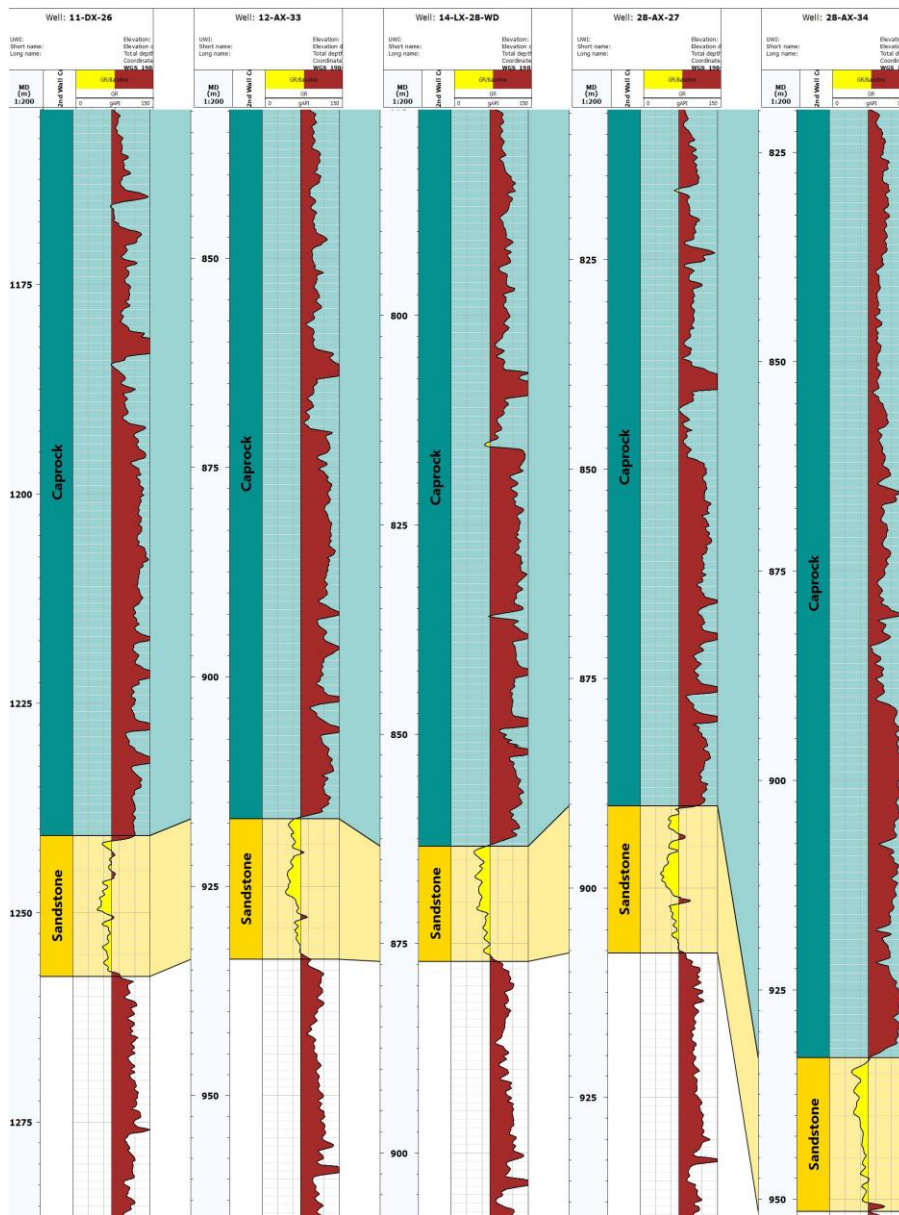


Figure 11 – Well correlation in the 2nd Wall Creek formation

Table 3 gives a summary of the thickness of both caprock and reservoir for each well. The average thickness of the caprock is 85 m and 19 m for the reservoir. Those values are similar to the ones showed in the stratigraphic column of the Teapot Dome obtained from the Rocky Mountain Oilfield Testing Center (RMOTC). The minimum thickness value for the caprock in the 2nd Wall Creek reservoir is 68.66 m and the

maximum 114.01 m. Even though the minimum thickness of the caprock is 67.48 m, the 2nd Wall Creek reservoir is still acceptable for CO₂ geological storage.

Table 3 – Thickness summary for the 2nd Wall Creek formation

Well	Caprock	Reservoir
	[m]	[m]
11-DX-26	86.78	16.81
12-AX-33	84.80	16.76
14-LX-28	88.06	13.77
28-AX-27	83.23	17.57
28-AX-34	113.32	18.35
34-TX-3	80.44	19.10
36-11-SX-2	73.20	14.28
36-MX-10	75.06	16.56
41-2-X-3	112.53	19.56
41-AX-3	74.61	22.14
53-LX-3	114.01	18.34
62-TpX-10	67.48	22.16
64-JX-15	70.30	19.35
67-1-TpX-10	68.66	20.99
71-1-X-4	104.73	20.84
75-AX-28	71.45	18.34
88-AX-28	81.23	18.36
88-DX-3	81.23	20.99
Average	85	19
Min value	67.48	13.77
Max value	114.01	22.16

4.3. Petrophysical Analysis

Qualitative and quantitative analyses were carried out over the caprock of the 2nd Wall Creek formation to describe its petrophysical properties. The interpretation was made through analyses of the well log data by a probabilistic approach to determine the volume of shale, porosity, fluid saturation, and lithology. For a better understanding of those parameters, several histograms are presented for each case.



The input data for the petrophysical analysis were obtained from the available logs for each well described in *Table 2*.

4.3.1. Volume of shale

The volume of shale expresses the shale percentage contained in the formation. It is useful to determine if there is a different lithology than shale in caprock. Gamma ray log is used for the computation of the shale volume because the shale is more radioactive than the sandstone or carbonates. The calculation is based on the *Eq. 2* which is implemented in Techlog©.

$$V_{sh} = \frac{GR - GR_{min}}{GR_{max} - GR_{min}} \quad \text{Eq. 2}$$

Where GR, is the value read at particular depth; GR_{max} is the value read in 100% shale, and GR_{min} corresponds to 100% matrix rock (22). In *Figure 12*, GR_{min} represents GR_{Matrix} , and GR_{max} is GR_{Shale} . For the well 11-DX-26, a baseline of 75 API was chosen for sand, and a baseline of 105 API was chosen for the shale. The same procedure was repeated for the 18 wells.

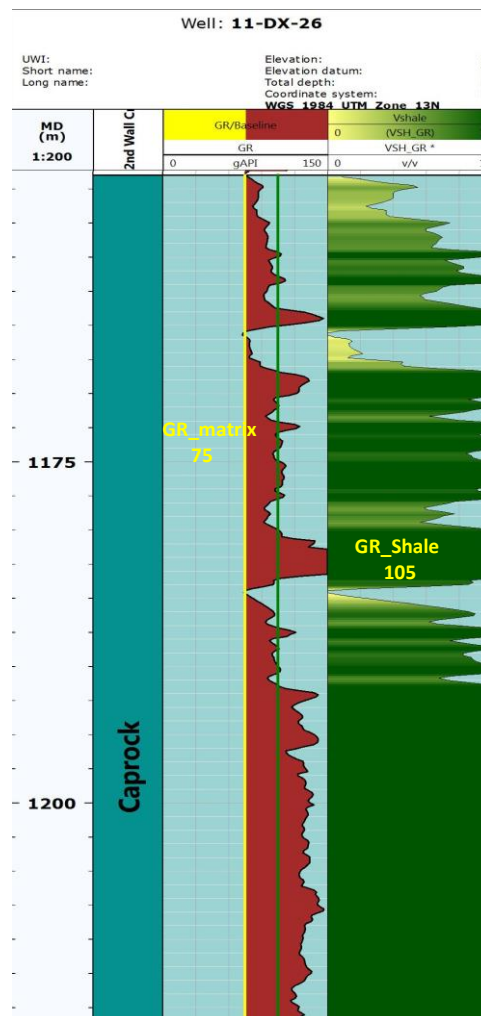


Figure 12 – Determination of GR_Matrix and GR_Shale

The computation of the volume of shale for 5 wells from left to right (28-AX-27, 36-MX-10, 67-1-TpX-10, 11-DX-26, 12-AX-33) is presented in *Figure 13*. This is an exemplification of the pattern found across the wells in 2nd Wall Creek reservoir. The shale is represented with the green color, and the yellow color shows other lithology. It can be noticed that the volume of shale is bigger at the caprock bottom than at the top. This result is similar to the one presented by Towse (1954). He described the shale unit in the 2nd Wall Creek reservoir as sandy shale with sandstone streaks (18). The distribution of volume of shale for the 18 wells can be found in APPENDIX 3

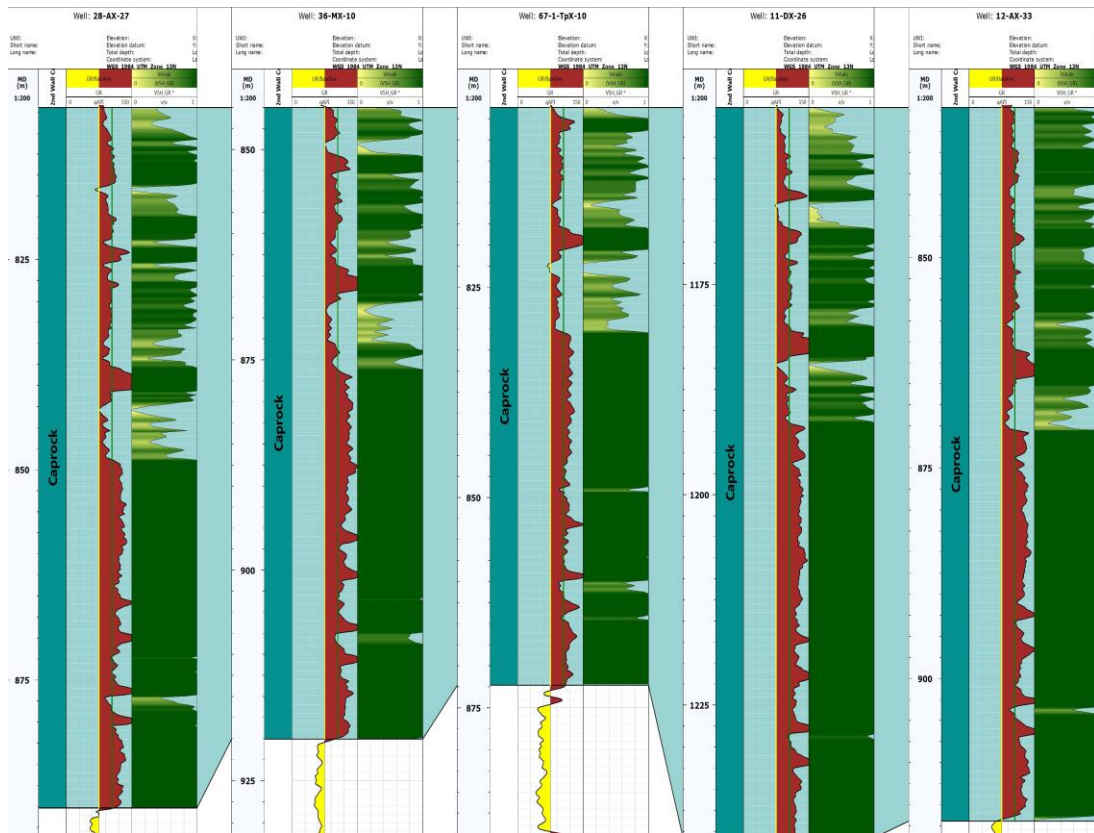
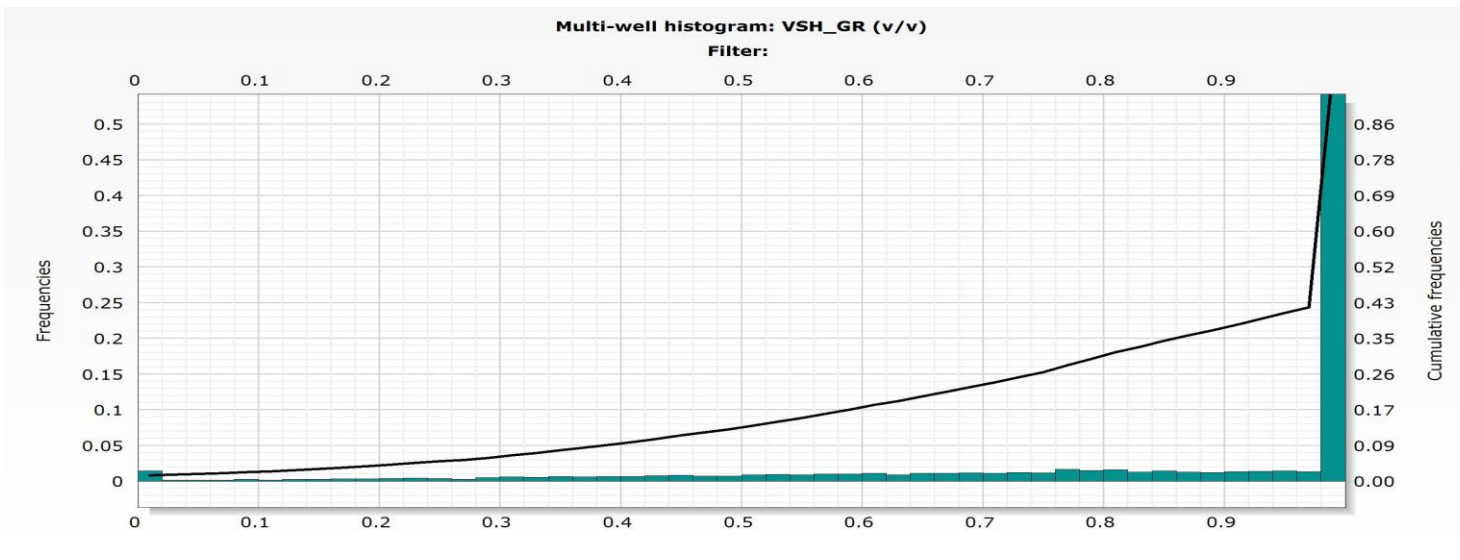


Figure 13 – Computation of shale volume (V_{sh}) for the wells: 28-AX-27, 36-MX-10, 67-1-TpX-10, 11-DX-26, 12-AX-33

Figure 14 shows a histogram of the volume of shale with an accumulative frequencies line for the 18 wells that penetrates the 2nd Wall Creek reservoir. It can be observed that the histogram is not normally distributed. The minimum volume of shale is 0 v/v; corresponding to sandy streak and the maximum is 1 v/v which represents pure shale. The average value for the 18 wells in the zone of interest is 0.8388 v/v. This means that 84% of the caprock is shale and the 16% is another lithology.



Well:

11-DX-26: [9.7536 - 1559.36]
 28-AX-27: [0 - 1265.53]
 36-11-SX-2: [6.7056 - 1288.85]
 41-AX-3: [9.144 - 1736.75]
 64-JX-15: [0.1524 - 1297.23]
 75-AX-28: [3.048 - 1221.64]

12-AX-33: [0.1524 - 1258.21]
 28-AX-34: [18.7452 - 1286.26]
 36-MX-10: [191.719 - 1246.63]
 53-LX-3: [6.096 - 1258.21]
 67-1-TpX-10: [17.6784 - 1725.78]
 88-AX-28: [6.096 - 1251.2]

14-LX-28-WD: [0 - 1219.2]
 34-TX-3: [0.1524 - 1264.62]
 41-2-X-3: [0 - 1763.57]
 62-TpX-10: [1.524 - 1708.1]
 71-1-X-4: [17.3736 - 1773.02]
 88-DX-3: [8.9916 - 1244.19]

Statistics:

Mode: 0.99
 Arithmetic mean: 0.838802
 Average deviation: 0.200151
 Number of missing values: 8
 Minimum value: 0
 Skewness: -1.60321

Median: 1
 Possible values: 10032
 Standard deviation: 0.25278
 Variance: 0.0638976
 Maximum value: 1
 Kurtosis: 1.66742

Zonation: 2nd Wall Creek

Figure 14 – Shale Volume histogram for all the wells



4.3.2. Porosity Calculation

The porosity represents the fraction of the rock filled with fluids. It can be determined from laboratory measurements or well logs; being neutron porosity (NPHI), bulk density (RHOB) and sonic (DT) the logs used for the calculation. There are two types of porosity: total and effective. The total porosity is the ratio of the total pore volume to the bulk volume. On the other hand, the effective porosity is the total porosity minus the fraction of the pore volume occupied by shale or clay. In the present study, both total and effective porosity are analyzed. Neutron and bulk density log combination is used for the calculation.

Porosity calculation using neutron-density log combination

The neutron log (NPHI) measures the hydrogen index and therefore responds to the volume of water that fills the pore space. It gives an indication of porosity which is display directly in the log. Porosity can also be found by using the bulk density log (RHOB). The equation that links together porosity and density is:

$$\phi_d = \frac{\rho_{matrix} - \rho_b}{\rho_{matrix} - \rho_{fluid}} \quad \text{Eq. 3}$$

Where ϕ_d is the total porosity in the caprock, the ρ_{matrix} , g/cm^3 , is the matrix density in the formation and ρ_{fluid} , g/cm^3 , is the fluid density in the wellbore and ρ_b , g/cm^3 is the value read in the log. The input parameters in Techlog© are ρ_{matrix} and ρ_{fluid} .

The combination of both neutron-density logs is used to determine the porosity without being affected by lithology. In this method, the values of apparent neutron and density porosities are averaged. In this way, the effects of dolomite and quartz tend to cancel out. It is also employed a square root to eliminate the effects of residual gas in the flushed zone (23). The total porosity is estimated by the Eq. 4 where ϕ_n and ϕ_d are the neutron and density porosities, respectively. This equation is implemented in Techlog©.

$$\phi = \sqrt{\frac{\phi_n^2 + \phi_d^2}{2}} \quad \text{Eq. 4}$$



Figure 15 shows the total and effective porosity results for 3 wells from left to right (28-AX-27, 36-MX-10, 67-1-TpX-10). The plot also includes the neutron (blue line) and density logs (red line). As it can be noticed, the effective porosity (white color) is lower than the total porosity (beige color). This occurs because the pore space can be occupied by particles and water bound. The porosity pattern from one well to another change because the formation is not isotropic and the rock properties vary vertically and horizontally. The complete porosity pattern is found in APPENDIX 4.

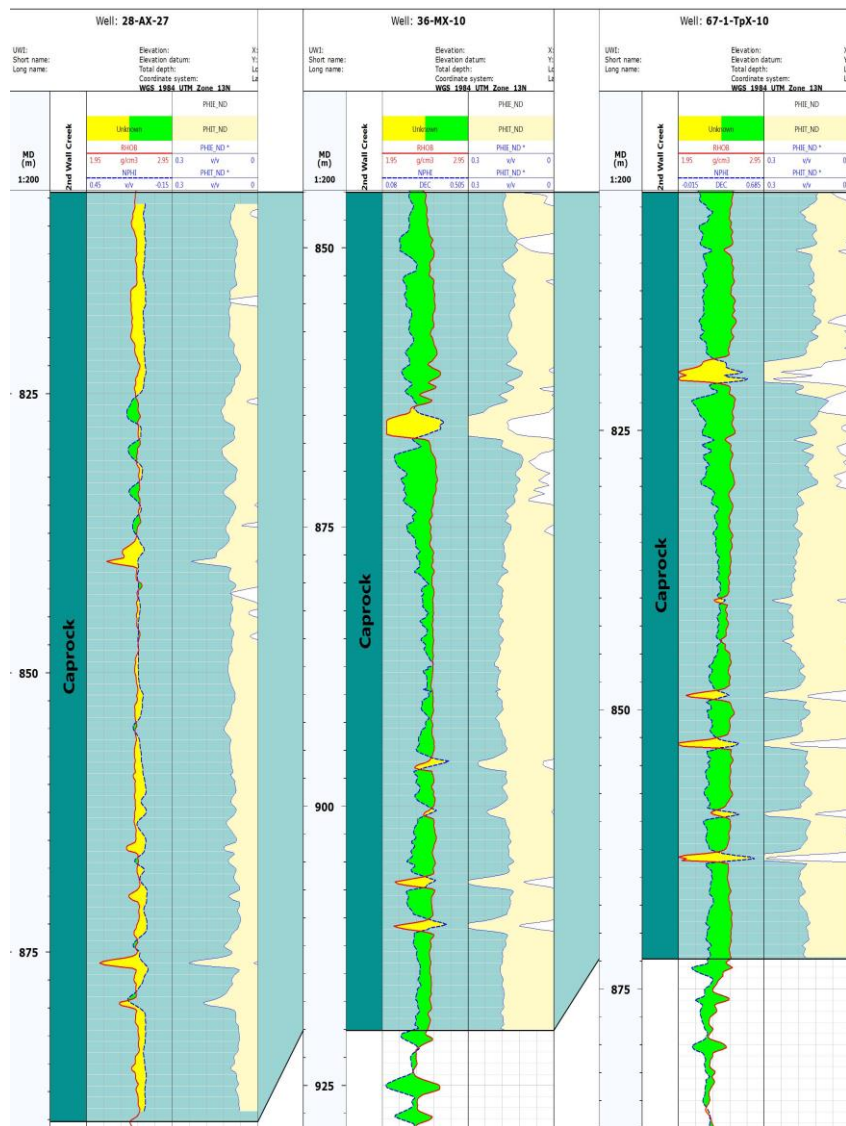
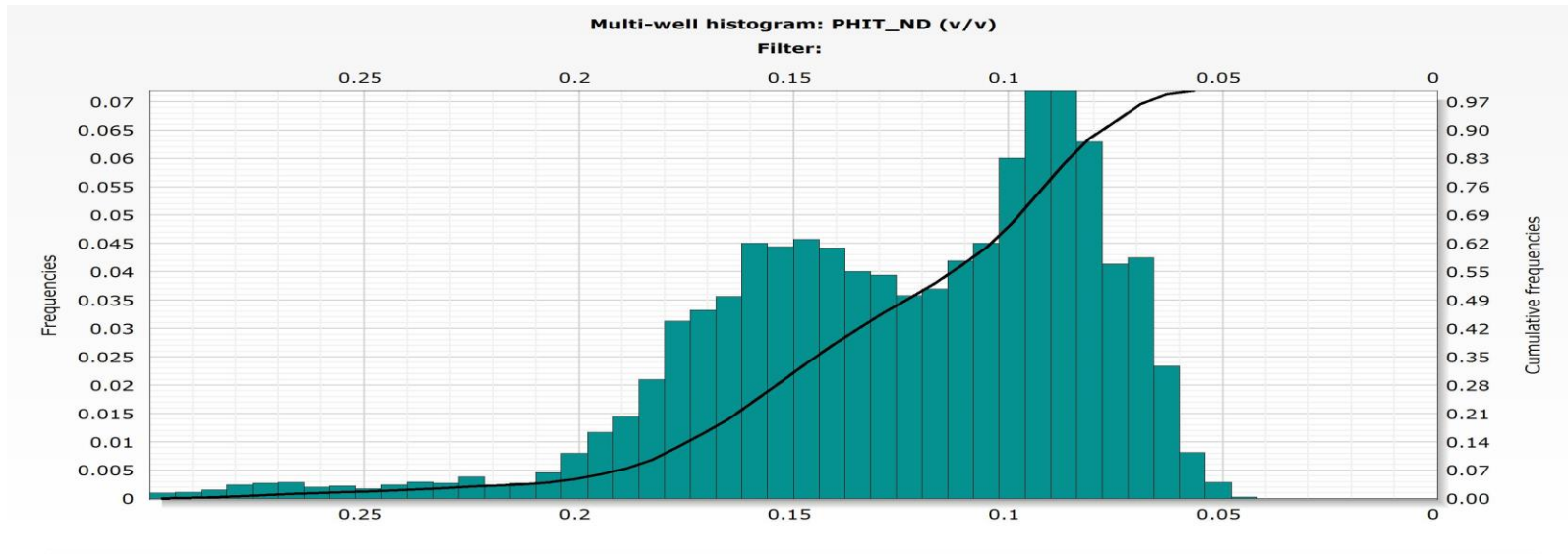


Figure 15 – Calculation of porosity by neutron-density logs for the wells: 28-AX-27, 36-MX-10, 67-1-TpX-10

The obtained results from the total and effective porosity are presented in the *Figure 16 Figure 17*. The total porosity histogram is moderately asymmetrical with a kurtosis of 4.7 and a skewness of 1.51. The peak of the data is between 0.085 and 0.095 v/v; meaning that the total porosity values are mostly concentrated in this range. Also, it can be seen that the minimum value for the total porosity is 0.04612 v/v, the maximum is 0.5207 v/v, and the average is 0.1270 v/v.

The effective porosity histogram (*Figure 17*) corresponds to a matrix histogram plot with cumulative frequency. The effective porosity value ranges between 0-0.10 v/v which is within the range suggested by the literature (22). As it can be noticed, the histograms in most of the wells are left skew, and the peak of the data is concentrated in 0 v/v. Consequently, the effective porosity in the caprock is negligible.



Well:

11-DX-26: [9.7536 - 1559.36]
 28-AX-27: [0 - 1265.53]
 36-11-SX-2: [6.7056 - 1288.85]
 41-AX-3: [9.144 - 1736.75]
 64-JX-15: [0.1524 - 1297.23]
 75-AX-28: [3.048 - 1221.64]

12-AX-33: [0.1524 - 1258.21]
 28-AX-34: [18.7452 - 1286.26]
 36-MX-10: [191.719 - 1246.63]
 53-LX-3: [6.096 - 1258.21]
 67-1-TpX-10: [17.6784 - 1725.78]
 88-AX-28: [6.096 - 1251.2]

14-LX-28-WD: [0 - 1219.2]
 34-TX-3: [0.1524 - 1264.62]
 41-2-X-3: [0 - 1763.57]
 62-TpX-10: [1.524 - 1708.1]
 71-1-X-4: [17.3736 - 1773.02]
 88-DX-3: [8.9916 - 1244.19]

Statistics:

Mode: -9999
 Arithmetic mean: 0.127036
 Average deviation: 0.0377006
 Number of missing values: 140
 Minimum value: 0.0461182
 Skewness: 1.51238

Median: 0.119009
 Possible values: 10032
 Standard deviation: 0.0486412
 Variance: 0.00236596
 Maximum value: 0.520712
 Kurtosis: 4.74477

Zonation: 2nd Wall Creek

Figure 16 – Histogram of total porosity



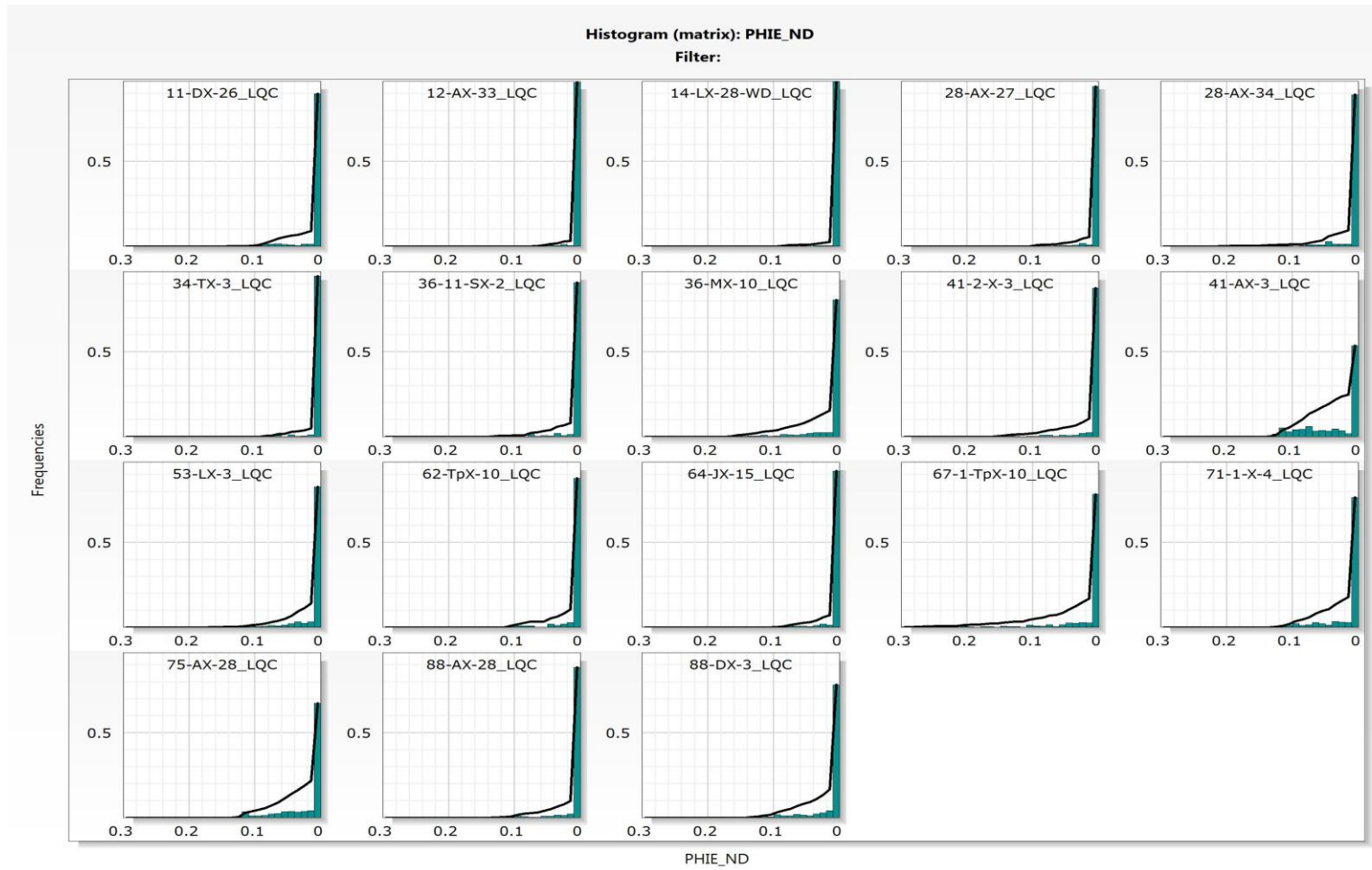


Figure 17 – Matrix histogram for effective porosity



4.3.3. Fluid Saturation

The water saturation is calculated through Archie's equation (Eq. 5) which is part of the typical petrophysical workflow in Techlog®. It is important to highlight that this calculation was performed since it is an input for the lithology estimation.

$$S_w = \left(\frac{a R_w}{\phi^m R_t} \right)^n \quad \text{Eq. 5}$$

Where S_w is the water saturation, a is the tortuosity factor in the zone of interest, R_w is the formation water resistivity, ϕ is porosity, m is the cementation factor, R_t is the formation resistivity, and n is the saturation exponent.

The calculation of S_w requires as an input data, the formation resistivity which corresponds to deep resistivity log and the porosity that was calculated previously. The parameters of cementation factor, saturation exponent and tortuosity were set as default; being the values 2, 2, 1 respectively. In order to get meaningful results, the value of R_w was set between 0.14 and 0.18 ohm.m.

Figure 18 shows the distribution of the water saturation for 3 wells from left to right (36-MX-10, 67-1-TpX-10, 11-DX-26,) along with the resistivity and total porosity logs. The reading values from the resistivity log (blue dashed line) are in the range from 1 to 5 ohm.m, which corresponds to a conductive fluid. As a consequence, the bearing fluid in the pore space is water. The calculated water saturation log, displayed in blue, shows that the value of S_w is more than 80 v/v. This result was expected because the shale in the caprock does not contain any hydrocarbons. APPENDIX 5 shows the distribution of water saturation across the 18 wells.

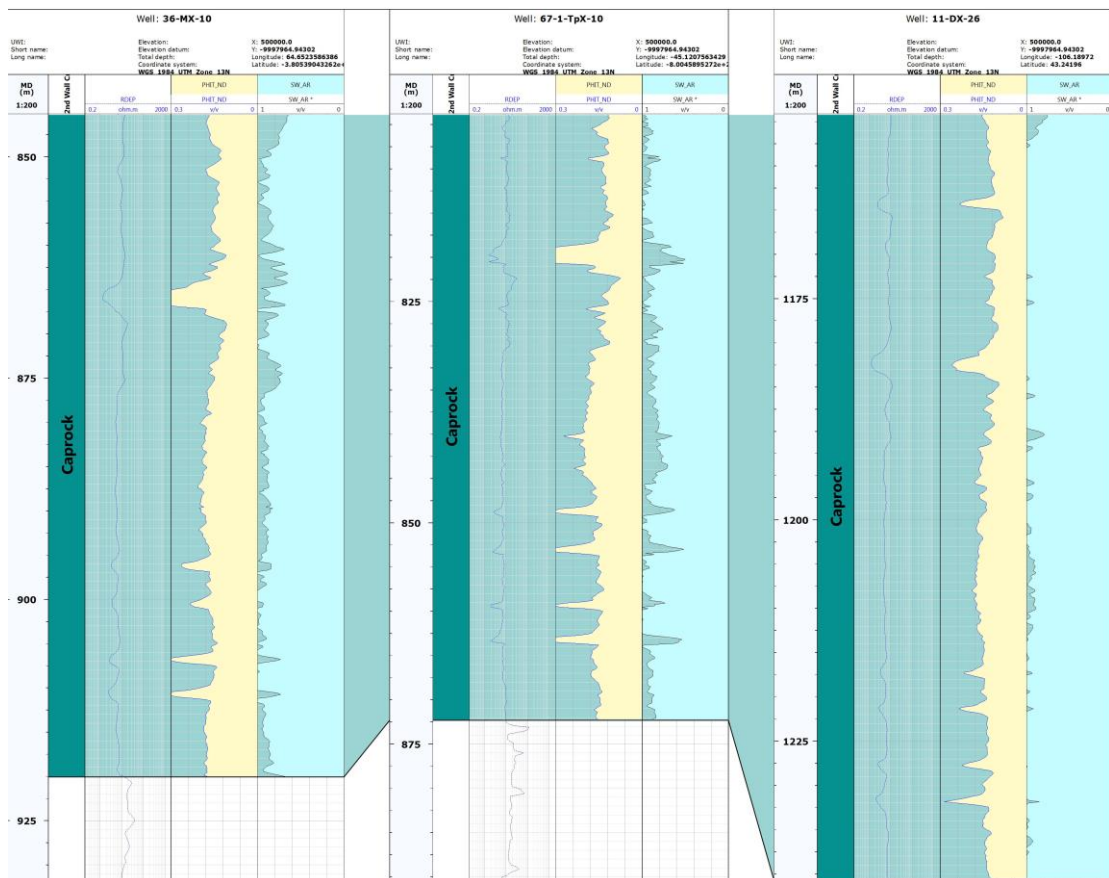


Figure 18 – Distribution of water saturation across the wells in the caprock

4.3.4. Lithology estimation

The well log data can be used to infer or determine the lithology, mainly speaking the mineralogy. Cross-plots, two-dimensional representations of the log response of different mineralogies, are the primary tool to evaluate the mineralogical composition. The crossplots: RH_{maa} (apparent grain density) vs. U_{maa} (matrix apparent volumetric photoelectric factor) and RH_{maa} vs. DT_{maa} (matrix apparent compressional slowness) are used in the present project since they predict complex lithologies. It was observed in the volume of shale calculation that the caprock is mainly composed of shale but also includes another type of lithology. Therefore, the aim of this section is to estimate the mineral content of that percentage of the caprock that is not shale.

The matrix apparent volumetric photoelectric factor (U_{maa}) is computed from photoelectric adsorption (P_e) and porosity by Eq. 6 (24).

$$U_{maa} = \frac{P_e \rho_e - \phi U_f}{1 - \phi} \quad \text{Eq. 6}$$

Where ϕ is the apparent porosity determined by the well logs, U_f is the apparent fluid volumetric cross section and ρ_e is the electron density which is calculated from Eq. 7 in which ρ_b is the bulk density

$$\rho_e = \frac{\rho_b + 0.1883}{1.0704} \quad \text{Eq. 7}$$

The apparent grain density (RH_{maa}) is determined by the Eq. 8 (24).

$$RH_{maa} = \frac{\rho_b - \phi \rho_f}{1 - \phi} \quad \text{Eq. 8}$$

Where ρ_f is the density of the fluid that is 1 considering that water is the bearing fluid in the pore space.

The matrix apparent compressional slowness (DT_{maa}) is calculated by combining neutron porosity and sonic log (25). The Eq. 9 is used to determine the value of DT_{maa} .

$$DT_{maa} = \frac{\Delta t - \phi \Delta t_f}{1 - \phi} \quad \text{Eq. 9}$$

Where Δt is the wave transit time change, Δt_f is the pore fluid transit time change, and ϕ is the porosity.

The above calculations were done by the lithology computation utility in Techlog©; being the input data the following logs: bulk density (RHOB), compressional slowness (DT) and photoelectric factor (PE), effective porosity (PHIE_ND), shale volume (V_{SH}) and water saturation (S_w).

Figure 19 shows the minerals on a RH_{maa} and U_{maa} cross-plot for the 18 wells that penetrated the 2nd Wall Creek reservoir. The end-member minerals are linked to each other by straight lines; defining bounding triangles. The four end minerals are quartz, dolomite, calcite, and anhydrite. Other minerals such as kaolinite, illite, barite,



feldspar are also shown in the cross-plot. As can be noticed, the data points are concentrated in the quartz and feldspar zone, meaning that they are the main constituent minerals for the non-shaly part of the caprock. Notice that some points are shifted toward the dolomite and calcite region indicating the presence of calcareous minerals. This is due to the presence of some streak in the shale unit.

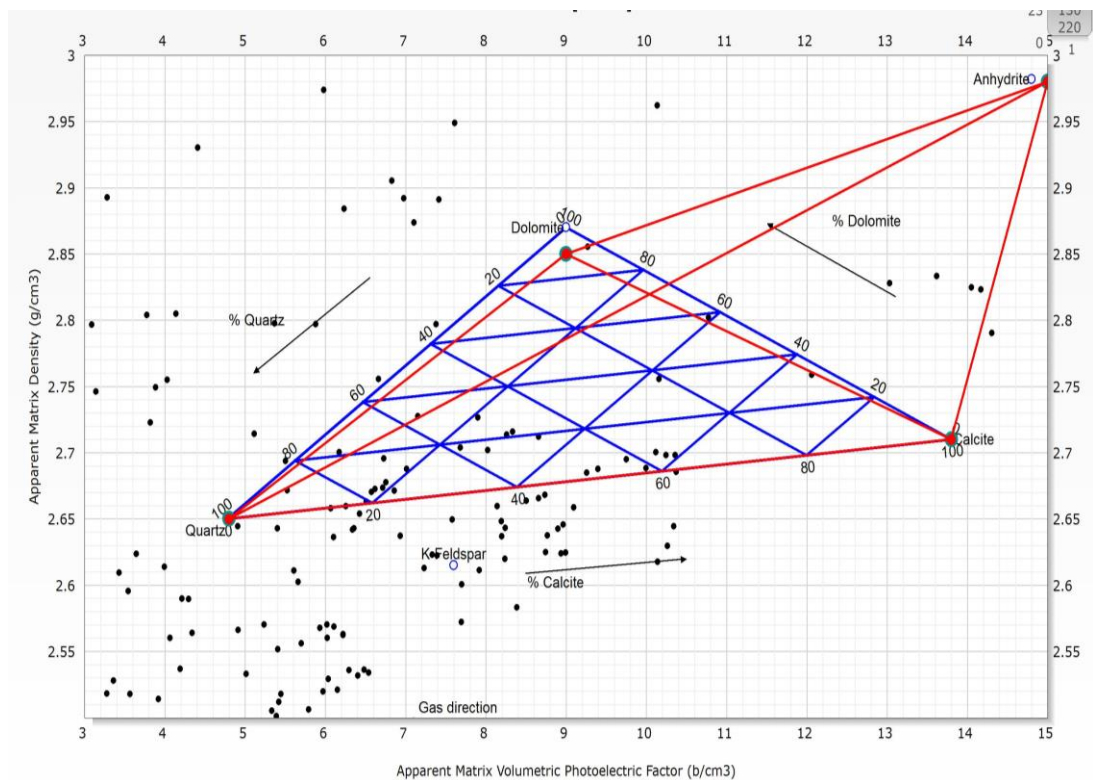


Figure 19 -Cross-plot RHoma vs. Umaa for mineralogy identification

Figure 20 shows the crossplot Rhomma vs. Dtmaa. It can be observed that the data points move to the quartz zone. This corroborates the mineral content obtained from the previous crossplot (Rhomma vs. Umaa).

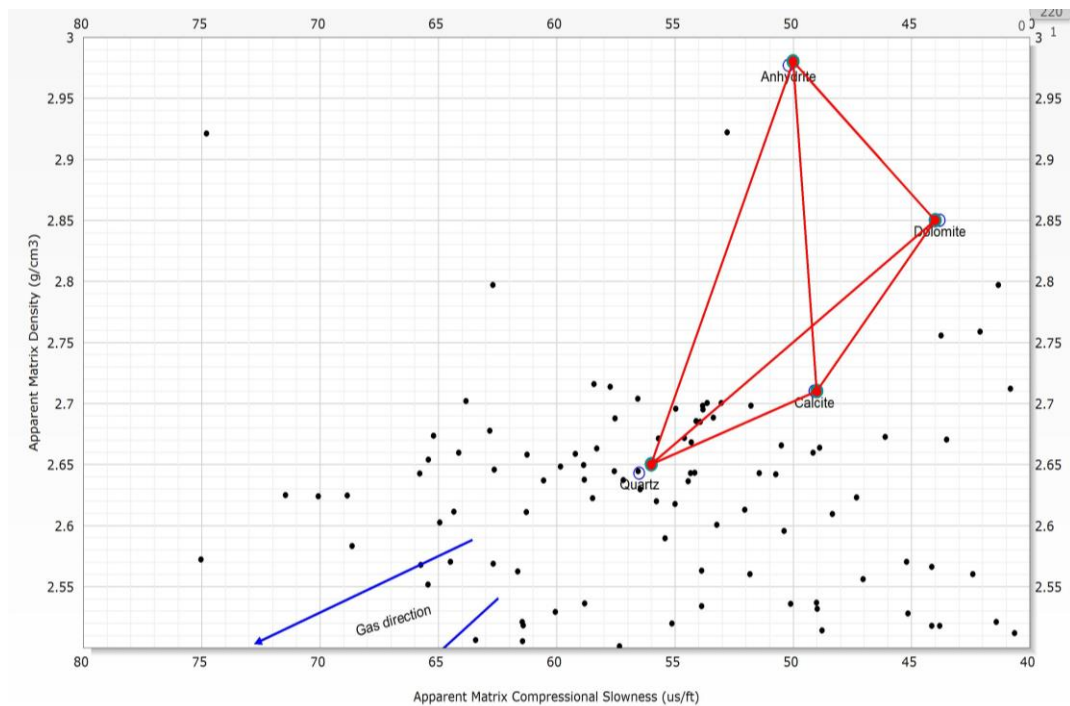


Figure 20 -Cross-plot RHomaa vs. DTmaa for mineralogy identification

A better illustration of the mineral content of the caprock is found in *Figure 21* which is the lithology log for the well 67-1-TpX-10. In this log is displayed the volume of shale (V_{SH}), quartz (V_{QTZ}), clay (V_{CLC}), dolomite (V_{DOL}) and anhydrite (V_{ANH}). It can be noticed that the caprock is mainly composed of shale which represents the 84% of the total mineral content. The remaining 16% is consists of the other minerals. The volume of dolomite for this well is higher than the other minerals. In order of importance, the log shows that the unit has quartz, calcite, and anhydrite. The mineralogy log for the 18 wells is found in APPENDIX 6.

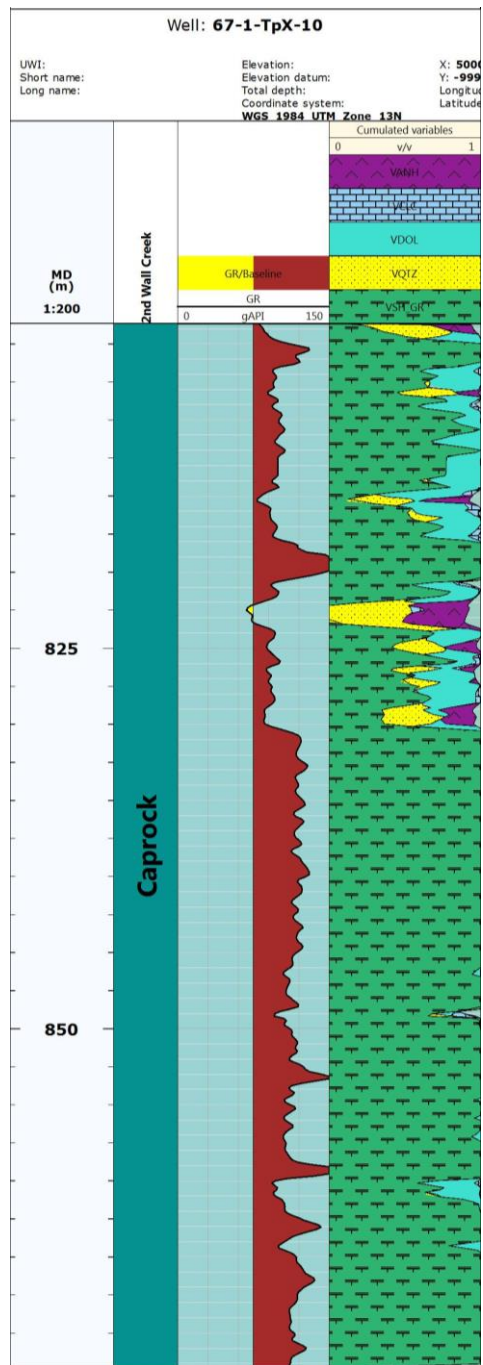


Figure 21 - Mineralogy log for well 67-1-TpX-1



CHAPTER V. GEOPHYSICS

The geophysics allows linking geologic properties (porosity, volume of shale, water saturation and lithology) with seismic properties such as acoustic impedance and elastic modulus. This section covers an overview of the theory behind the main elastic constants and the basic principles applied to calculate those properties based on the well log data.

5.1. Overview

Poisson's ratio, Young's modulus, shear modulus and bulk modulus should be taken into account in order to characterize the caprock. These parameters can be determined in static conditions from compressional tests or in dynamic conditions from well log data. *Table 4* shows the basic equations used in the determination of those parameters.

Table 4 – Mechanical parameters

Stress	Strain	Poisson's ratio	Young's modulus	Shear modulus	Bulk modulus
$\sigma = F/A$	$\epsilon = \Delta L/L$	$\nu = \frac{\epsilon_{trans}}{\epsilon_{axial}}$	$E = \frac{\sigma}{\epsilon}$	$G = \frac{T}{\gamma}$	$K = \frac{\Delta P}{\Delta V/V_0}$
σ : Stress F: Force A: Area	ϵ : Strain ΔL : Longitudinal change L: Longitude	ν : Poison's ratio ϵ_{trans} : Transverse strain ϵ_{axial} : Axial strain	E: Young's modulus σ : Tensile stress ϵ : Extensional strain	T: Shear stress Y: Shear strain	ΔP : Pressure change ΔV : Volume change V_0 : Initial volume

In the present project, those parameters are determined by dynamic conditions because of available well logs dataset.

5.2. Acoustic properties

The Techlog® toolbox function computes the formation acoustic properties: compressional velocity (VP), acoustic impedance (AI) and compressional modulus (M). The inputs for this method are compressional slowness (DT) and bulk density (RHOB) which are part of the primary log data.

The compressional velocity (VP), expressed in m/s, is the propagation of compressional principal waves (P-waves) in the medium which is longitudinal for isotropic and homogeneous solids. As a consequence, the particles in the rock vibrate parallel to the travel direction of the wave (26). It can be calculated by using the compressional slowness log which is the travel time per feet ($\mu\text{s}/\text{ft}$). The Eq. 10 shows the conversion between velocity and compressional slowness (27). In the equation, DT is the compressional slowness in microseconds per foot.

$$VP = \frac{10^6}{DT} \quad \text{Eq. 10}$$

The acoustic impedance (AI) is defined as the opposition that a rock presents to the wave propagation. It is computed as the product of the compressional velocity (VP) and the bulk density (ρ_b) which is expressed in MPa.s/m (Eq. 11) (27).

$$AI = (\rho_b)(VP) \quad \text{Eq. 11}$$

Compressional modulus (M) also called P-wave modulus, or longitudinal modulus is one of the elastic modules which is expressed in acoustic terms (Eq. 12). The unit of this modulus is GPa (27).

$$M = (\rho_b)(VP^2) \quad \text{Eq. 12}$$

Figure 22 shows the elastic properties along with the bulk density and compressional slowness logs for the well 67-1-TpX-10. The compressional slowness for the shale in the caprock is proximately 70 to 120 $\mu\text{s}/\text{ft}$. Consequently, the range of compressional velocity is low because it takes more time for the wave to travel a certain distance. As can be observed in the compressional velocity log (magenta color), the velocity varies between 2620 m/s and 4471 m/s which is in accordance with the values shown in the literature for this type of lithology (1600 – 5000 m/s) (22). The acoustic impedance



and compressional modulus are directly proportional to the bulk density and compressional velocity. It is noticed in the log that low values for acoustic impedance and compressional modulus correspond to low bulk density values. If the density is low, the pore space is higher, and therefore the sonic wave moves faster through the medium. APPENDIX 7 contains the computed elastic properties for the 18 wells.

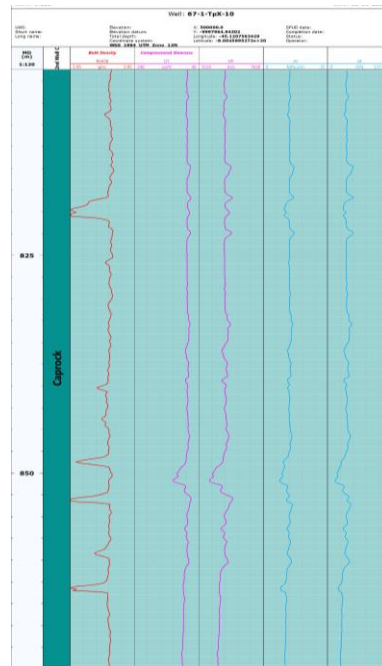


Figure 22 - Acoustic properties for well 67-1-TpX-10

The shear velocity (V_S), expressed in Km/s, is the propagation of secondary waves (S-waves) in the medium. In this case, the particles oscillate perpendicular to the travel direction of the wave (26).

The shear velocity is computed in Techlog© through the lithology dependent Greenberg- Castagna method. It gives empirical relations to estimate the shear velocity based on the compressional velocity in multiminerall, saturated brine rocks where the composed minerals are calcite, dolomite, quartz, and shale. The shear velocity is computed by the following equation which is used in Techlog© (Eq. 13)

$$V_S = \frac{1}{2} \left\{ \left[\sum_{i=1}^L \frac{V f_i}{a_i V P^2 + b_i V P + c_i} \right]^{-1} + \sum_{i=1}^L V f_i (a_i V P^2 + b_i V P + c_i) \right\} \quad \text{Eq. 13}$$

5.3. Dynamic Elastic Properties

The elastic properties measure the tendency of a rock to deform non-permanently when the stress is applied. The elastic properties are: Poisson's ratio (PR), Young's modulus (E), bulk modulus (K) and shear modulus (G)

The Poisson's ratio (PR) is the relationship between the lateral strain to longitudinal strain related to the elasticity of the material (28). In consequence, the static Poisson's ratio (VPVS) can be calculated as the ratio between the compressional and shear velocities. The dynamic Poisson's ratio (PR) can be found with the compressional and shear velocities through the following equation (Eq. 14) in Techlog©.

$$PR = \frac{1}{2} \frac{(VP^2 - 2VS^2)}{(VP^2 - VS^2)} \quad \text{Eq. 14}$$

In *Figure 24* are displayed the output logs from VPVS and PR along with compressional (VP) and shear velocities (VS) for the well 67-1-TpX-10. It can be seen that the trend of both static and dynamic Poisson's ratio logs is similar to the compressional and shear velocities but with an opposite tendency. This is because the value of the compressional velocity is higher than the value of the shear velocity; giving as a result lower values for the Poisson's ratio. The range of the static Poisson's ratio has higher values than the dynamic Poisson's ratio. Schultz (1995) suggests that this occurs because in the dynamic properties the effect of the pore fluid is not taking into account and therefore the intrinsic static/dynamic differences are measured (29).

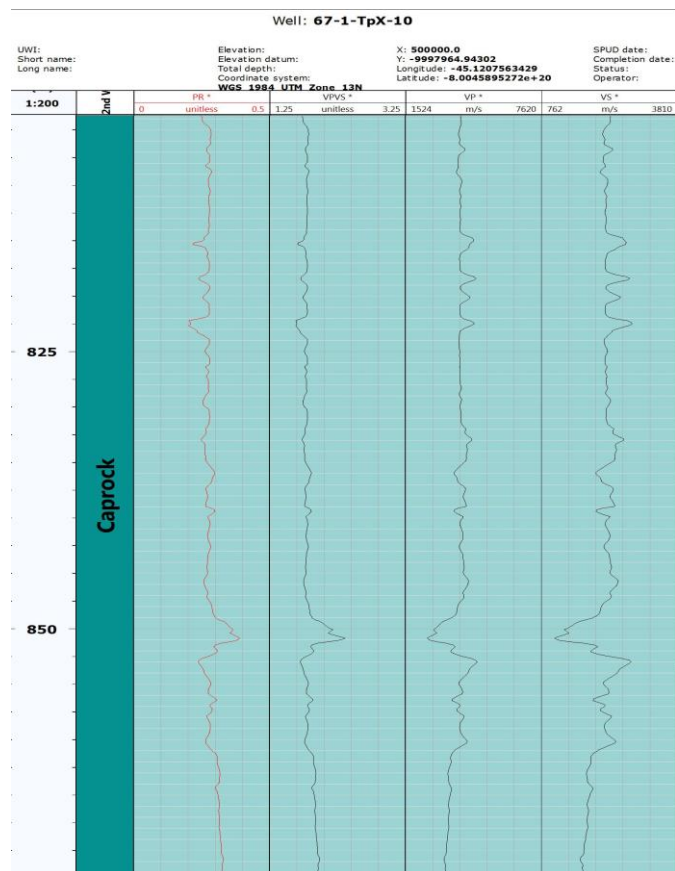


Figure 24 – Compressional to shear velocity ratio and dynamic Poison’s ratio for the well 67-1-TpX-10

The Young’s modulus is the ratio between the longitudinal stresses to the longitudinal strain of a material when there is no change in the orthogonal stress. The shear modulus also called modulus of rigidity is the ratio of shear stress to shear strain (28). Finally, the bulk modulus is the resistance of the material to isotropic volume change when there is an isometric compression.

The Dynamic elastic properties (Young’s modulus, shear modulus and bulk modulus) are calculated in Techlog© based on the Sonic Model in which the relationship between the sonic logs and the dynamic properties is considered.

The dynamic shear modulus (G_{DYN}), and bulk modulus (K_{DYN}) are computed in Techlog© by the following equations (Eq. 15 and Eq. 16) assuming a homogenous, isotropic and elastic formation.

$$G_{dyn} = (13474.45) \frac{\rho_b}{(\Delta t_{shear})^2} \quad \text{Eq. 15}$$

$$K_{dyn} = (13474.45) \rho_b \left[\frac{1}{(\Delta t_{comp})^2} \right] - \frac{4}{3} G_{dyn} \quad \text{Eq. 16}$$

Where ρ_b is the bulk density in g/cm^3 , Δt_{comp} is the bulk formation compressional slowness in us/ft , Δt_{shear} is the bulk formation shear slowness in us/ft . Note that 13474.45 is a conversion coefficient.

Once both dynamic shear and bulk modulus are determined, the Dynamic Young's Modulus is computed by Eq. 17.

$$E_{dyn} = \frac{9G_{dyn} (K_{dyn})}{G_{dyn} + 3K_{dyn}} \quad \text{Eq. 17}$$

The distribution of the dynamic elastic properties is presented in *Table 5*. The histograms for the analyzed elastic properties have a leptokurtic distribution because the points along the X-axis are cluster; giving, as a result a higher peak (kurtosis). The distribution of those properties is asymmetric. In the case of Young's modulus, shear modulus, and bulk modulus, the distribution is left-skewed because the majority of data points are concentrated on the right side. It can also be seen that the mean value for those properties is lower than the median; showing that the distribution is in fact left skewed. The literature shows that the typical values for shales in the case of Young's modulus is 1-70 GPa (30). The Young's modulus histogram ranges between the values suggested by the literature; indicating that the rock with low Young's modulus has a lower resistance to be deformed and with high values, the rock is stiffer. The range of bulk modulus according to the literature is between 6.4 to 21.6 GPa

Table 5 – Statistical parameters of dynamic properties for the caprock of the 2nd Wall Creek reservoir and histograms made for Young modulus, shear modulus, bulk modulus and Poisson’s ratio

Elastic Properties	Range of Value	Statistic Parameters	Histogram
<p>Young modulus (E_DYN) [GPa]</p>	<p>Min: 1.94 Max: 123.67</p>	<p>Mean: 28.198 Median: 28.64 Mode: 29.86</p>	
<p>Shear modulus (G_DYN) [GPa]</p>	<p>Min: 0.67 Max: 49.38</p>	<p>Mean: 11.029 Median: 11.19 Mode: 11.57</p>	
<p>Bulk modulus (K_DYN) [GPa]</p>	<p>Min: 5.84 Max: 90.29</p>	<p>Mean: 21.492 Median: 21.57 Mode: 21.989</p>	

CHAPTER VI. GEOMECHANICS

The investigation of the rock mechanical properties allows evaluating the forces acting on the caprock matrix. This is relevant in order to ensure the caprock integrity during and after the CO₂ injection. This chapter analyzes the in-situ stresses and the caprock strength regarding unconfined compressive strength and tensile strength.

6.1. Overview

The determination of the rock deformation process is based on the relationship between stress and strain (28)

The Stress (σ) is the force applied to a rock that tries to change its original dimensions; thus, it is the concentration of a force per unit area. The principal stresses that act on the rocks are tensile, compression and shear stress. The tensile stress (tension) is the resistance of the material against being pulling apart by forces. This leads to the elongation of the rock in the direction where the forces are applied. On the other hand, the compression stress tries to compact the material by forces directed toward each other in the same direction; thus, the material is shortening. Finally, the shear stress is the product of external forces applied in parallel and opposite direction on different planes. *Figure 25* represents those stresses.

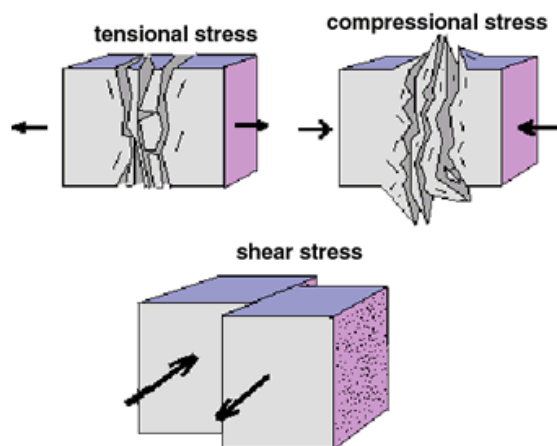


Figure 25 – Type of stresses (31)

The strain is the change of the rock original dimension as a result of the stresses applied to it. It is measured by the ratio of change in dimensions to the initial ones.

The stress-strain relationship is usually plotted on the stress vs. strain curve which is unique for each material (*Figure 26*). Under low values of stress, elastic region, the rock dimensions change. However, the dimensions are recovered when the stress is removed. If the rock matrix is beyond the yield point, plastic region, the original rock dimensions are deformed permanently from its original characteristics. (28)

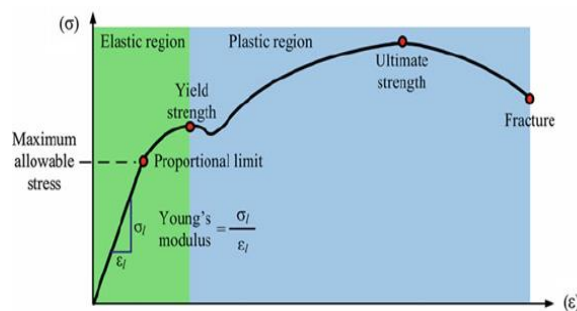


Figure 26– Stress-strain curve (32)

Depending on the relative behavior under stress, the rock matrix is classified in two categories: brittle or ductile. Those two classifications have different stress vs strain curves as can be seen in *Figure 27*. The brittle material has low or not plastic deformation until it reaches the brittle failure (B). On the other hand, the ductile rock has a clear plastic behavior where it is deformed before the ductile failure (B'). Consequently, the ductile rocks can absorb large energy amount before failure than the brittle rocks. (33)

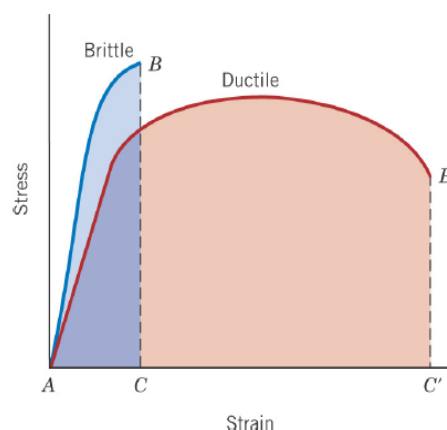


Figure 27 – Stress-strain curve for ductile and brittle rocks

6.2. In-Situ Stress

The principal in-situ stresses in the caprock are overburden stress or vertical stress (σ_v) and pore pressure (Pp) (34). Different equations and approximations are used to calculate the principal stresses in the caprock.

6.2.1. Overburden Stress

The overburden stress, also called vertical stress, is the pressure applied by the overlying sediments weight per unit of area. In order to compute the overburden stress is important to know the density of the overlying formations (35). Techlog® extrapolates the density up to the mud line by using the Eq. 18 to have an estimation of the density of the intervals where the log is not available.

$$\rho_{extrapolated} = \rho_{mudline} + A_o(TVD - AirGap - WaterDepth)^\alpha \quad \text{Eq. 18}$$

Where $\rho_{mudline}$ is the mud density at the ground level, A_o and α are fitting parameters, and TVD is the truth vertical depth. The values used for the calculation are 1.65 g/cm³ of the mud density, 0 m for both AirGap and WaterDepth. Note that those values were set as defaults in Techlog®.

The overburden stress is calculated with Eq. 19. Where $\rho_{extrapolated}$ is density that was extrapolated previously, σ_v is the overburden stress, TVD is the true vertical depth, and z is the depth.

$$\sigma_v = \int_0^{TVD} \rho_{extrapolated}(z) dz \quad \text{Eq. 19}$$

Figure 28 shows the overburden stress (SVERTICAL_EXT), vertical stress gradient equivalent (OBMW_EXT), extrapolated bulk density (DEN_EXTRAPOLATED) and bulk density (RHOB). The blue line corresponding to DEN_EXTRAPOLATED was interactively adjusted by changing the position of the points in both density and depth axes in order to get more accurate results. It can be seen that the overburden stress trend is linear and is increasing with depth because the geostatic load increased likewise.



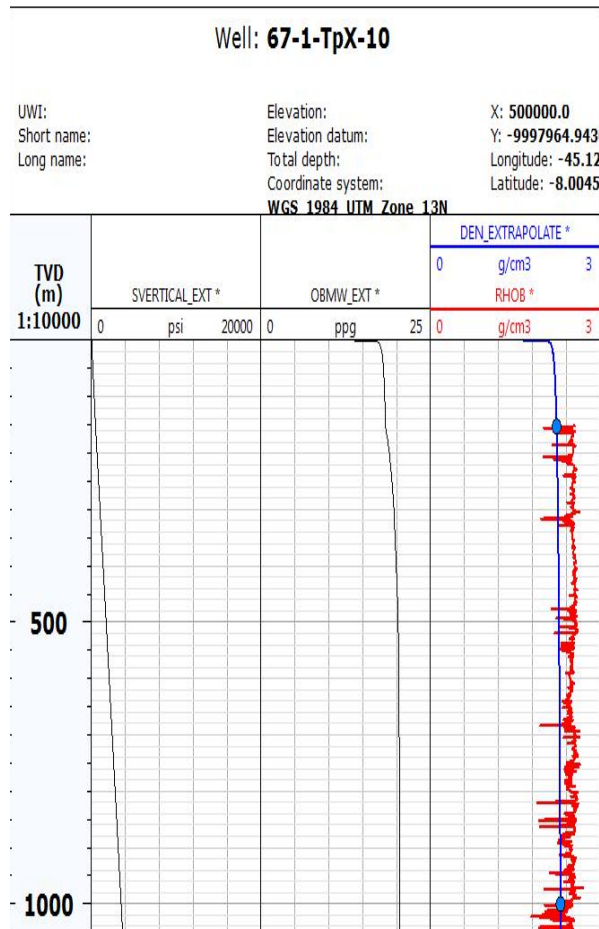


Figure 28 – Overburden stress

In *Figure 29* is presented the overburden stress histogram for all the wells. There are two data sets in the picture, the first one is approximately from 15 MPa to 23 MPa and the second goes from 27 MPa to 29 MPa. The second distribution is due to the displacement of the 2nd Wall Creek reservoir, which can be seen in well correlation study. The histogram is moderately asymmetric since the formation depth varies from one well to another. Therefore, the overburden stress changes accordingly to it. In overall, the average overburden stress is approximately 19 MPa.

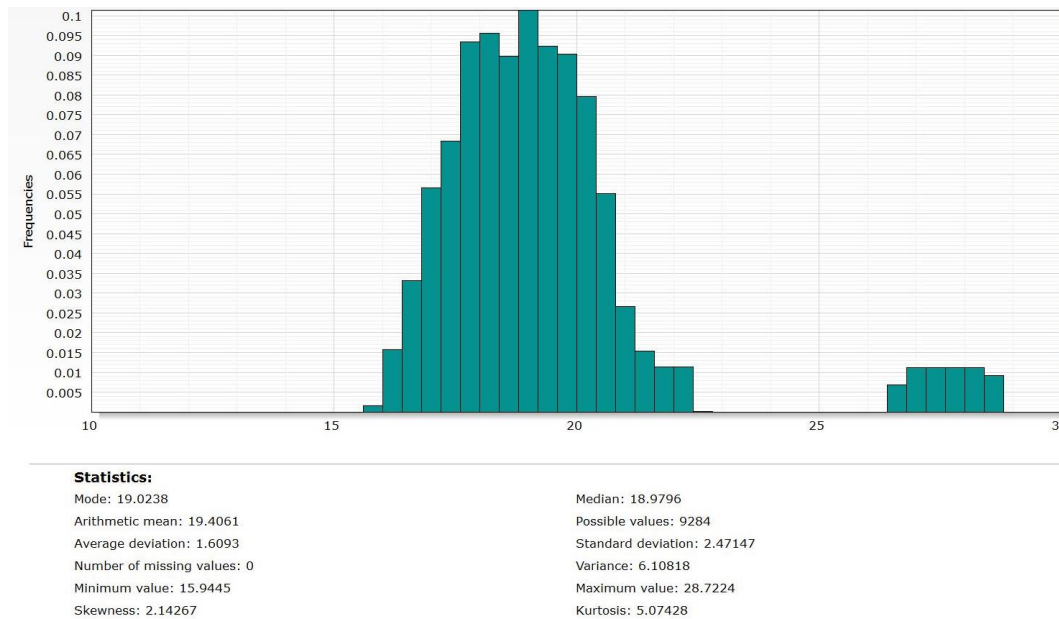


Figure 29 – Overburden stress histogram

6.2.2. Pore Pressure

The pore pressure is the fluid's pressure inside the pore space, and it is given by the hydrostatic pressure of the overlying formation water (36).

In the case of shales, the prediction of the pore pressure is based on different vertical effective stress approaches: Eaton, Bowers, and Traugott. Those methods use the Terzaghi's law which states that pore pressure is a function of the overburden stress (total stress) and the effective vertical stress (36). The pore pressure method used in this study is the Eaton since it is widely used for shales.

The Eaton method uses the resistivity and compressional slowness log to estimate the pore pressure.

The pore pressure computed by resistivity (P_{p_R}) is based on the following equation (Eq. 20)

$$P_{p_R} = \sigma_v - (\sigma_v - P_{pnorm}) (a) \left(\frac{R}{R_{norm}} \right)^n \quad \text{Eq. 20}$$

Where σ_v is the vertical stress, R is a value from the resistivity log, R_o is the initial sediments resistivity, R_{norm} is a measurement value assuming that formation is frequently pressured, P_{pnorm} is the normal pore pressure, a and n are fitting parameters which are set by default as a=1 and n=3

Notice that the P_{pnorm} and R_{norm} are calculated through Eq. 21 and Eq. 22. Where P_o is the pressure at sea floor, k is a constant gradient, and Z is depth measured from the sea floor

$$P_{pnorm} = P_o + kZ \quad \text{Eq. 21}$$

$$\ln R_{norm} = \ln R_o + kZ \quad \text{Eq. 22}$$

The pore pressure is calculated through Eq. 23 when the compressional slowness log (DT) is used instead. In this equation DT is value from the compressional slowness log, DT_o is the initial travel time, DT_{norm} is a measurement value assuming that formation is normally pressured

$$P_{p_DT} = \sigma_v - (\sigma_v - P_{pnorm}) (a) \left(\frac{DT}{DT_{norm}} \right)^n \quad \text{Eq. 23}$$

The values for the fitting parameters are a=1 and n=1.2. The Eq. 24 represents DT_{norm} in this case.

$$\ln DT_{norm} = \ln DT_o + kZ \quad \text{Eq. 24}$$

Figure 30 shows the pore pressure calculation for the well 67-1-TpX-10. The second and third track displays the compressional slowness and the resistivity log for this well. The magenta color line represents the compaction trend which has been adjusted in each case to give accurate results. The calculated pore pressure by using compressional and resistivity logs is shown in the last track. As can be noticed, the computed logs are close to each other; following a similar trend which is increasing with depth. Note that the pore pressure is lower than the overburden pressure because it only takes into account the overlying pore fluids (formation water) but not the overlying sediments. The normalized value of pore pressure (P_p) is calculated through the normalization of P_{p_R} and P_{p_DT} which in Techlog© the variable is called



PPRS_NORM displayed with a sky-blue line. APPENDIX 9 shows the pore pressure for all the wells.

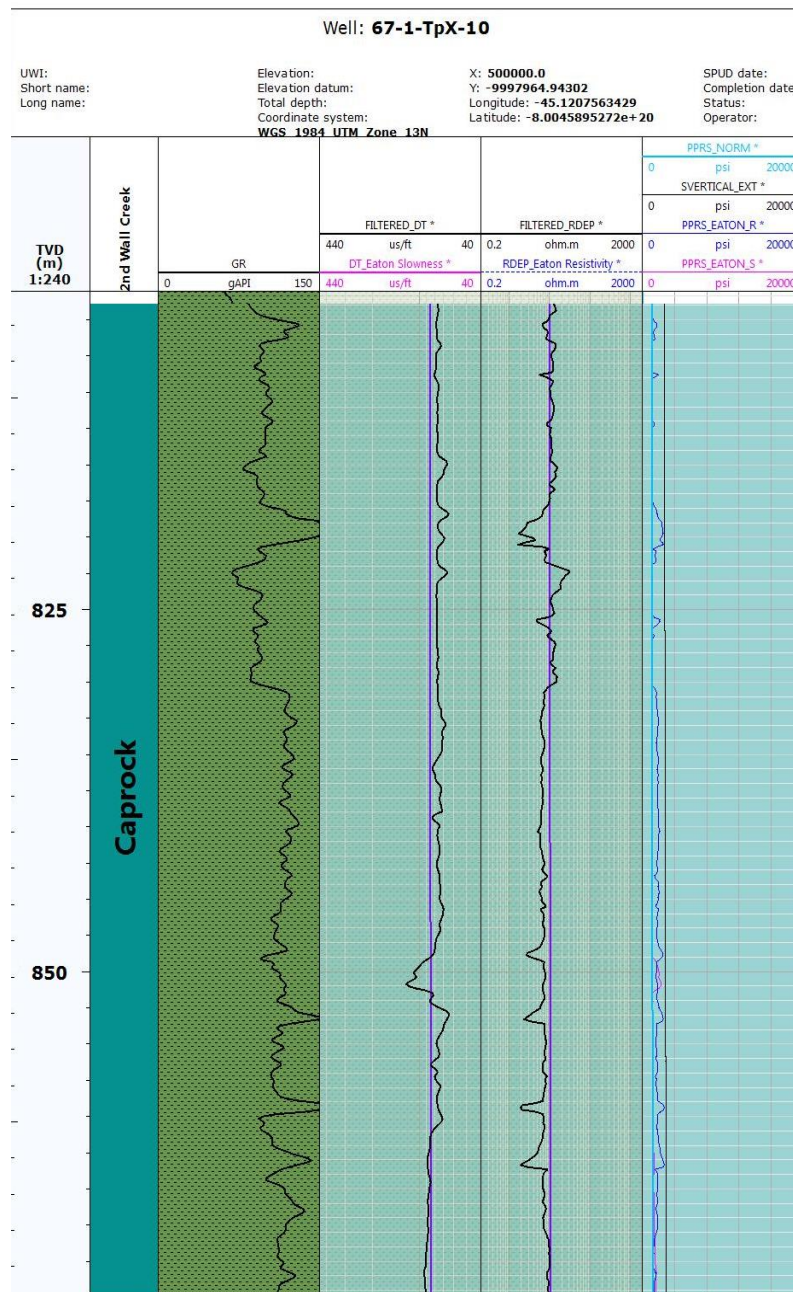


Figure 30 – Pore pressure calculation by using the Eaton’s method



The pore pressure (P_p) histogram is similar to the overburden stress histogram since there are 2 data sets which can be seen in *Figure 31*. This distribution occurs due to the displacement of the 2nd Wall Creek reservoir and therefore the pore pressure increases likewise. The caprock average pore pressure is 9 MPa; being the minimum value approximately 8 MPa and the maximum around 13 MPa. The P_p gradient is 0.010 MPa/m (0.456 psi/ft); meaning that P_p in SG is 1.05.

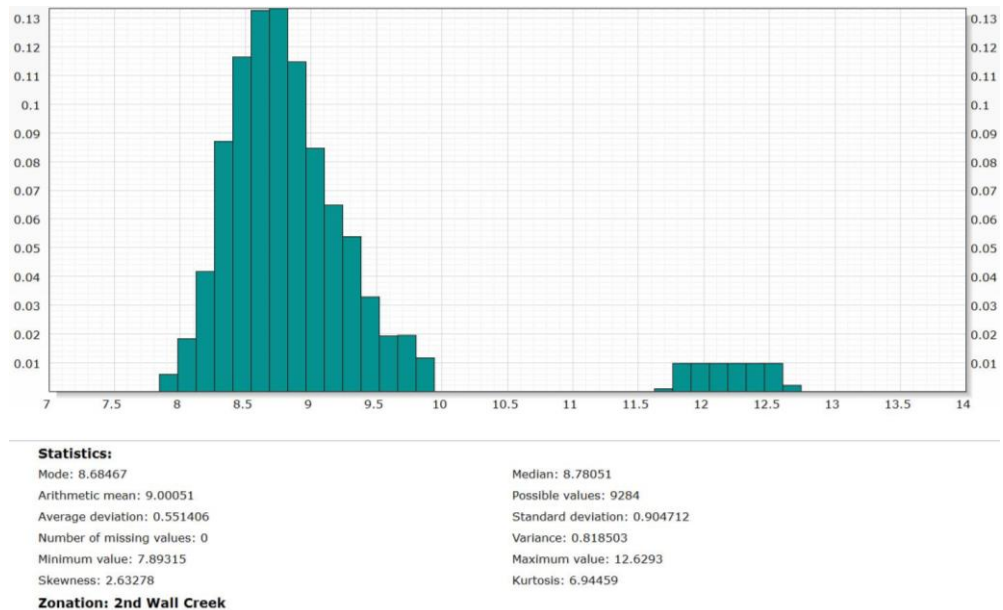


Figure 31 – Pore pressure histogram

6.3. Rock Strength

The ability of the rock to resist the deformation induced by external forces is called strength. It is affected by its mineralogical composition, external pressure and temperature. Some minerals such as quartz, feldspars are very brittle while clay, mica and calcite are more ductile. The temperature influences the rock strength because at high temperatures the molecules can move freely and therefore the rock is more ductile.

In this section, different equations are applied in order to find the unconfined compressive strength (UCS) and tensile strength (TS) of the caprock (37).

6.3.1. Unconfined Compressive Strength

The unconfined compressive strength (UCS), also called uniaxial compressive strength, measures the strength of a material (rock) which is stressed axially under unconfined conditions (38).

The unconfined compressive strength of the caprock can be estimated from the elastic properties calculated from the log data. It can be calculated through the Coates and Denoo equation which is the most common for shales (Eq. 25).

$$UCS = 0.0866 \left(\frac{E_{dyn}}{C_{dyn}} \right) (0.008V_{sh} + 0.0045(1 - V_{sh})) \quad \text{Eq. 25}$$

Where UCS is the unconfined compressive stress in MPa, E_{dyn} is the dynamic Young's modulus in MPa, K_{dyn} is the dynamic bulk modulus in MPa and C_{dyn} is the dynamic bulk compressibility which is expressed by the Eq. 26.

$$C_{dyn} = \frac{1}{K_{dyn}} \quad \text{Eq. 26}$$

Figure 32 presents the elastic properties and the unconfined strength of the rock. The first and second track presents Young's modulus (E_{DYN}) in GPa and Poisson's ratio. The last track shows the caprock unconfined compressive strength in GPa. The calculation results show that the trend of the UCS is similar to E_{DYN} but differs from the Poisson's ratio. The lithology type plays a major role in the unconfined compressive stress because both density and porosity change depending on the mineralogy. Xu, Hao, et al. (2016) show that UCS of a rock increases with the rock density but decreases with the porosity.

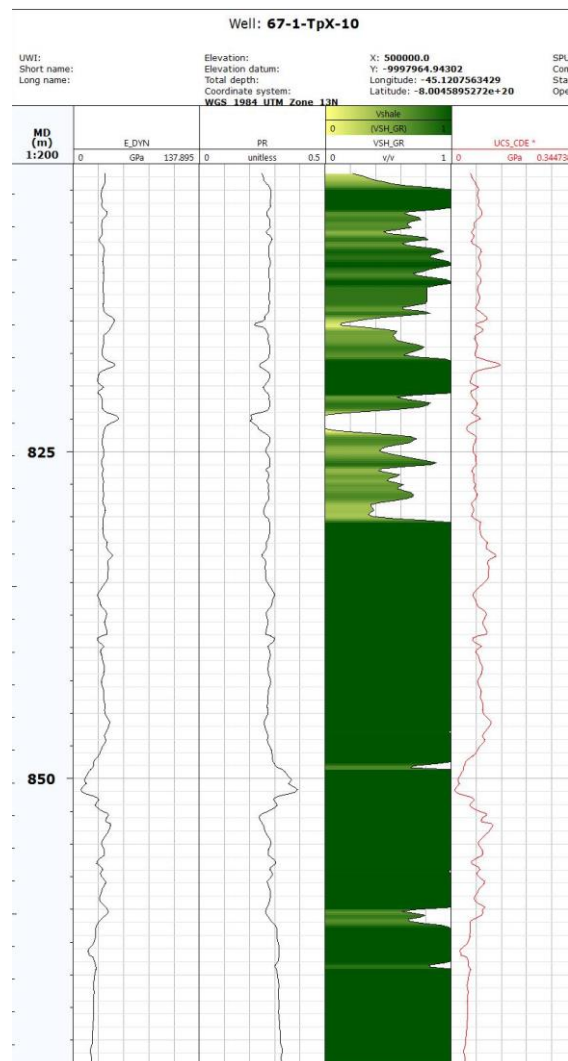


Figure 32 – Unconfined compressive strength

Different authors related the unconfined compressive strength with the compressional transit time (DT), Young's modulus (E_DYN) and porosity (\emptyset) in order to evaluate it (39) (40). UCS vs. DT and UCS vs. E_DYN crossplots are presented in the *Figure 33*. *Figure 33 a*) shows that the UCS is negatively correlated with DT. In other words, UCS is decreasing with increasing of compressional transit time. On the other hand, it is observed a positive correlation between UCS and E_DYN because as E_DYN increases, the UCS is increasing likewise (*Figure 33 b*).

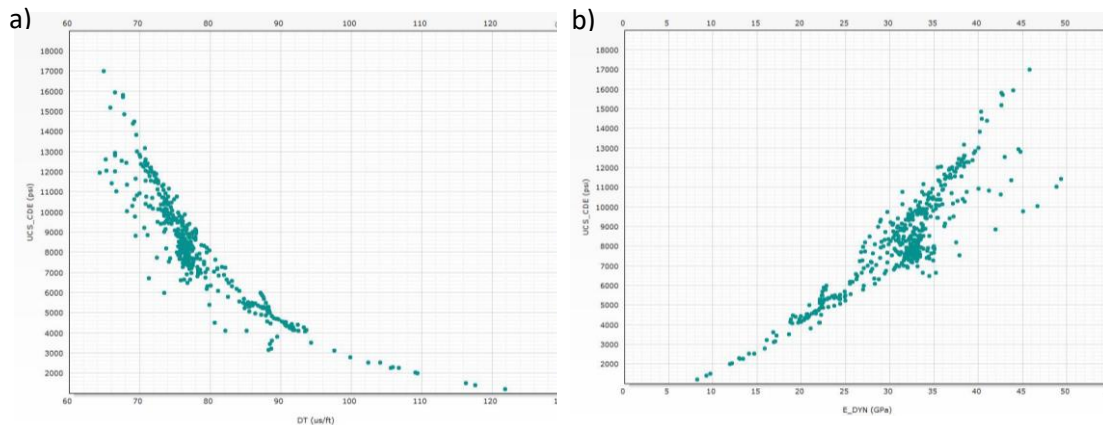


Figure 33 – Unconfined compressive strength crossplots

Figure 34 presents the unconfined compressive strength (UCS) histogram for all the wells. The distribution is slightly symmetrical because the values of the median, mode and mean values are close to each other. The average value of the UCS for the 18 wells is 57 MPa. According to the strength classification proposed by Afrouz (1992), the caprock has low to moderate strength because the UCS value is between 40 to 80 MPa (37).

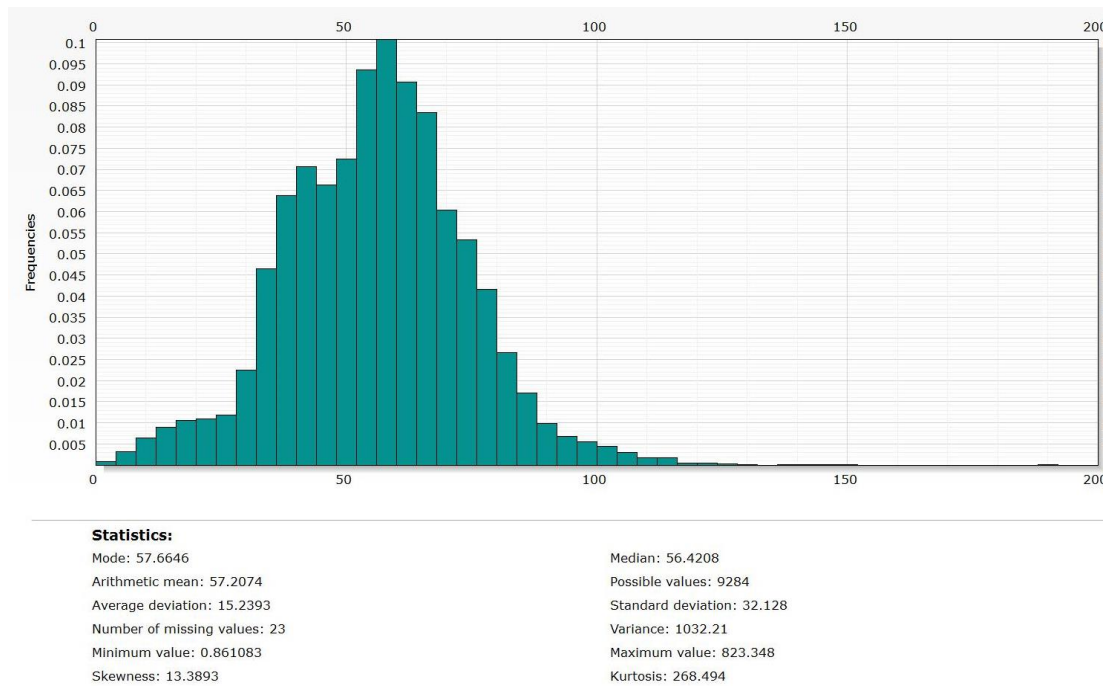


Figure 34 – Unconfined compressive strength histogram



6.3.2. Tensile Strength

The tensile strength is the maximum load that a material can support without being elongated which is opposed to the compressive strength (37). In order to calculate its magnitude, it was used in Techlog© the Eq. 27.

$$TS = 0.1(UCS) \quad \text{Eq. 27}$$

The tensile strength histogram is presented in *Figure 35*. The statistics show that the average tensile strength is 5.7 MPa which is in the range suggested by the literature (2-10 MPa) for shales. Notice that there are some outliers in the distribution such as 0.086 MPa (minimum value) and 82 MPa (maximum value) and therefore they should not be considered.

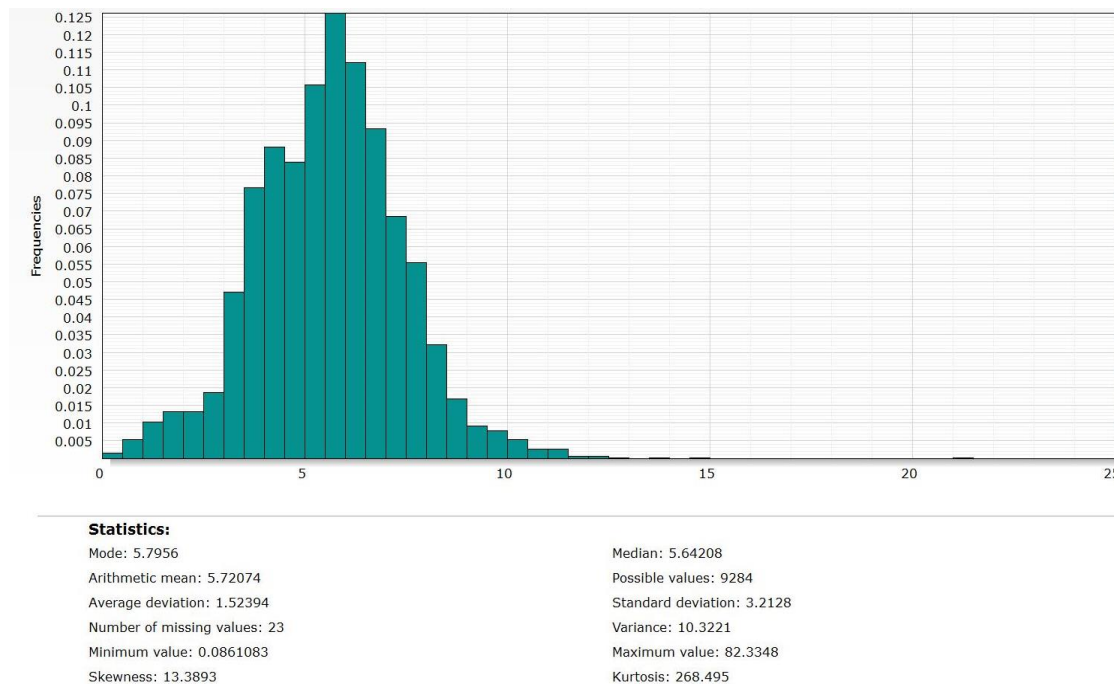


Figure 35 –Tensile strength histogram

The presence of outliers for both UCS and TS can be noticed in the box plots shown in *Figure 36*.

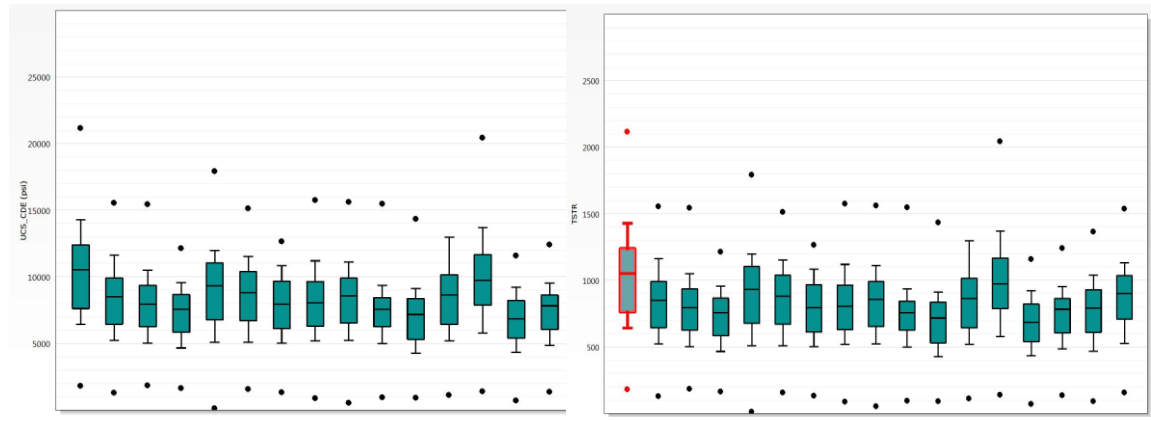


Figure 36 –Box plots for UCS and TS

According to Nygaard (2010), two modes controls the rock failure. The first one occurs when the rock reaches the limit for tensile failure and the rock is pulled apart. The second one is when the shear stress is above the critical level. Note that the tensile strength is the critical limit for tensile failure, and unconfined compressive strength is the limit for shear stress (41). Consequently, the caprock will fail in tensile, if the stress is greater than 5.7 MPa (tensile strength) and will fail in shear if the stress is bigger than 57 MPa (unconfined compressive strength).

CHAPTER VII. CAPROCK INTEGRITY

The caprock integrity is related to ductility and tendency of fracturing. Even though the ductile rocks have a low strength, they are less likely to develop CO₂ migration pathways through fracturing (8).

In order to determine the caprock integrity of the 2nd Wall Creek reservoir, two approaches are taken into account. The first one is a detailed understanding of the ductility and brittleness of the caprock. The dynamic elastic properties, Poisson's ratio and Young' modulus and the neural network analysis, IPSOM, in Techlog© are used for this purpose. The second one is the brittleness index calculation using different methods. This information is then correlated with the IPSOM results to give a final indication of the caprock integrity.

7.1. Dynamic elastic properties analysis

According to Perez (2013), crossplotting Young modulus (E_DYM) vs Poisson's ratio (PR) indicates the brittleness or ductility of the rock (33). The brittle rocks have a low PR and moderate/high E_DYM and the ductile rocks have a high PR and low E_DYM. A crossplot E_DYM vs PR for the well 67-1-TpX-10 was done in order to determine qualitatively if the caprock is brittle or ductile. Note that this information was retrieved from the previous section (Geophysics)

It can be seen in *Figure 37* that there is a clear distinction between ductility and brittleness for the shale unit. Notice that the concentration of points is higher in the ductile part than in the brittle part. According to the color scale between green and red, the GR is high which indicates ductility.



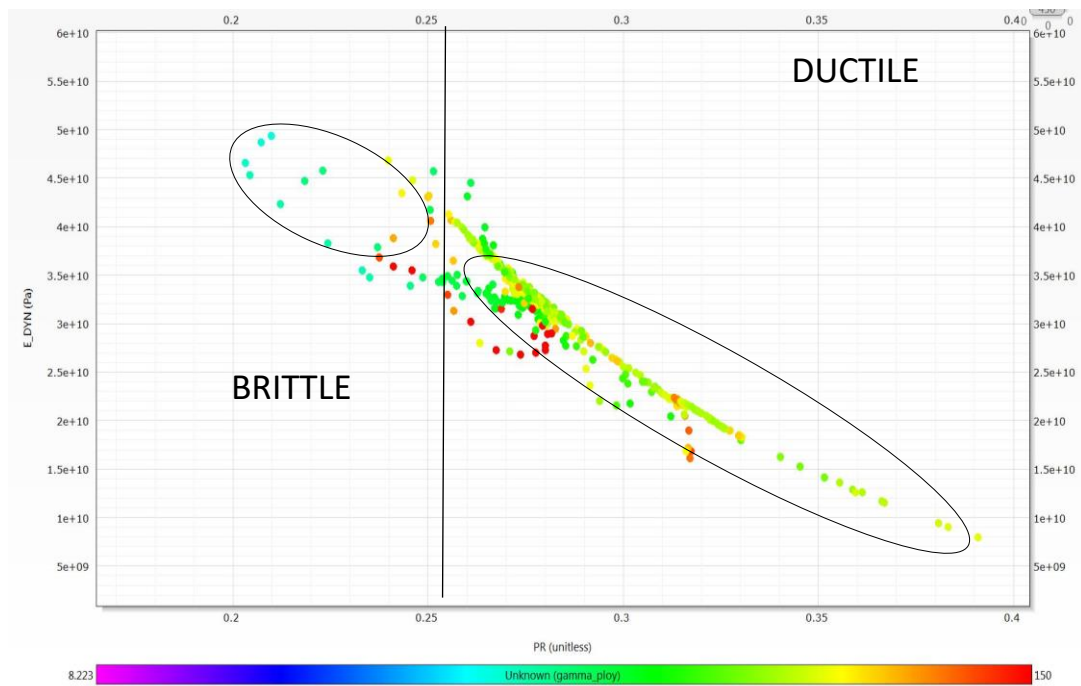


Figure 37 –Young's modulus vs Poisson's ratio crossplot colored by gamma ray

Perez (2013) suggests that the zones with the high content of quartz and calcite are more brittle than the zones with high clay content which are more ductile. Chao, D, et al (2014) suggests that the quartz content lowers the Poisson's ratio and increases the Young's modulus; representing that the rock is more easily fractured and also can maintain a fracture. The presence of quartz and dolomite can be seen in the upper part of the caprock; meaning that this zone is more likely to be brittle (*Figure 38*)

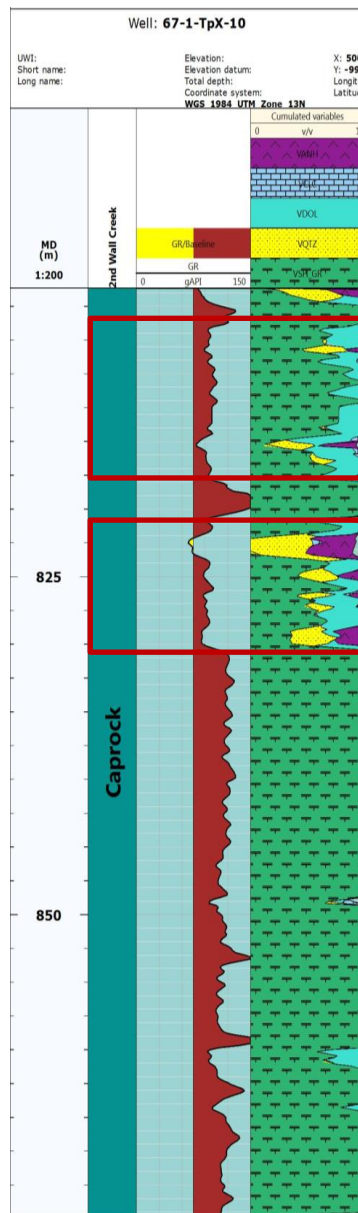


Figure 38 - Mineral content of the caprock in the well 67-1-TpX-10

7.2. IPSOM Classification

The caprock behavior subjected to stress is classified by using the neural network analysis module in Techlog© called IPSOM (Index and Probability Generating a Self-Organizing Map). This module is based on the Kohonen algorithm which learns the neuronal network in one well and then applies it to the other wells.

IPSOM module uses the following logs in order to identify the characteristics of the caprock: bulk density (RHOB), gamma ray (GR) and compressional slowness (DT). Also, the volume of shale was taken into account in order to refine the IPSOM's results. Notice that the neutron log (NPHI) was not used because of redundancy with the sonic log. *Figure 39* indicates the variables employed in the neuronal analysis.

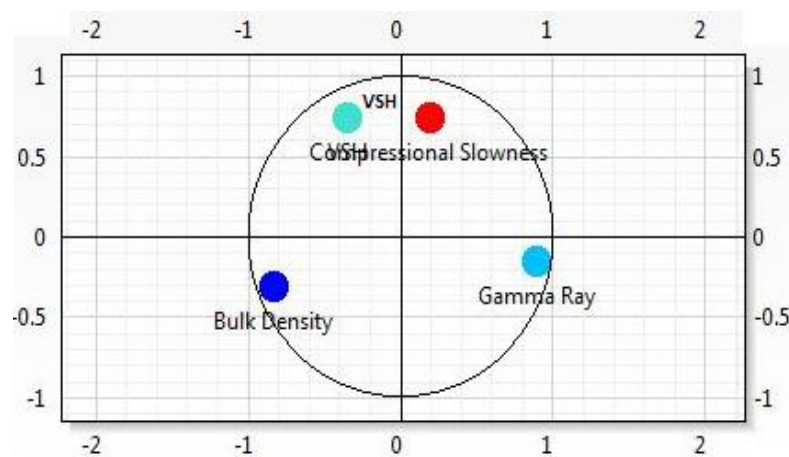


Figure 39 – Correlation of variables used for IPSOM classification

The well 67-TpX-10 is selected as a reference well for the neuronal network analysis because it contains all the log data. The obtained model from this well is then applied to the other wells. In IPSOM, the user can set the number of indexation depending on the seeking classification. The crossplot Young Modulus (E_DYN) vs Poisson's ratio (PR) (*Figure 37*) shows that the caprock can be ductile or brittle. Therefore, it was chosen an indexation of 2.

The IPSOM map classification for the caprock is shown in the *Figure 40*. In this classification, there are two main regions, one displayed in sky-blue and the other one in royal blue. Notice that the meaning of this classification is only known when the results are compared with the dynamic elastic properties. However, it is assumed that

the royal blue region, which occupied the map majority, denotes ductility and the sky-blue section represents brittleness.

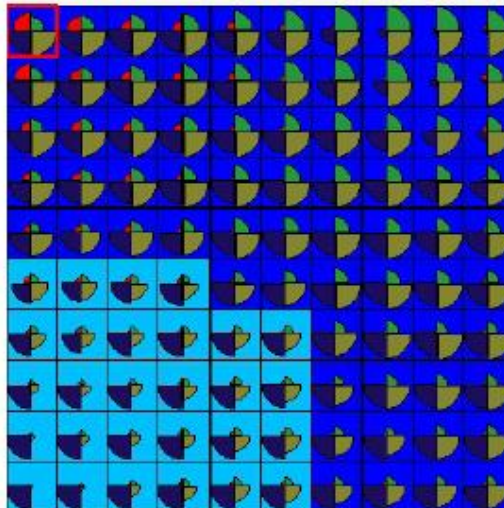


Figure 40 – IPSOM classification using an indexation of 2

Table 6 contains the variables utilized in the IPSOM classification. The volume of shale is the variable with the highest contribution because it gives more than 53% of the information employed by the neuronal analysis. Gamma ray is the second variable with 38% of the information, bulk density and shear slowness have approximately 3%.

Table 6 – Variable correlation and contribution

Variables Classification			
1	Variable	Correlation	Information
2	Shale Volume	0.7774807	0.5381371
3	Gamma Ray	0.5603807	0.3878703
4	Bulk Density	0.05373505	0.03719298
5	Shear Slowness	0.05316667	0.03679957

Table 7 presents the statistics for the group 1 (ductile in royal-blue) and group 2 (brittle in sky-blue); showing the mean and variance for the input parameters (Gamma ray, shear slowness, bulk density and shale volume). It can be noticed that the difference of each group is considerable; meaning that IPSOM classification is accurate.

Table 7 – IPSOM classification statistics

Name	1		2	
Color				
Variables	Mean	Variance	Mean	Variance
Gamma Ray	116.69	128.5293	91.5567	32.1725
Shear Slowness	147.5748	506.3431	137.3566	56.8426
Bulk Density	2.4919	0.0195	2.5557	0.0021
Shale Volume	0.9663	0.0042	0.5328	0.0292

Figure 41 shows the IPSOM classification results along with the dynamic elastic properties and the mineral content of the caprock in the well 67-TpX-10. Comparing the IPSOM results with the dynamic elastic properties, it can be inferred that the sky-blue color sections represent brittleness because the Poisson’s ratio is low and the Young modulus is moderate to high (the curves are deflected to the left side). The royal blue color sections denote ductility since the Poisson’s ratio is high and the Young’s modulus is low (the curves are deflected to the right). Also, notice that the IPSOM classification matches with the mineral content of the rock since the sky-blue sections are displayed in the regions where there is quartz/dolomite. The IPSOM classification for the 18 wells is presented in APPENDIX 10.

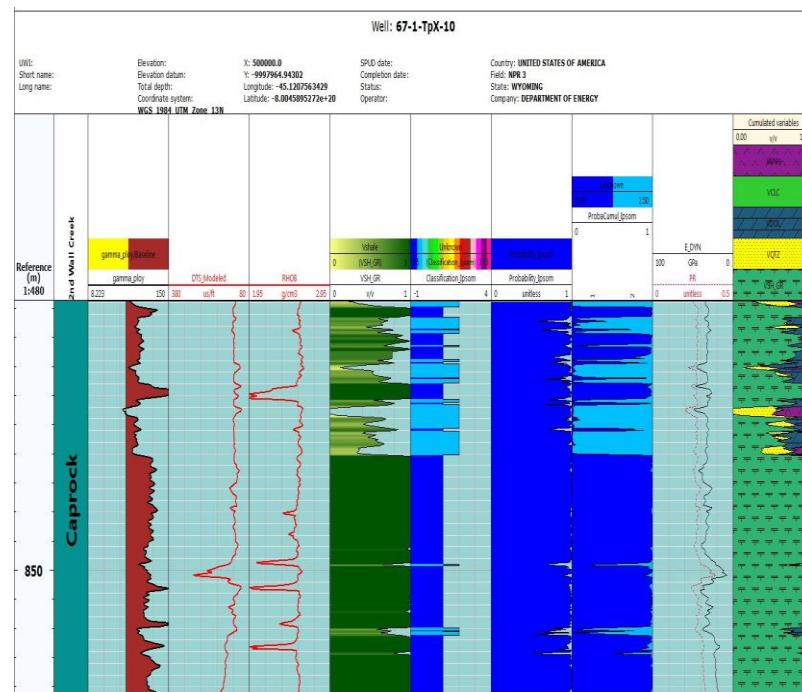


Figure 41 - IPSOM classification results using an indexation of 2

Figure 42 a) presents a crossplot of E_DYN vs PR colored by IPSOM classification for the well 67-1-TpX-10 and the Figure 42 b) shows a crossplot of E_DYN vs PR colored by Gamma ray for the well 67-1-TpX-10. It is observed that the ductility group according to the IPSOM classification matches with moderate to high GR values and the brittle group corresponds to low GR values.

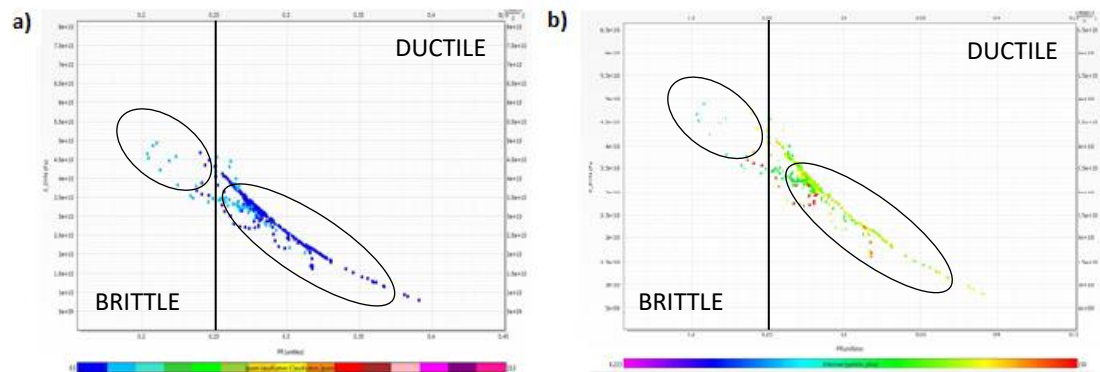


Figure 42 – a) Young's modulus vs Poisson's ratio crossplot colored by IPSOM classification and b) Young's modulus vs Poisson's ratio crossplot colored by gamma ray

A pie chart for the IPSOM classification for the well 67-TpX-10 can be seen in Figure 43. According to this plot, 74% of the caprock is ductile (group 1) and 26% is brittle (group 2). The pie charts for all the wells are presented in APPENDIX 11.

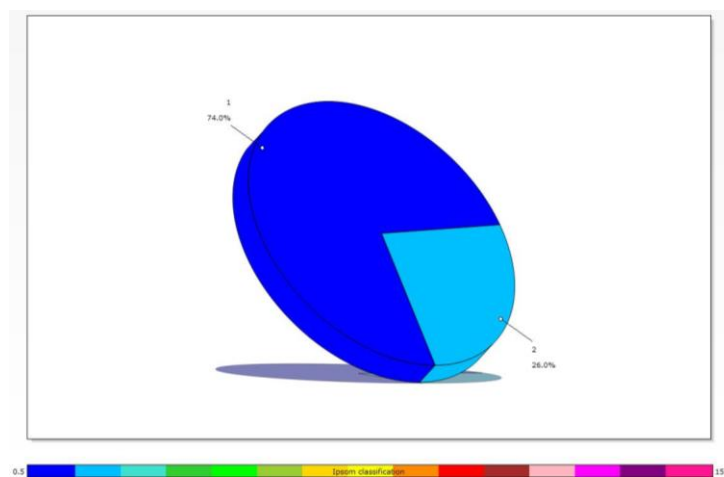


Figure 43 – IPSOM classification pie chart for the well 67-TpX-10

Figure 44 is a pie chart for brittleness and ductility in the whole caprock. This chart was done by summing up all the IPSOM classification values for all the wells. In average the 74% of the caprock can be described as ductile and the remaining 26% as brittle.

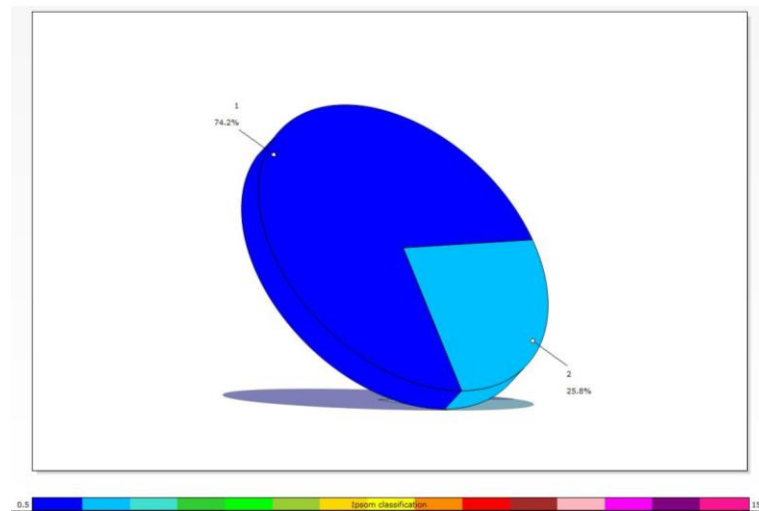


Figure 44 – IPSOM classification pie chart for all the wells

7.3. Brittleness Index

The Brittleness is the lack of ductility in tensile or shear stress which causes the rupture or failure of a material with a small or no plastic behavior (33). Some of the characteristics of brittleness are (42)

1. Low elongation/strain when a force is applied.
2. Fracture failure can be observed in the material surface such as cracks and ruptures
3. Higher ratio of compressive strength to tensile strength
4. Higher v/v concentration of brittle minerals such as quartz, dolomite compared to the ductile ones (clay).
5. Higher Young's modulus and lower Poisson's ratio values compared to their average values.

The Brittleness index (BI) is used to quantify the brittleness of the rock matrix. It has diverse expressions depending on the available data such as mineral composition or in-situ stresses. Different equations can be used for each case (42). The BI calculation

for this project was done by various methods like Ingram and Urai (1999), Rickman, et al. equation (2008), modified Wang and Gale equation (2009).

Ingram and Urai (1999) (BI_H) used the relationship between the estimated in-situ unconfined compressive strength (UCS) and the unconfined compressive strength of a consolidated rock (UCS_{NC}) (8). The brittleness index calculated with this method is presented in the Eq. 28.

$$BI_H = \frac{UCS}{UCS_{NC}} \quad \text{Eq. 28}$$

The unconfined compressive strength of a consolidated rock is equal to the effective vertical stress which is calculated by Eq. 29. In this equation, S_v is the vertical stress and P_p is the pore pressure.

$$UCS_{NC} = S_v - P_p \quad \text{Eq. 29}$$

The BI computed by the Rickman's equation (BI_R) (Eq. 30) is based on the dynamic elastic properties (Young's modulus and the Poisson's ratio) which are related to the stress and strain applied to the rock matrix. Qualitative analysis shows that rocks with high Young's modulus and low Poisson's ratio are potentially brittle. In addition, the effect of both stresses and strains is established by the relationship between those parameters (43).

$$BI_R = \frac{1}{2} \left[\frac{E - E_{min}}{E_{max} - E_{min}} + \frac{v_{max} - v}{v_{max} - v_{min}} \right] \quad \text{Eq. 30}$$

The modified Wang and Gale's method (44) (BI_M) is based on the mineral composition of the rock. In this approach, the BI is calculated by dividing the percentage of the most brittle minerals such as quartz and dolomite by the total mineral composition (Eq. 31).

$$BI_M = \frac{V_{QTZ} + V_{DOL}}{V_{QTZ} + V_{CLC} + V_{DOL} + V_{ANH} + V_{SH}} \quad \text{Eq. 31}$$



The methods that were used to calculate BI are plotted beside the IPSOM classification (Figure 45). Notice that each BI method gives different values at the same point. This is because they are based on different rock properties. The modified Wang and Gale's brittleness index (BI_M) in blue line reflects that the zones with a high concentration of quartz and dolomite are more brittle (high brittleness index) than the sections in which those minerals are not present. This method is used to give an indication/suggestion of the possible brittle zones. The Rickman's brittleness index log (BI_R) displayed with the red line and Ingram and Urai (BI_H) displayed with the black line follows a similar trend; however, the values of BI_H are higher than BI_R. This is because each method is based in different parameters. In APPENDIX 12 is shown the brittleness index for all the wells

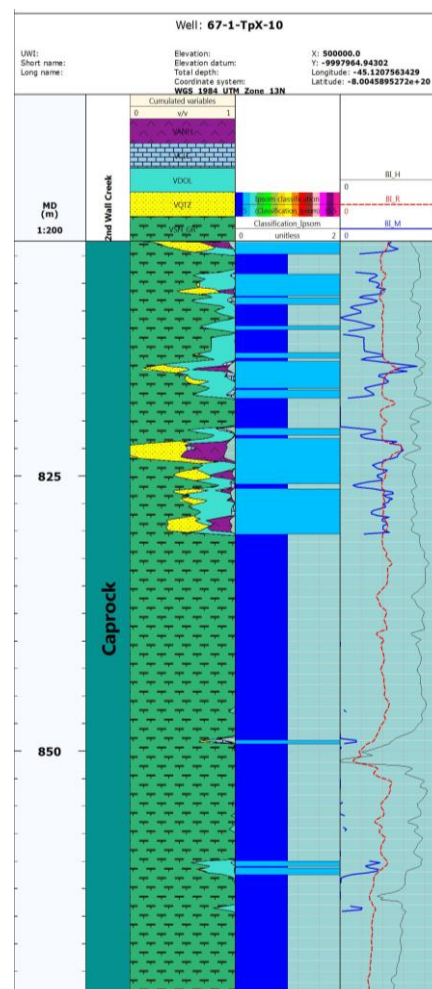


Figure 45 – Brittleness index comparison for the well 67-1-TpX-10

According to Perez (2013) (33), the most widely used methods for the brittleness index calculation in shales are based on the mineral content, Young's modulus and Poisson ratio. Zhang, et al. (42) suggests that the Rickman's method is more precise in quantifying the rock brittleness index because it evaluates the mutual effect of stresses and strains. In the (Figure 45) is observed that BI_R shows a positive response when there is a high concentration of quartz and dolomite, and a moderate/lower response when there is a high concentration of shale. On the contrary, the Ingram and Urai index method (Bi_H) shows abnormal high brittleness values in zones where there is a high concentration of shale (clay); being opposite to the expected behavior; thus, this method is discarded for future evaluations. Moreover, the IPSOM classification has a better correlation with BI_R than with the others. For example, the IPSOM classification indicates that the sky-blue sections denote brittleness which is confirmed by high values of BI_R (BI>4) and the royal-blue (ductility) has moderate/lower values of BI_R (BI<4).

In conclusion, the BI_M indicates the brittle zones in the caprock and Rickman's brittleness index method (Bi_R) is used for its evaluation because it is more precise in quantifying the brittleness of the rock. Note that this approach was not calibrated due to the lack of laboratory results from mechanical tests.

7.3.1. Evaluation of Brittleness Index

Brittleness index and gamma ray crossplot is used to evaluate the brittleness index (Lou et.al, 2016). For the present study, the brittleness index calculated through Rickman's equation is plotted against the volume of shale, VSH, which is shown in Figure 46. Eq. 32 shows the correlation between those variables and it was obtained from the regression line (blue line) added to the crossplot.

$$BI_R = -0.1795596(VSH) + 0.5119376$$

Eq. 32



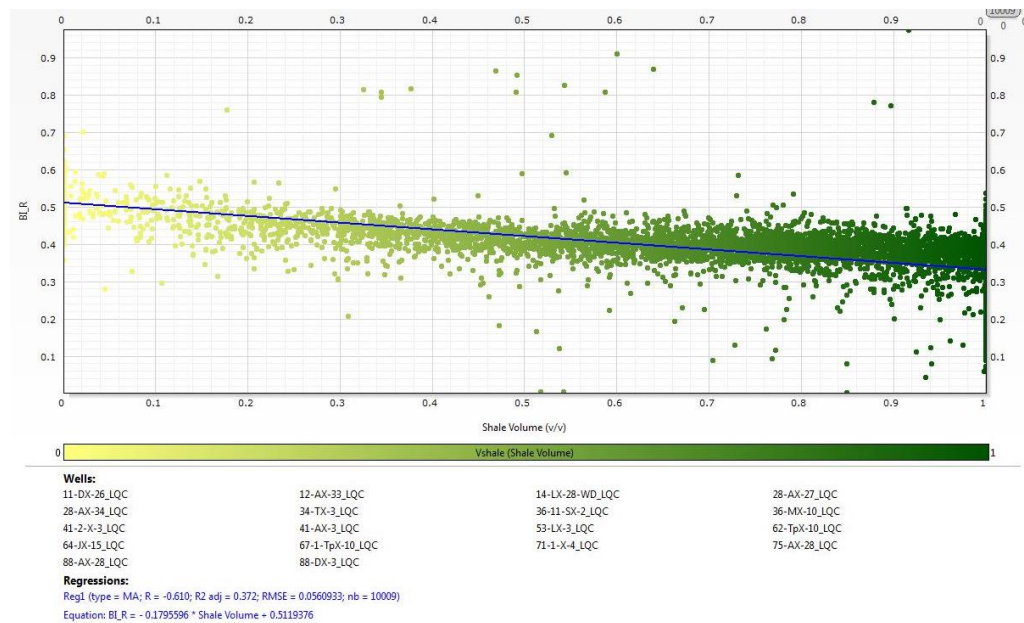
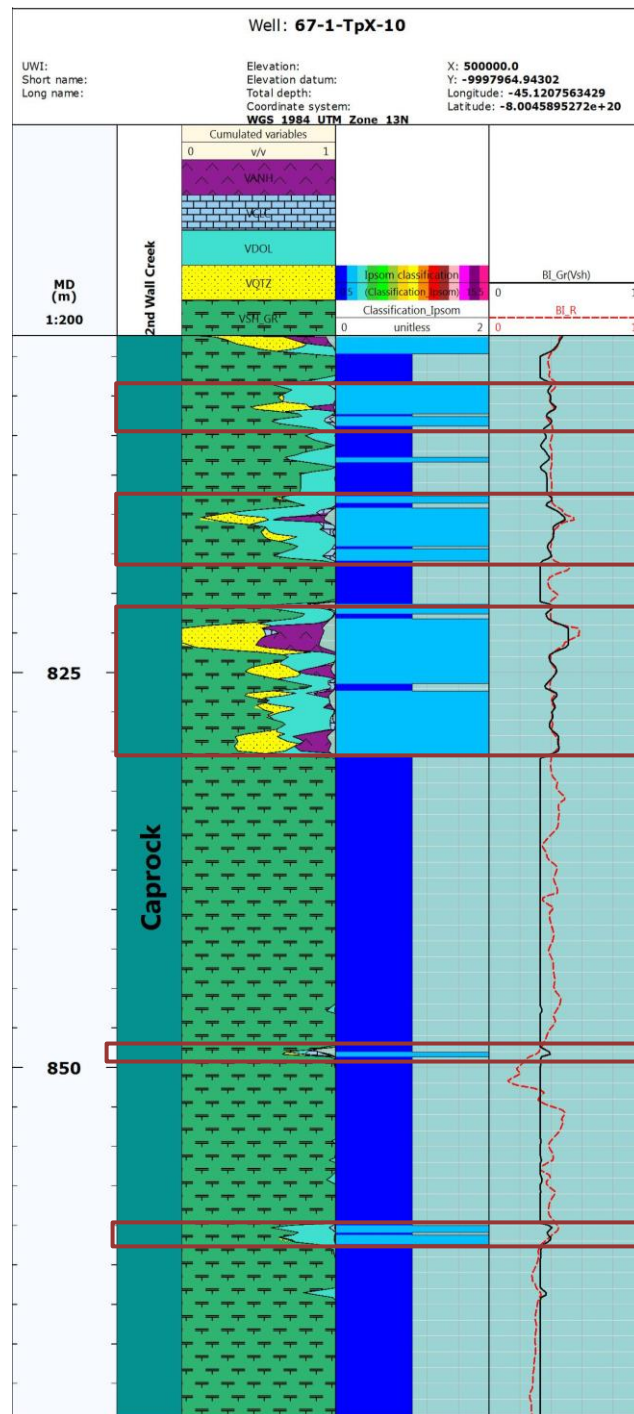


Figure 46 – Brittleness index vs volume of shale for all the wells

The first track of the *Figure 47* displays the mineral content of the caprock. The following tracks shows the IPSOM classification, Rickman's brittleness index and its evaluation. It can be noticed that the brittleness index curve and the brittleness evaluation curve follows a similar trend; fluctuating at the regions where there is a high concentration of quartz and dolomite and lower shale volume. Therefore, the BI_R is confirmed. In addition, it can be noticed that both IPSOM classification and brittleness index evaluation match consistently with the mineral content. Therefore, the Rickman's brittleness index and IPSOM classification can be used for the modeling of the caprock integrity.



CHAPTER VIII. CAPROCK MODELING

When assessing the caprock integrity, the numerical modeling plays a crucial role since it gives a reasonable understanding of its behavior in the whole area. Two types of modeling are carried out in Petrel (Schlumberger modeling platform) based on the obtained results in the previous chapters. The first one corresponds to facies modeling in which the discrete attributes derived from the IPSOM classification are populated into the grid cells. Then, this model is used to constrain the petrophysical modeling in which the continuous property, brittleness index (BI_R), is simulated in the caprock.

The ultimate goal of this section is to develop a robust model to represent the most suitable areas for CO₂ storage and CO₂ injection wells in the Teapot Dome Field.

8.1. Data and Methods

The caprock brittleness and ductility of the 2nd Wall Creek reservoir were modeled by using the Schlumberger modeling platform, Petrel. The information imported to build the models consists of the data retrieved from Techlog© such as well tops, IPSOM classification and the Rickman's brittle index. Besides, it was included the available seismic and topography information for the Teapot Dome field. The flowchart presented in *Figure 48* shows the methodology carried out in the present section.



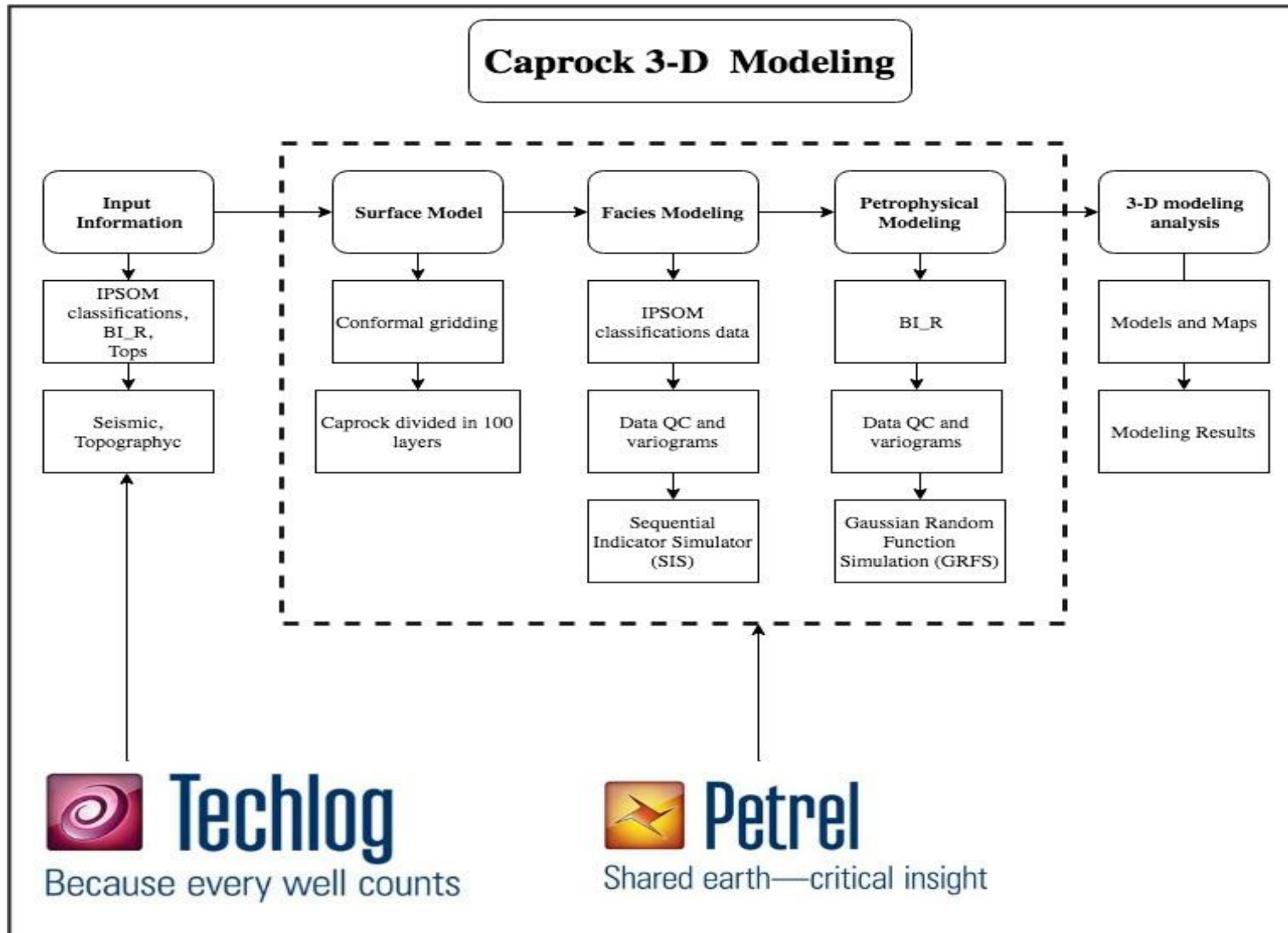


Figure 48 – Modeling flowchart for the simulation

8.2. Surface Model

The gridded surface and zone layering were done in Petrel. The caprock gridded surface was done by using the conformal gridding method in which the wanted surface is confined by 2 horizons (seismic top and seismic base) as can be observed in *Figure 49*. Notice that a suitable surface can be created based on the seismic data.

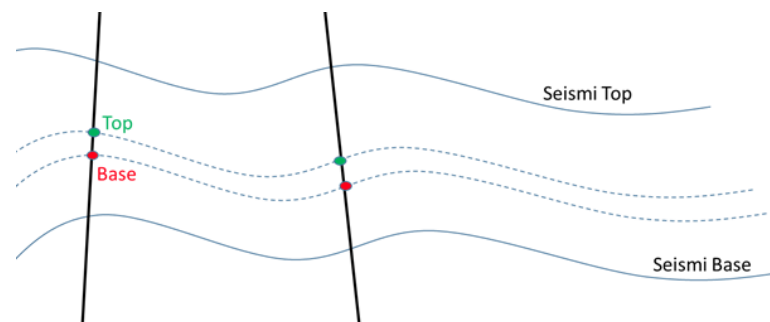


Figure 49 – Conformal gridding example

The Teapot Dome seismic data has a good resolution only at deeper depths; meaning that there are not good seismic horizons between the wanted surface. *Figure 50 a)* on the left side shows that the seismic data between the caprock limits (blue lines) is insufficient. *Figure 50 b)* indicates the maximum seismic magnitude that can be extracted from the top shale and top reservoir. The purple region in this map, which covers the majority of the area, represents the lack of information and the blue sections denote the available seismic data in the zone. As can be seen, the available seismic data around the 2nd Wall Creek reservoir cannot be used for making the surface

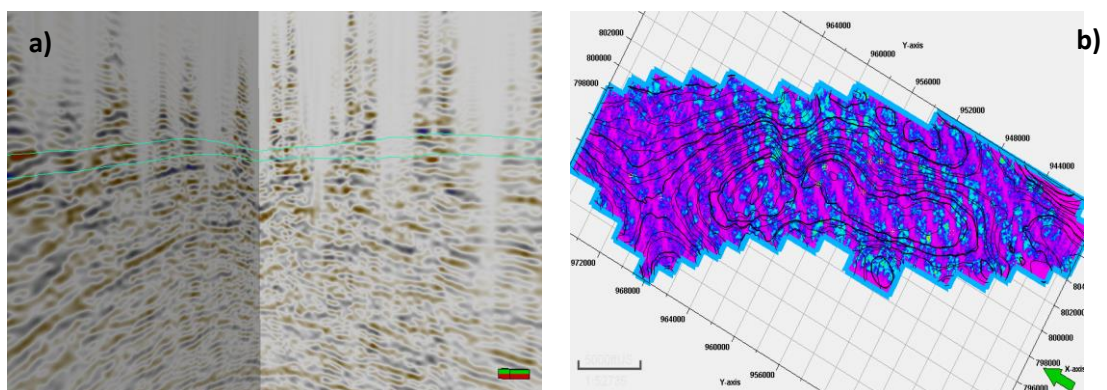


Figure 50 – Available seismic data for Teapot Dome field

Since the seismic data at the upper parts of the Teapot Dome field could not be used, the regional topography was employed as the top horizon and the deeper seismic (better resolution) as the bottom horizon. *Figure 51* represents the conformal grid obtained between the topography surface and the deep seismic surface.

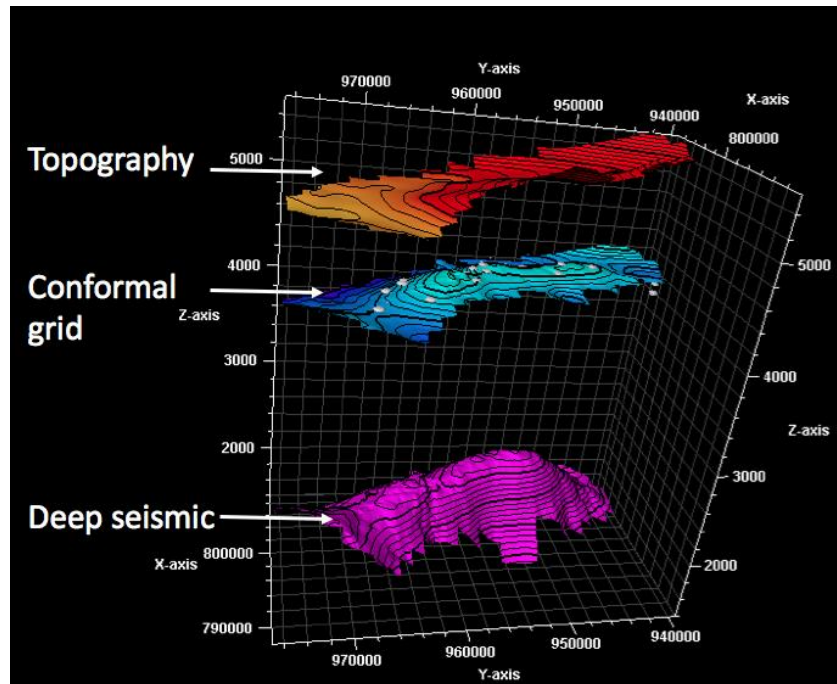


Figure 51 – Available seismic data for Teapot Dome field

The final conformal grid was built by adding the caprock zone tops and bases for all the wells. The layering to divide the caprock was 100; meaning that the average thickness of each layer is 0.8 m which give a good resolution as can be observed in *Figure 52*. Notice that the reservoir is displayed in green color with just one layer because it is no part of the present study.

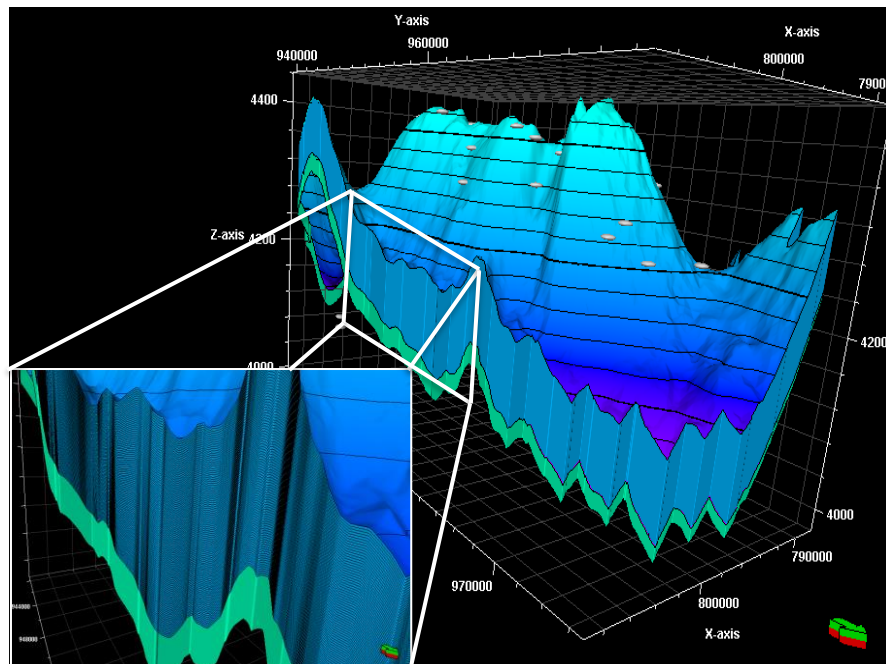


Figure 52 – Conformal 3D grid

8.3. Facies Modeling

The facies modeling is the interpolation of the discrete data in the grid cells (45). This kind of simulation is usually done to build a superior model.

The facies modeling of the present study is based on the Sequential Indicator Simulation (SIS) which uses variograms and directional trends to create a stochastic distribution of the property. The variograms and trends (major range, minor range and vertical range) are adjusted to refine the data. This method is reasonable when there is uncertainty in the shape of the subsurface body (caprock) (46), as it was observed in the conformal gridding

In the facies analysis was used the Techlog© IPSOM classification data (ductile or brittle) for the 18 wells. The first step in the modeling is upscaling the IPSOM classification and then analyzing this qualitative property.

Figure 53 indicates the data distribution and the estimated facies proportion in each layer of the model. The ductility is represented by the blue columns and brittleness by the purple ones. The distribution of the estimated facies follows a similar trend

that was observed before in which the bottom of the caprock is more ductile than the top which is more brittle.

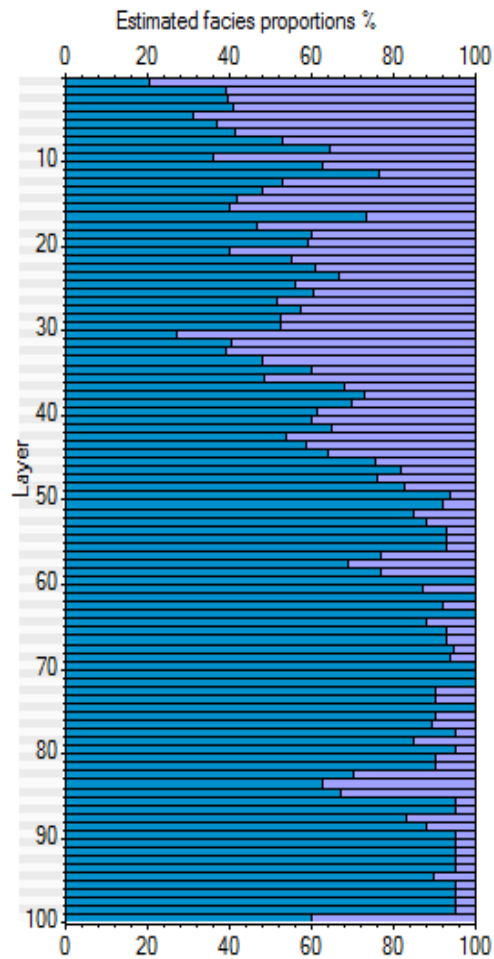


Figure 53 – Estimated facies proportions percentage

It can be seen in *Figure 54* that the estimated facies proportion data has a high variance in each classification (rough distribution). Therefore, the data was smoothed by adjusting the proportional curves (blue lines) in order to get a better distribution.

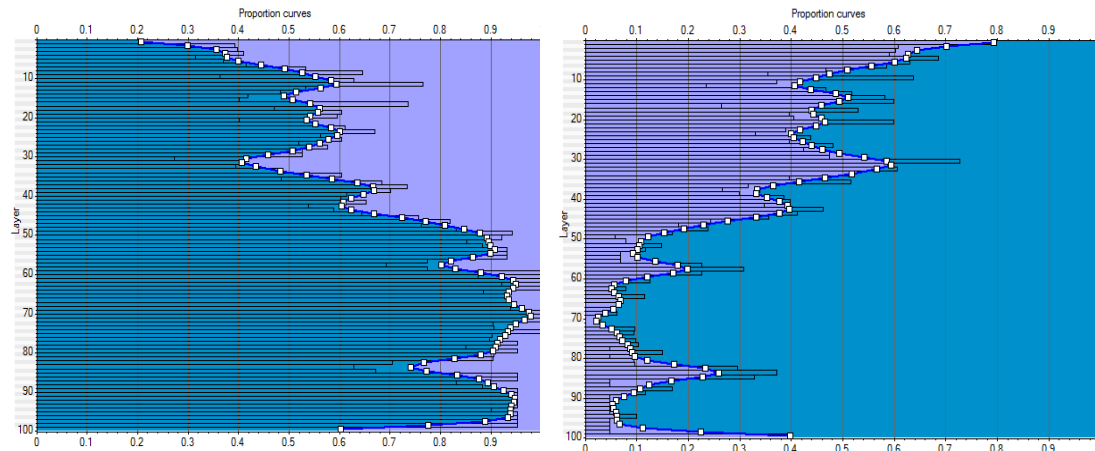


Figure 54 – Proportion curves for each facie (ductile and brittle)

After adjusting the proportional curves for each facie (ductile and brittle), the data is analyzed to specify the variograms (description of a property variation). Major, minor and vertical ranges were adjusted in order to specify the variograms that will be used in the simulation. This process is presented in *Figure 55*. It is important to highlight that the azimuth in the major direction was set as 330° because the anticlinal of the Teapot Dome field is oriented NE/ SW approximately at 30°.

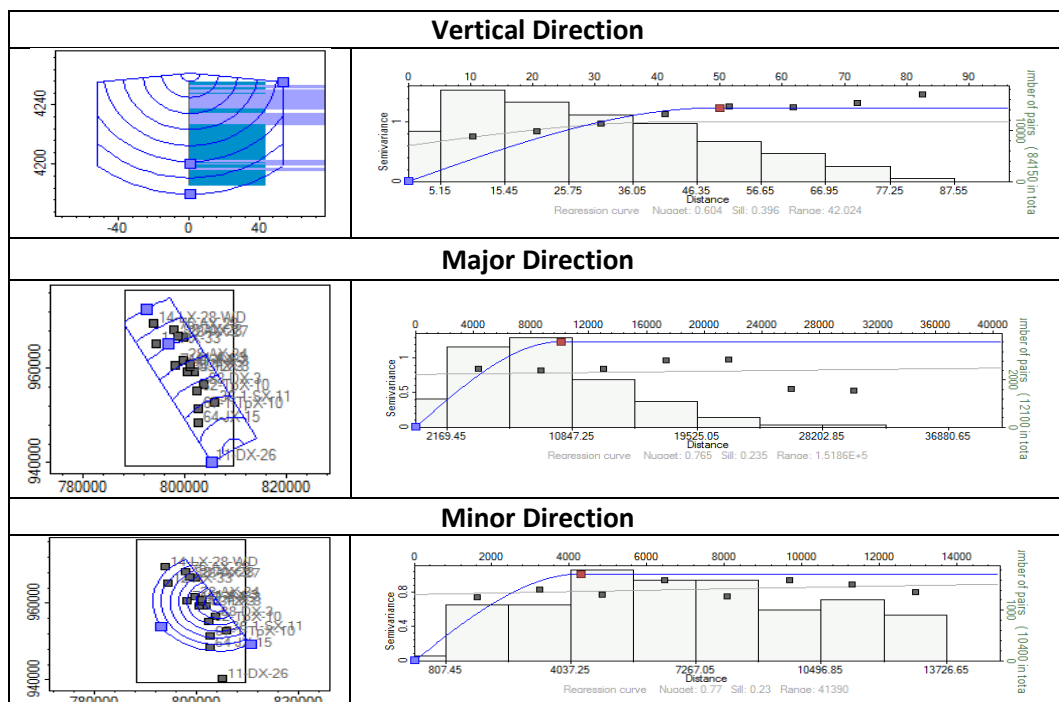


Figure 55 – IPSOM variogram

Once the proportional curves and variograms were adjusted, the Sequential Indicator Simulation (SIS) was used to model the facies (IPSOM classification) in the caprock.

The volumetric distribution of ductility (blue) and brittleness (purple) with the location of some wells can be observed in *Figure 56*. This 3D grid shows the location of the ductile and brittle regions. In overall, there are more ductile regions than brittle regions in the Teapot Dome field.

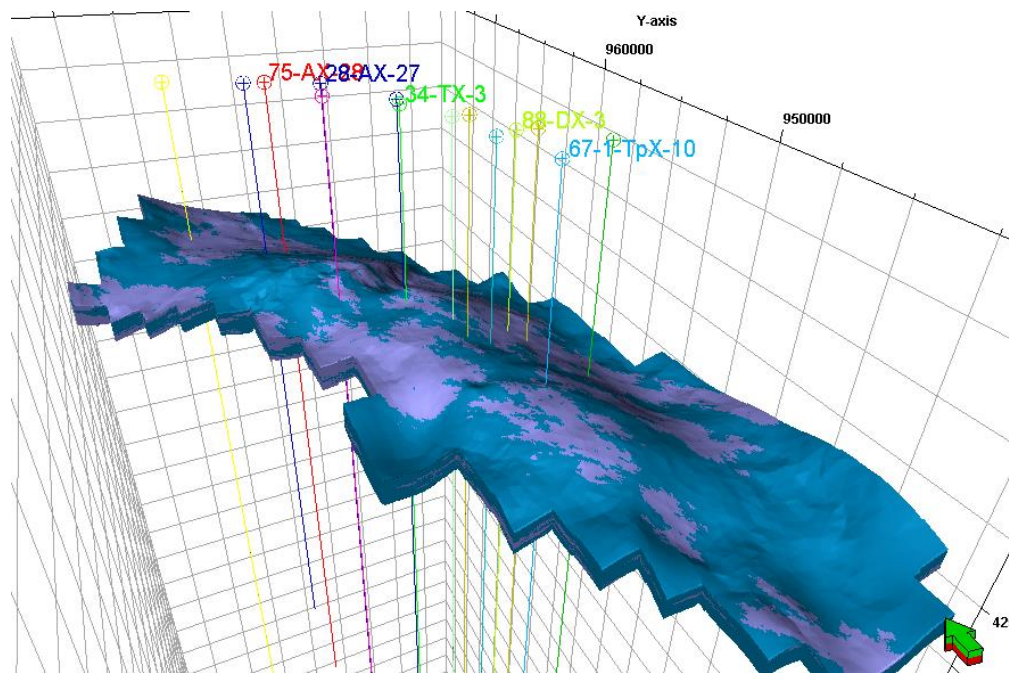


Figure 56 – Facies volume height map

8.4. Petrophysical Modeling

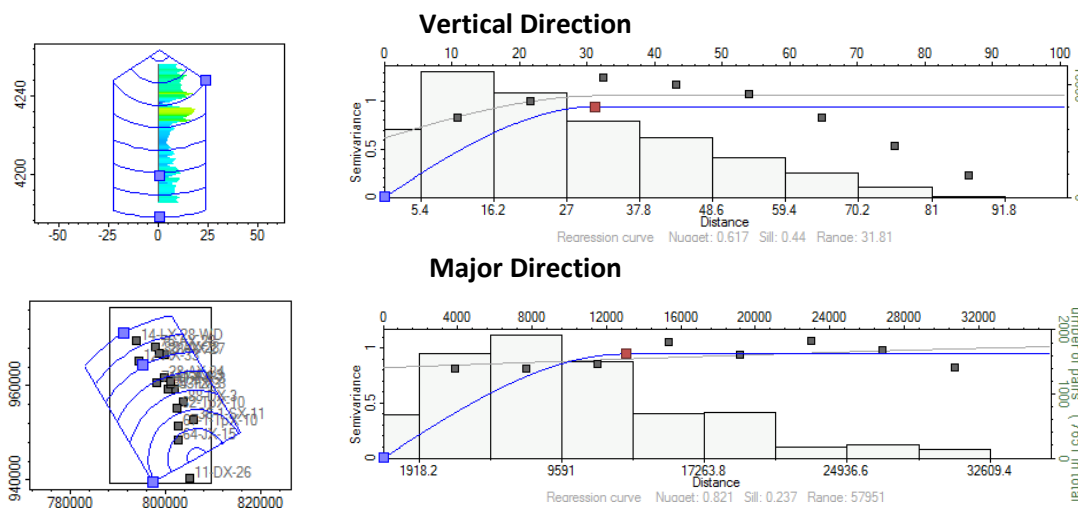
For the petrophysical modeling, it was used a conditional simulation, series of methods that simulates spatial and statistical characteristics. In this type of simulation, a random function of multivariate Gaussian form is assumed to represent the sample data, histograms and model variograms. In the simulation, each variable is transformed beforehand into a normal distribution because the technique requires a multi-Gaussian framework. Afterwards, the simulation results are back-transformed to the raw distribution. This transformed data is used to represent the sample values on a multivariate Gaussian function and to determine a probability function at each unsampled location (47).

Gaussian Random Function Simulation (GRFS) was chosen to simulate the mechanical strength of the caprock because it accurately reproduces the brittleness index distribution. Moreover, it is faster and efficient because of its parallel algorithm which is split into the Kriging base algorithm and the unconditional simulation that uses a fast Fourier transformation which gives an excellent variogram reproduction (47).

Instead of simulating the brittleness index and the IPSOM classification separately, the model was constrained to facies. This means that the IPSOM classification defines variograms and data distribution coming from raw logs. In other words, the group 1 (ductility) and group 2 (brittleness) delimit the distribution upfront which will resemble the final distribution.

The first step of the petrophysical modeling comprises the data analysis in which variograms and property transformations are defined by constraining the brittleness index with each IPSOM group.

Figure 57 shows the filtered data for vertical, major and minor direction for the group 1. It is observed that the points were adjusted in each case. Similar to the facies data analysis, the azimuth of the major direction was set as 330°.



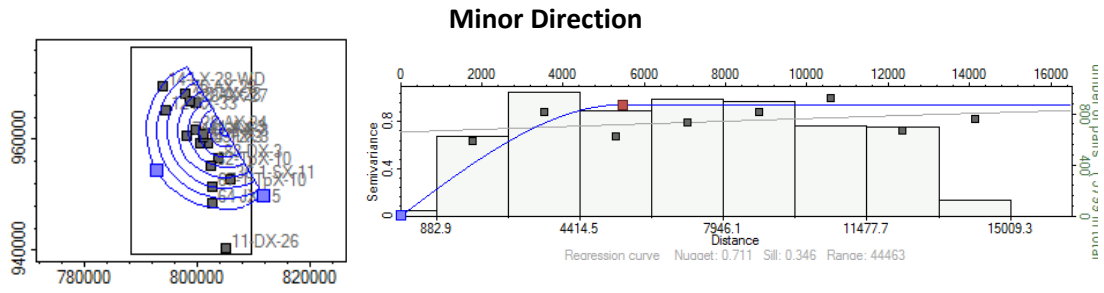


Figure 57 – Vertical, Major and minor direction for group 1

The procedure done for the group 1 was repeated for the group 2 of the IPSOM classification where the vertical, major and minor directions were adjusted and also the azimuth was set as 30° for the major direction.

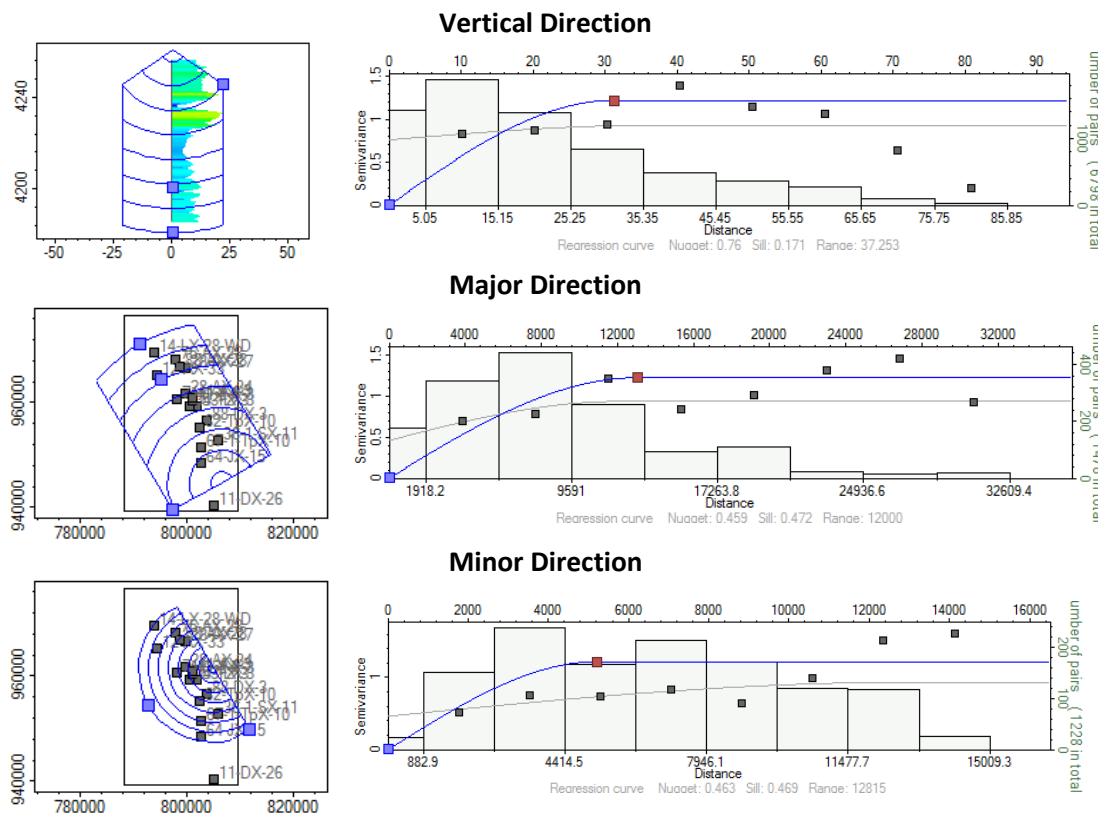


Figure 58 – Vertical, Major and minor direction for group 2

The only information available for the simulation are the variograms, and property transformation acquired previously. Usually, it would be preferred to model the brittleness using elastic properties obtained from seismic inversion. However, the

seismic data of the 2nd Wall Creek reservoir has a weak resolution at a depth of interest as can be seen in *Figure 50*.

Figure 59 shows the brittleness index distribution constrained to facies modeling obtained from petrophysical simulation and also the distribution resulting from facies modeling (purple color). Notice that the distribution in yellow color represents ductility because the data was filtered with the IPSOM classification group 1 and the distribution in pink color denotes the brittle classification. It can be seen that the results obtained from the simulation are consistent since there is a distinction between the group 1 (ductility) and group 2 (brittleness). In other words, the ductility distribution is moved to the left side (low values of BI), and the brittleness distribution is displaced to the right side (high BI values).

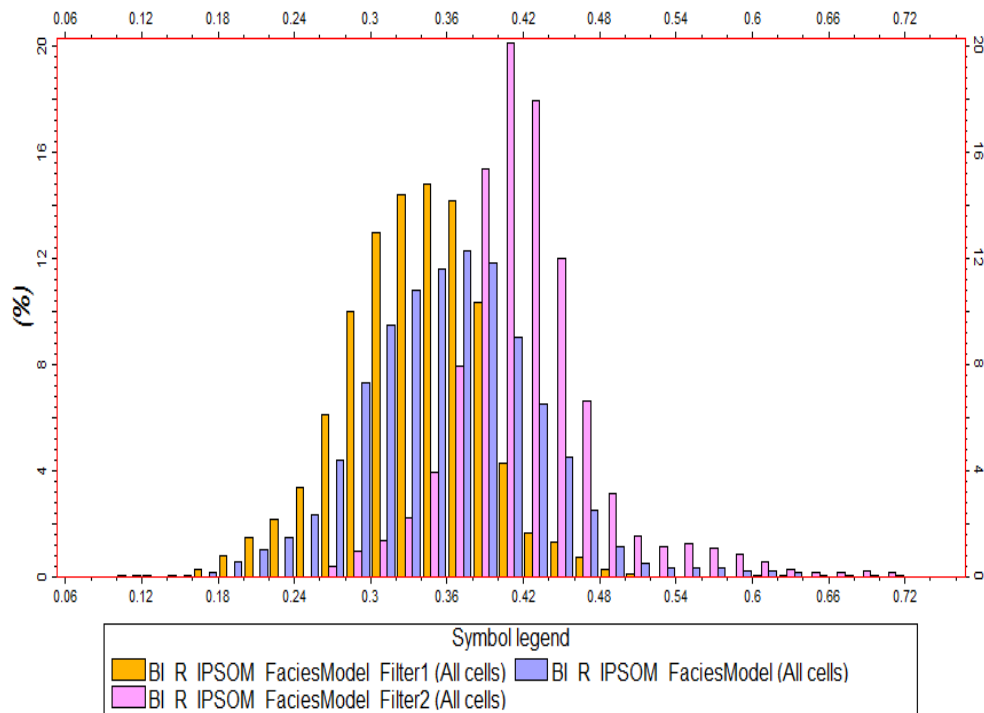


Figure 59 –Distribution of the modeled Brittleness index

Figure 60 presents a 3D volume height maps for the brittleness index filtered with the IPSOM classification and the location of some of the wells that penetrate the 2nd Wall Creek reservoir. It is important to highlight that *Figure 60 a)* was filtered with ductility



which has as thicker height column compared to *Figure 60 b)* which was filtered with brittleness.

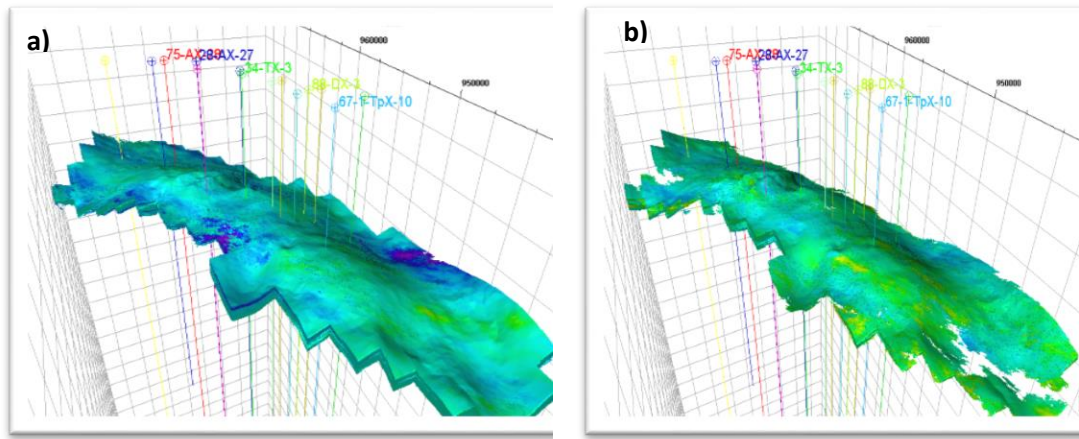


Figure 60 – Brittleness index volume height maps filtered with IPSOM classification

The average brittleness map can be found in *Figure 61*. In this map is represented the average values of BI. It can be noticed that there are two patches. The first patch has a high average BI (0.42); meaning that that region is highly brittle. The second patch, the purple area, is considered ductile since presents the lowest average BI. Notice that the zones with a BI < 0.4 have a good integrity.

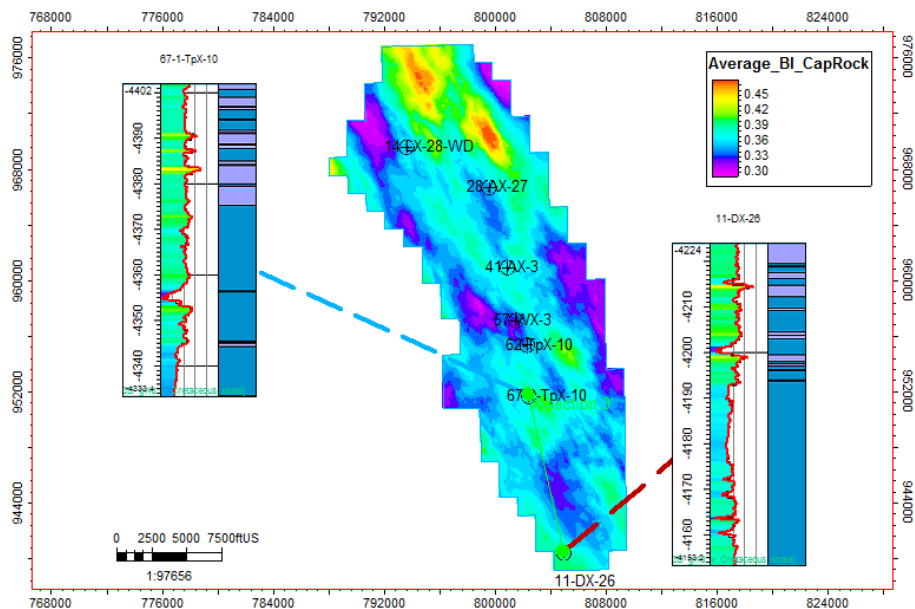


Figure 61 – BI average thickness map

8.5. Modeling Results

The results of the facies and petrophysical simulation are presented in the following proportional maps in which there is a clear distinction between the ductile and brittle zones in the caprock.

Figure 62 shows the ductility proportional thickness map and two reference wells, in which the first track corresponds to the brittleness index in the grid and the second track is related to the IPSOM classification. According to the color scale, the most ductile regions in the field are the ones highlighted with yellow and orange color. Those regions have a ductility percentage of 75% or higher. It is observed that those areas can be found widely distributed in the field.

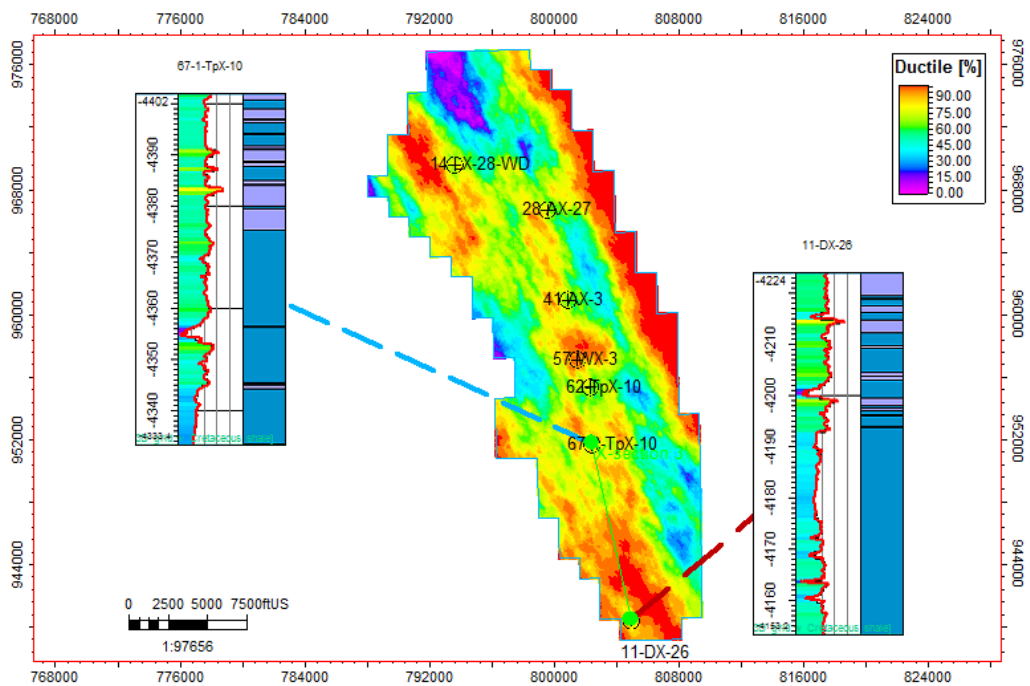


Figure 62 – Ductility proportional thickness map

The brittleness proportional map is found in *Figure 63*. According to this map, the most brittle areas within the field are the ones colored with yellow and orange color (75-90% brittleness). There are only 2 patches highly brittle in the caprock.

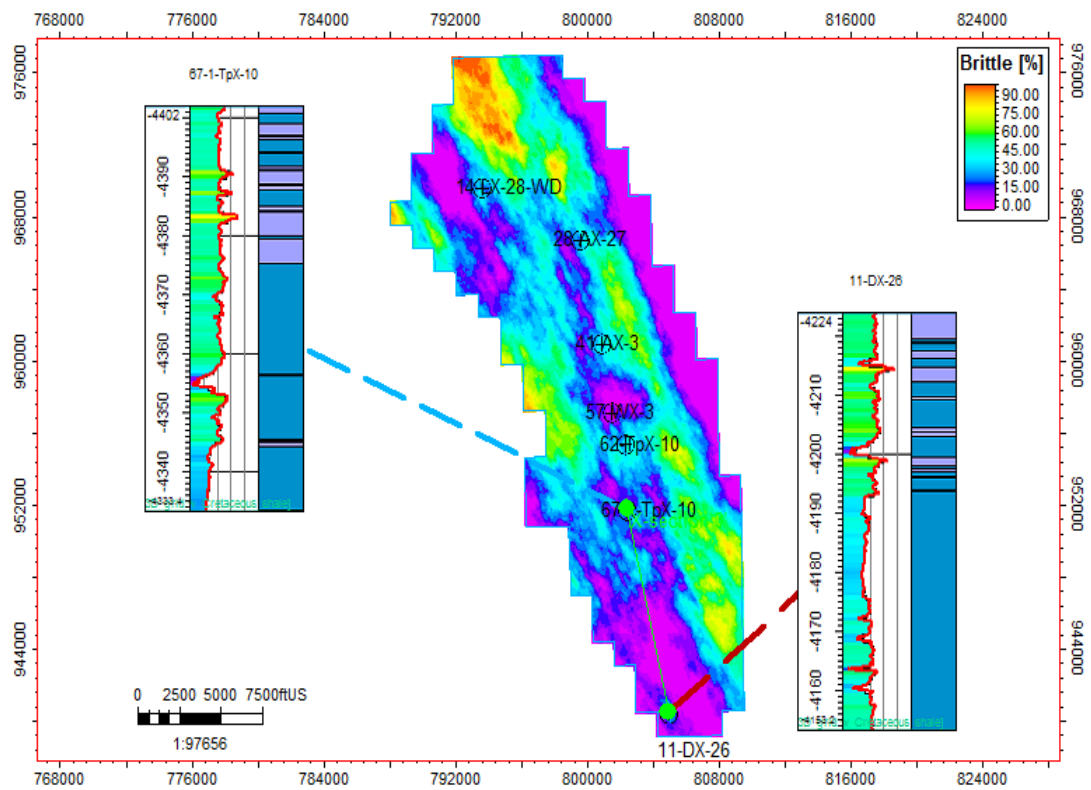


Figure 63 – Brittleness proportional thickness map

8.6. Drilling locations for the CO₂ injection wells

The CO₂ injection wells should be drilled in the areas where the caprock is highly ductile and has sufficient thickness. This will ensure the seal potential and therefore a long-term CO₂ storage.

The possible location of the new injector wells is represented with some stars in *Figure 64*. This map is based on the following relationship (Eq. 33), which relates the facies model to the petrophysical model since the caprock ductility percentage retrieved from the facies simulation (IPSOM classification group 1) and the average brittleness index was computed by the petrophysical simulation.

$$HighThickness_LowBI = \frac{Ductile}{(Average\ BI_R)(100\%)} \quad \text{Eq. 33}$$

According to the color scale, the most suitable drilling locations for CO₂ storage are the areas displayed in green color, high values of the parameter HighThickness_LowBI, because in those places, the ductility and thickness of the caprock are the highest (*Figure 64*). On the other hand, the patches in red/orange color, low values of the parameter HighThickness_LowBI, have small ductility and thickness and cannot be considered for CO₂ injection wells because the caprock is highly brittle which can cause an earlier failure. The zones in which the parameter HighThickness_LowBI is higher than 1.2, can be still considered for CO₂ injection. It can also be observed that the 18 wells are located in places where the caprock effectiveness is not compromised (green areas), and therefore they can be used for CO₂ injection into the 2nd Wall Creek reservoir.

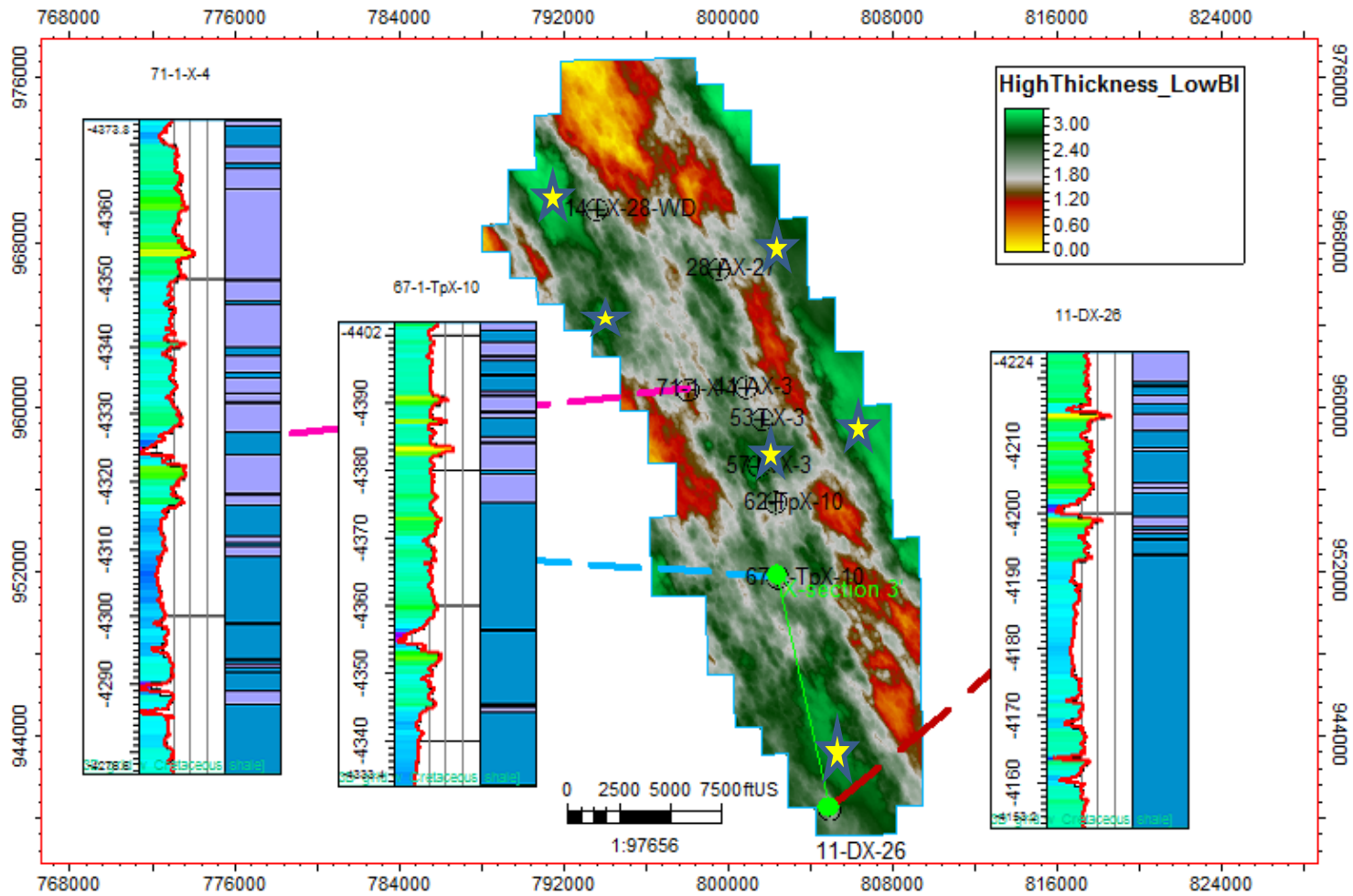


Figure 64 –Possible drilling locations for CO₂ storage

CONCLUSIONS

The petrophysical results indicated that the caprock of the 2nd Wall Creek reservoir could prevent the CO₂ horizontal leakage since the average thickness of this unit is approximately 85 m which is about 4.5 times thicker than the average reservoir height (approximately 19 m). Therefore, the caprock is reasonable for CO₂ storage even though its minimum thickness is 67.48 m at some places.

The mineralogical evaluation showed that shale mainly composes the 84% of the caprock and the remaining 16% corresponds to quartz, clay, dolomite and anhydrite. It can be inferred that clay is the principal mineral in the caprock; being highly concentrated at the base than at the top of the caprock as was presented in the Vsh figures.

The geomechanical study indicated that the caprock pore pressure is 1.05 SG; meaning that the horizontal stresses are lower and therefore faulting is less likely to occur. In addition, the results showed that caprock strength is relatively low since the unconfined compressive strength is 57 MPa and the tensile strength is 5.7 MPa

The dynamic elastic properties, Poisson's ratio and Young's modulus, suggested that the caprock is more ductile than brittle since the overall tendency of those parameters is high Poisson's ratio and low Young's modulus which corresponds to a ductile behavior.

The IPSOM classification predicted that the group 1 represents the 74% of the caprock and the group 2 the remaining 16%. By comparison with the dynamic elastic properties (Poisson's ratio and Young's modulus) it is concluded that group 1 denotes ductility and the group 2 indicates brittleness.

Different methods were used to calculate the brittleness index. However the most accurate approach was the Richman's method (BI_R) since it presented a good correlation with the IPSOM classification and the mineralogic composition of caprock. The BI_R showed low to moderate brittleness values in the ductile zones and high values in the brittle ones.

The caprock integrity was simulated by using facies modeling and petrophysical modeling. In the first one, the IPSOM classification groups (ductile and brittle) were



interpolated in the cells of the grid. The brittleness index was used in the petrophysical modeling. Due to the lack of properties derived from seismic inversion, this model was constrained to facies to get better results.

The average thickness map of brittleness index (BI) obtained from the petrophysical modeling showed that the caprock is mainly ductile since there are only two patches with a BI bigger than 0.4. in the full extension of the caprock. This result is confirmed in the ductility proportional map in which can be clearly seen a high percentage of ductility in the area. There are several zones with high thickness and low brittle index which are the most appropriated for drilling the new wells for CO₂ storage.

After the integrated petrophysical, geophysical and geomechanical analysis, it can be concluded that the caprock has a satisfactory integrity due to its thickness and reasonable ductility. Therefore, the 2nd Wall Creek reservoir can potentially be used for CO₂ storage.



FUTURE WORK

Future study will provide a better understanding in the caprock integrity of the 2nd Wall Creek reservoir. Specific investigation efforts can include:

- Obtain geomechanical properties of the caprock based on cores or core plugs from the Frontier formation and validate the results achieved with Techlog©
- Analyze leak-off tests (LOT) and fracture tests for geomechanical evaluation of the caprock
- Rerun the caprock simulation using a seismic survey that has a good resolution at the Frontier formation
- Use stochastic analysis to determine the sensitivity of the parameters, brittleness index and IPSOM classification
- Assess the geomechanical impact of having a compartmentalized reservoir
- Conduct a critical stress fault analysis and fluid flow simulation to model the CO₂ migration.
- Evaluate the volumes of CO₂ than can be injected into the reservoir without compromising the caprock integrity



REFERENCES

1. **Okojie, Anita.** *An Approach to Mapping of Shallow Petroleum Reservoirs Using Integrated Conventional 3D and Shallow P- and SH-Wave Seismic Reflection Methods at Teapot Dome Field in Casper, Wyoming.* Provo : Brigham Young University, 2007.
2. **Metz, Bert, et al.** *Carbon Dioxide Capture and Storage.* New York : Cambridge University Press, 2005. 13 978-0-521-68551-1.
3. **Friedmann, Julio and Stamp, Vicki.** *Teapot Dome: Site Characterization of a CO₂- Enhanced Oil Recovery Site in Eastern Wyoming.* Livermore : Lawrence Livermore National Laboratory, 2005.
4. **Chiaramonte, Laura, et al.** *Fracture Characterization and Fluid Flow Simulation with Geomechanical Constraints for a CO₂- EOR and Sequestration Project Teapot Dome Oil Field, Wyoming.* s.l. : ELSEVIER, 2011.
5. **Fleury, M, et al.** *Evaluating Sealing Efficiency of Caprocks for CO₂ Storage: an Overview of the Geocarbone-Integrity Program and Results.* Malmaison : Institut Français du Pétrole, 2010.
6. **Chantsalmaa, Dalkhaa.** *Caprock Integrity in CO₂ Storage.* Ankara : Middle East Technical University, 2010.
7. **Busch, A, et al.** *The Significance of Caprock Sealing INtegrity for CO₂ Storage.* New Orleans : Society of Petroleum Engineers, 2010.
8. **IEAGHG.** *Caprock Systems for CO₂ Geological Storage.* Cheltenham : International Energy Agency, 2011.
9. **Khan, S, et al.** *An Integrated Geomechanics Workflow for Caprock-Integrity Analysis of a Potential Carbon Storage.* New Orleans : Society of Petroleum Engineers, 2010.
10. **Downey, Marlan W.** *Evaluating seals for hydrocarbon accumulations.* s.l. : The american association of petroleum geologist, 1984. pp. 1752-1763.
11. **Allen, Philip and Allen, Jhon.** *Data Analysis: Principles and Applications.* Billiton : WILEY, 1990.



12. **Niemi, Auli, Bear, Jacob and Bensabat, Jacob.** *Geological Storage of CO₂ in Deep Saline Formations.* Dordrecht : Springer, 2017.
13. **Chang, Yang.** *CO₂ Sequestration and EOR Cooptimization in a Mature Field: TEAPOT DOME, WYOMING.* Ann Arbor : ProQuest LLC, 2014.
14. **Fox, J., Dolton, G. and Clayton, J.** *Power River Basin.* s.l. : US: Geological Society of America, 1991.
15. **Cooper, Scott, Laurel B, Goodwin and Lorenz, John.** *Fracture and fault patterns associated with basement-cored anticlines: The example of Teapot Dome.* Wyoming : AAPG, 2006.
16. **Cooper, S.** *Deformation within a basement-cored anticline Teapot Dome.* Wyoming : New Mexico Institute of Mining and Technology, 2000.
17. **Zhang, Ye, et al.** *An Uncertainty Analysis of Modeling Geologic Carbon Sequestration in a Naturally Fractured Reservoir at Teapot Dome.* Wyoming : University of Wyoming, 2014.
18. **Towse, Donald.** *The Frontier Formation in the Southwest Power River Basin, Wyoming.* Massachusetts : Massachusetts Institute of Technology, 1951.
19. **Merewether, E.A.** *Stratigraphy and Tectonic Implications of Upper Cretaceous Rocks in the Powder River Basin, Northeastern Wyoming and Southeastern Montana.* Denver : U.S.Geological Survey Bulletin, 1917.
20. **Lawrence, Anna.** *Geologic Assessment of Undiscovered Oil and Gas in the Powder River Basin Province, Wyoming and Montana.* Virginia : USGS, 2009.
21. **Cant, Douglas.** *Subsurface Facies Analysis.* Calgary : s.n., 2000.
22. **Rider, Malcolm.** *The Geological Interpretation of Well Logs.* Scotland : Rider-French Consulting Ltd, 2000. 0-9541906-0-2.
23. **Glover, Paul.** *Petrophysics Notes.* Aberdeen : University of Aberdeen.
24. **Rockhold, ML, Sullivan, EC and Murray, CJ.** *Data Assimilation Tools for CO₂ Reservoir Model DEvelopment- A Review of Key Data Types, Analyses, and Selected Software.* Springfield : Pacific Northwest National Laboratory, 2009.
25. **Hallenburg, James.** *Standard Methods of Geophysical Formation Evaluation.* New York : Lewis Publishers, 1998.



26. **Bery, Andy and Saad, Rosli.** *Correlation of Seismic P-Wave Velocities with Engineering Parameters (N Value and Rock Quality) for Tropical Environmental Study.* Penang : International Journal of Geosciences, 2012.
27. **Mavko, Gary, Mukerji, Tapan and Dvorkin, Jack.** *The Rock Physics Handbook.* Edinburgh : Cambridge University Press, 2009.
28. **Dandekar, Abhijit Y.** *Petroleum Reservoir Rock and Fluid Properties.* 2nd edition. s.l. : Taylor & Francis Group, 2013.
29. **Schultz, Richard.** *Rock Mechanics Proceeding of the 35th U.S. Symposium.* Rotterdam : University of Nevada, 1995.
30. **Emujakporue, G and Ekine, A.** *Determination of Rocks Elastic constants from Compressional and Shear Waves Velocities for Western Niger Delta, Nigeria.* Nigeria : Journal of Applied Sciences and Environmental Management, 2009.
31. **Joo, Tat, Yang, Guilin and Ming, I.** *Compliant Manipulators.* s.l. : Springer, 2014.
32. **Perez, Roderick.** *Brittleness Estimation from Seismic Measurements in Unconventional Reservoirs: Application to the Barnett Shale.* Oklahoma : University of Oklahoma, 2013.
33. **Zoback, M, et al.** *Determination of stress orientation and magnitude in deep wells.* California : PERGAMON, 2003.
34. **Peng, Suping and Zhang, Jincai.** *Engineering Geology for Underground Rocks.* Berlin : Springer, 2007.
35. **Zhang, Jincai.** *Pore Pressure Prediction from Well Logs: Methods, Modifications, and New Approaches.* Houston : ELSEVIER, 2011.
36. **Afrouz, Andy.** *Rock Mass Classification Systems and Mode of Ground Failure.* Boca Raton : CRC Press, 1992.
37. **Fox, Amy, et al.** *Geomechanical Principles for Unconventional Reservoirs.* s.l. : MicroSeismic, 2003.
38. **Xu, Hao, et al.** *Characterization of Rock Mechanical Properties Using Lab Tests and Numerical Interpretation Model of Well Logs.* Chengdu : Hindawi Publishing Corporation, 2016.



39. **Tove, Linn.** *Relating Acoustic Wave Velocities to Formation Mechanical Properties.* Trondheim : Norwegian University of Science and Technology, 2012.
40. **Nygaard, Runar.** *Wabamun Area CO2 Sequestration Project.* Calgary : Energy& Environmental Systems, 2010.
41. **Zhang, Decheng, Ranjith, P.G. and Perera, M.** *The Brittleness Indices Used in Rock Mechanics and Their Application in Shale Hydraulic Fracturing: A Review.* Australia : Journal of Petroleum Science and Engineering, 2016.
42. **Rickman, R, et al.** *A Practical Use of Shale Petrophysics for Stimulation Design Optimization: All Shale Plays Are Not Clones of the Barnett Shale.* s.l. : Society of Petroleum Engineering, 2008.
43. **Wang, F. and Gale, J.** *Screening criteria for shale-gas systems.* s.l. : Gulf Coast Association of Geological Transactions, 2009.
44. **Schlumberger.** Glossary Oilfield. [Online] Schlumberger. [Cited: may 24, 2017.] http://www.glossary.oilfield.slb.com/Terms/f/facies_modeling.aspx.
45. **Deutsch, Clayton V.** *A Sequential Indicator Simulation Program for Categorical Variables with Point and Block Data: BlockSIS.* Alberta : Computer and Geosciences, 2006.
46. **Ersoy, Adem, Yusuf, Tayfun and Atici, Umit.** *Geostatistical Conditional Simulation for the Assessment of Contaminated Land by Abandoned Heavy Metal Mining.* Nigde : Wiley Periodicals, Inc, 2007.
47. **Hyne, Norman J.** *Nontechnical Guide to petroleum geology, exploration, drilling & production third edition.* 3rd edition. s.l. : Pennwell, 2012.
48. **Bassiouni, Zaki.** *Theory, Measurements, and Interpretation of Well Logs.* Richardson : Society of Petroleum Engineers, 1994.
49. **Donnez, Pierre.** *Essentials of reservoir engineering Volume II.* Paris : Technip, 2012. Vol. II.
50. **Asquith, George and Krygowski, Daniel.** *Basic well log analysis, second edition.* 2nd edition. s.l. : AAPG, 2004.



APPENDIXES

APPENDIX 1 – WELL LOGGING TOOLS AND PRINCIPLES

Well logs are different measurements made in the well bore space by different tools that work under mechanical, radioactive, acoustic and electric principles. They are used to identify the key rock properties such as lithology, porosity and fluid composition (47). Even though the measurements can be done in an open-whole or cased-hole (open-whole indicates that the formation has not been covered by a casing, as opposed to cased-hole, in which the casing lines the well), most logs are recorded in open whole in order to evaluate all the petrophysical properties of the subsurface formation.

Figure 1. 1 is a schematic diagram of a wireline logging setup. After the last casing shoe has been cemented and the well has been cleaned, a logging truck, unit that contains a logging cable, winch, self-contained generator and a digital recording system, place down logging tools attached to a wireline in the well where the measurements are recorded. The logging data is transmitted digitally by the electrical wire and recorded for further processing and analysis (47).

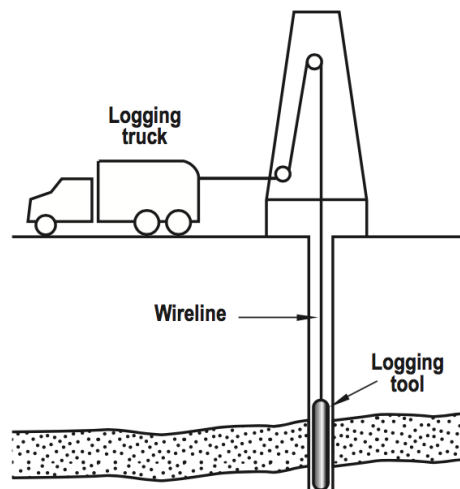


Figure 1. 1 – Well logging setup (47)

The most common wireline logs are: gamma ray (GR), bulk density (RHOB), photoelectric effect log (PEF), neutron (NPHI), compressional slowness log (DT) and resistivity logs. Other logging tools such as spontaneous potential log (SP) and caliper can also be included in the assembly. In this section, it is described the well logs that were used for the petrophysical analysis of the caprock of the 2nd Wall Creek reservoir.

1.1. GAMMA RAY (GR)

The gamma ray tool uses a non-artificial radiation source to measure the natural radioactivity of the formation since the rocks contain various amounts radioactive minerals such as potassium, thorium and uranium. Those elements are concentrated in shales because the surface of clay particles absorb them. On the other hand, the amount of radioactive minerals in the shale-free sandstones and carbonates is small because the chemical environment during the deposition of the sediments is not favorable for the accumulation of radioactive minerals. Figure 1. 2 is an illustration of the gamma ray log. It can be noticed that the response is higher in shales than sandstones.

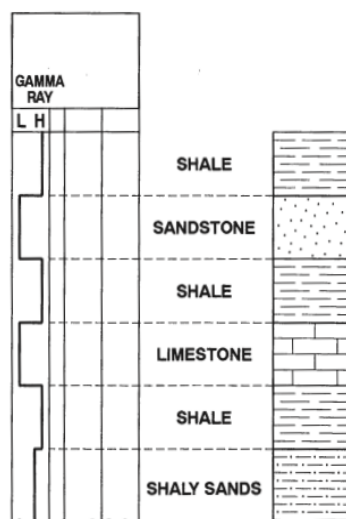


Figure 1. 2 – Gamma Ray response (47)

Principle

The gamma rays are electromagnetic waves emitted by some radioactive elements such as potassium, potassium, thorium and uranium. The gamma rays scattered and lose energy due to the following interactions: Compton scattering (energy loss because of collision with atoms in the formation), photo electric effect (low-energy gamma photon transfers all its energy to an inner orbital electron and as a consequence the electron is ejected from the atom) and pair production (the photon interacts with a nucleus and creates a positron, e^+ , and negatron, e^-) (48).

The gamma ray sonde contains a detector with a scintillation crystal counter. It is used to measure the natural radioactivity of the formation by a photomultiplier that

records the light produced by the gamma rays when they strike the scintillation. The measurement unit is API and counts the amount of gamma ray striking the detector in a period of time. (49) (50)

Use

- Identify bed boundaries for stratigraphic correlations
- Determine the shale content of the formation
- Depth control
- Identify radioactive deposits

1.2. BULK DENSITY LOG (RHOB)

The density logging tool records the formation's bulk density which includes both minerals forming the rock and fluids filling the pore space. It can be run into the well alone or in combination with another tool such as neutron logging tool (NPHI) and used as an indicator of primary porosity. This log has a shallow depth of investigation so the tool is placed against the wellbore in order to record the density of the formation (49). In Figure 1. 3 is represented that bulk density for different lithologies.

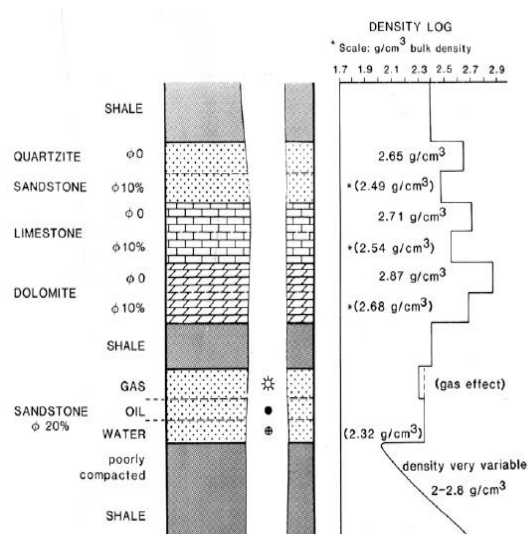


Figure 1. 3 – Bulk Density log (22)

Principle

The density logging tool uses a radioactive source such as Cesium-137 to emit medium- high energy gamma rays to the formation. It scatters the attenuation of the gamma rays between the source and detectors. This occurs because of the Compton effect in which the gamma rays lose energy when they pass through the formation.

Therefore, the attenuation is a function of the number of electrons contained by the formation which is related to its density. When the formation is denser, a few detectable gamma rays reach the detector because the rock has more atoms per unit of volume. Conversely, the scattering is higher in porous rocks (49) (50).

Use

- Determination of porosity and lithology
- Identification of mineral content in evaporites
- Gas detection
- Evaluation of complex lithologies such as shaly sands
- Overpressure identification
- Determination of hydrocarbons density

1.3. PHOTOELECTRIC FACTOR LOG (PEF)

This log records the effective photoelectric absorption index (PE) of the formation which depends on the average atomic number of the elements that constitute the formation. Figure 1. 4 indicates the response of the photoelectric factor log for different lithologies, including shale, dolomite, limestone, sandstone (2).

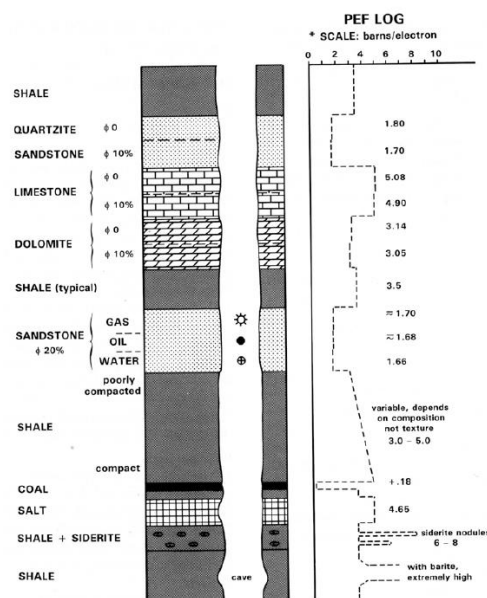


Figure 1. 4 – Photoelectric Factor log (22)

Principle

The photoelectric factor logging tool measures the formation photoelectric absorption index by using a radioactive source that emits gamma ray that collides with the formation. The absorption depends on the average atomic number of the rock matrix and it is not affected by the pore space (47).

Use

- Evaluation of the lithology and composition of the formation
- Matrix indicator

1.4. NEUTRON LOG (NPHI)

The neutron log is used to evaluate the formation's porosity by measuring the hydrogen index. In clean formations, the pore space is filled with hydrocarbons or water; thus, it gives a real value of the pore space filled with fluids (47) (50). Figure 1.5 shows the neutron porosity values for different lithologies.

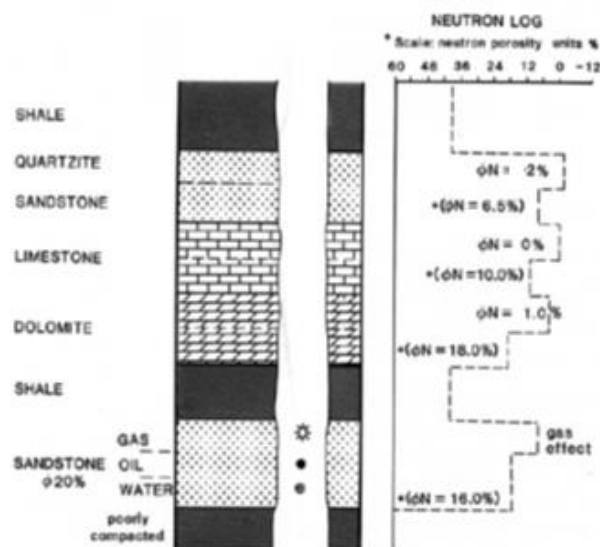


Figure 1.5 – Neutron log (22)

Principle

The neutron logging tool has a radioactive source that uses a mixture of americium and beryllium to emit continuously high-speed neutrons to the formation. When the neutrons collide elastically with particles that has the same mass (hydrogen nuclei), there is significant energy loss. As a consequence, most of the neutrons lose velocity

and are captured within short time. On the other hand, if the neutrons collide with heavy particles, there is not a significant velocity loss (inelastic scattering) and they can travel further from the source before being captured. In this case, the lecture of the logging tool is higher (47) (50).

Use

- Determination of porosity directly from the log
- Interpretation of lithology
- Gas identification
- Evaluation of clay content, shaliness in the rock

1.5. RESISTIVITY LOGS

The resistivity logging tool measures the formation's resistivity (resistance of a compound to the passage of the current) to identify the fluid type in the pore space. Since the formation water is less resistive than the hydrocarbons, this log is used to distinguish between zones bearing hydrocarbons and formation water. The resistivity log for different lithologies is shown in Figure 1. 6. It can be seen that the reading values in the sandstone unit are high which indicates that the main fluid in the pore space is hydrocarbons.

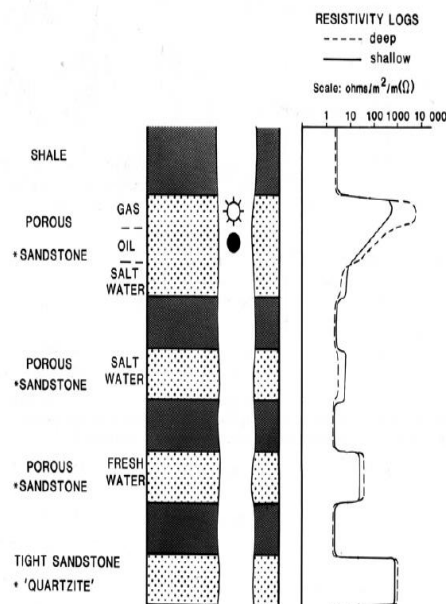


Figure 1. 6 – Resistivity logs (22)

Principle

A localized electrical current is sent through the formation by some electrodes and is measured the potential drop between other electrodes. The advantages of using focused currents are: reduce the borehole effects and can be sent directly to the required areas (22) (47)

Use

- Define oil and water bearing zones
- Estimation of the porosity
- Calculation of water saturation
- Formation correlation
- Indication of lithology changes based on a resistivity map

1.6. COMPRESSIONAL SLOWNESS LOG (DT)

The compressional slowness log records the capacity of the formation to transmit sound waves which is a function of porosity, lithology and rock texture. This is expressed as interval transit time (Δt) and is measured in $\mu\text{ft}/\text{ft}$. Figure 1. 7 indicates the capacity of different lithologies to transmit the sound waves.

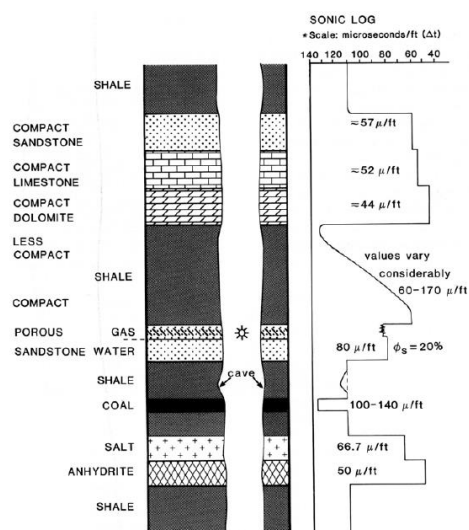


Figure 1. 7 –Compressional Slowness log (22)

Principle

The compressional slowness logging tool uses transducers and receivers to measure the travel time that the sound wave takes to reach the receivers. The transducer,

which is piezoelectric, converts an electrical signal into an ultrasonic vibration that is sent to the formation. The receivers, on the other hand, provide the logging signal by converting the pressure waves into electromagnetic signals. The sound speed depends on the type of rock. It is slow for shale, intermediate for sandstones and fast for dolomite and limestone (47) (50).

Use

- Lithology indicator
- Porosity
- Well correlation
- Indication of fractures
- Estimation of mechanical properties
- Identify over-pressure

APPENDIX 2 – WELL CORRELATION

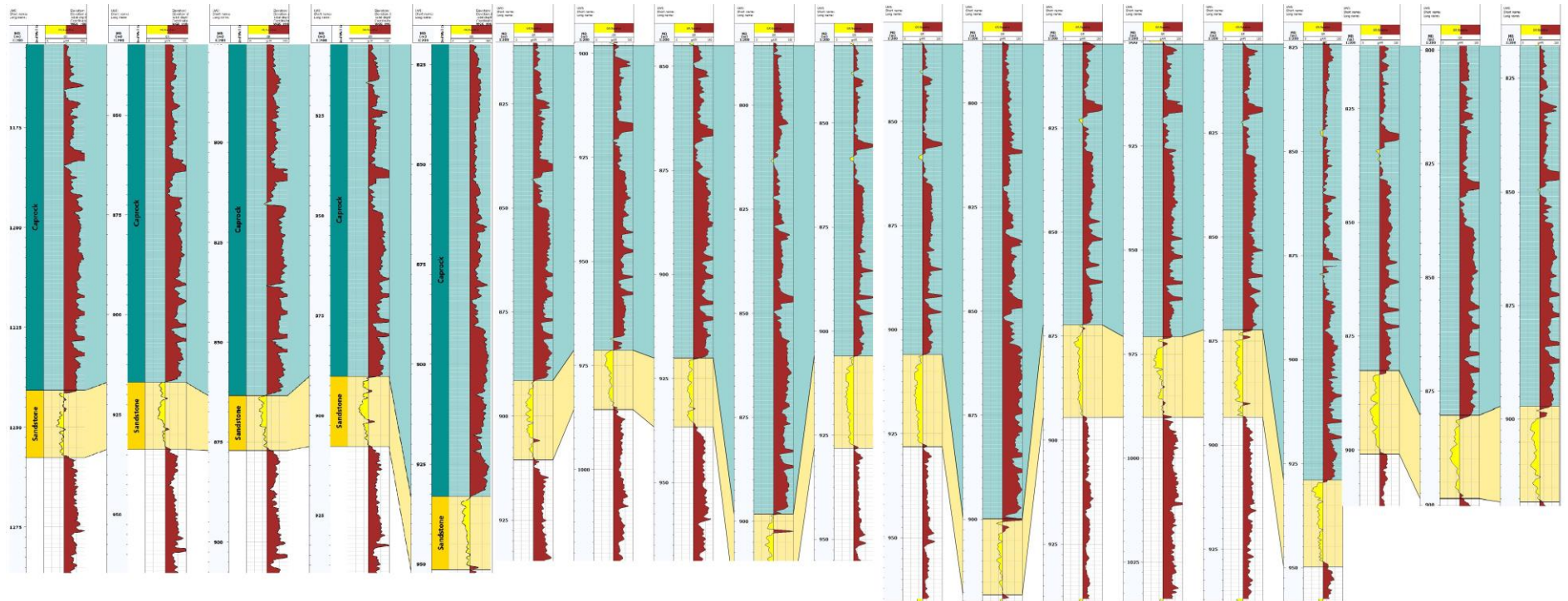


Figure 2. 1 – Correlation across the 18 wells that penetrates the 2nd Wall Creek Reservoir

APPENDIX 3 – SHALE VOLUME

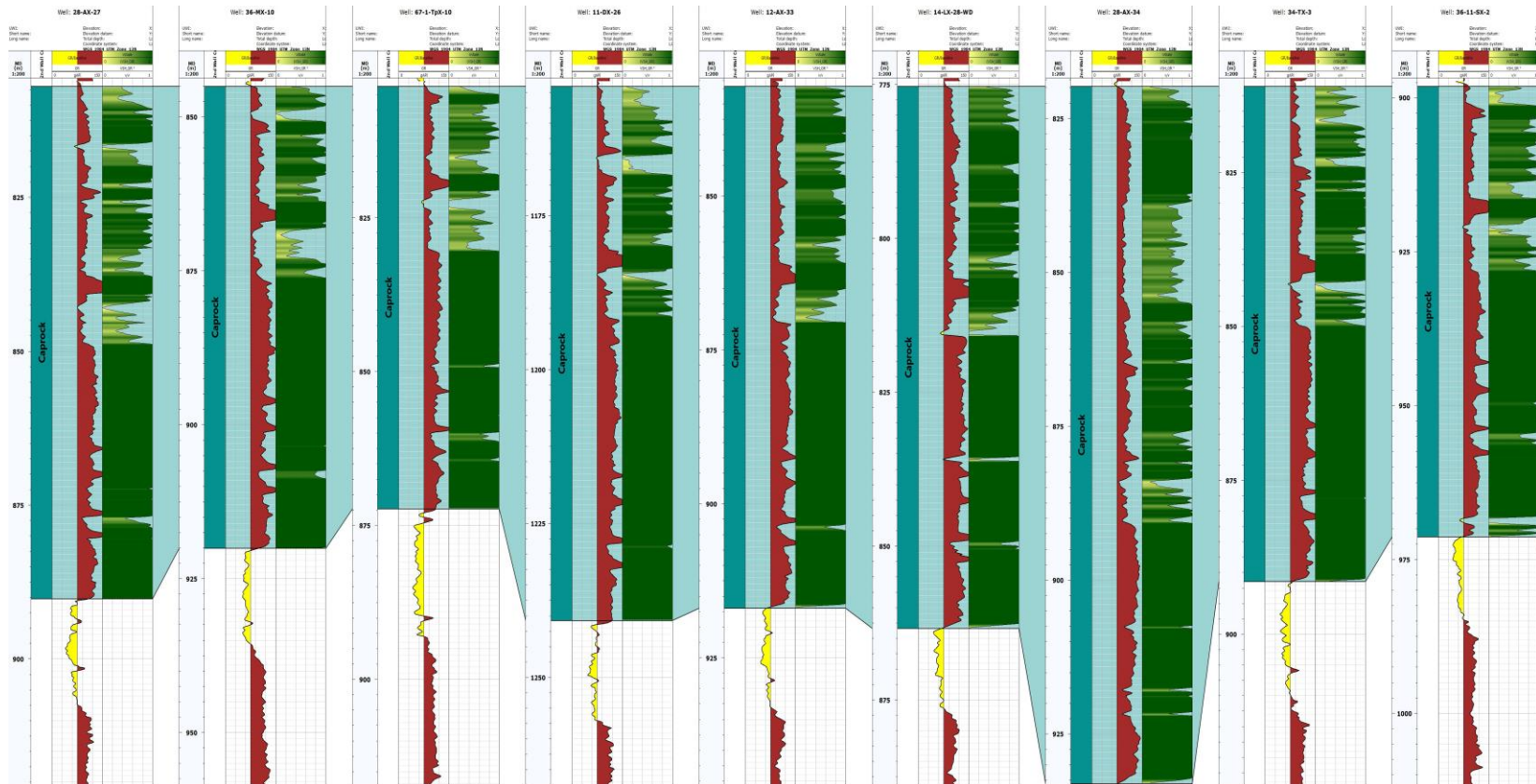


Figure 3. 1 - Shale volume calculation for the wells from left to right: 28-AX-27, 36-MX-10, 67-1-TPX-10, 11-DX-26, 12-AX-33, 14-LX-28-WD, 28-AX-34, 34-TX-3, 36-11-SX-2

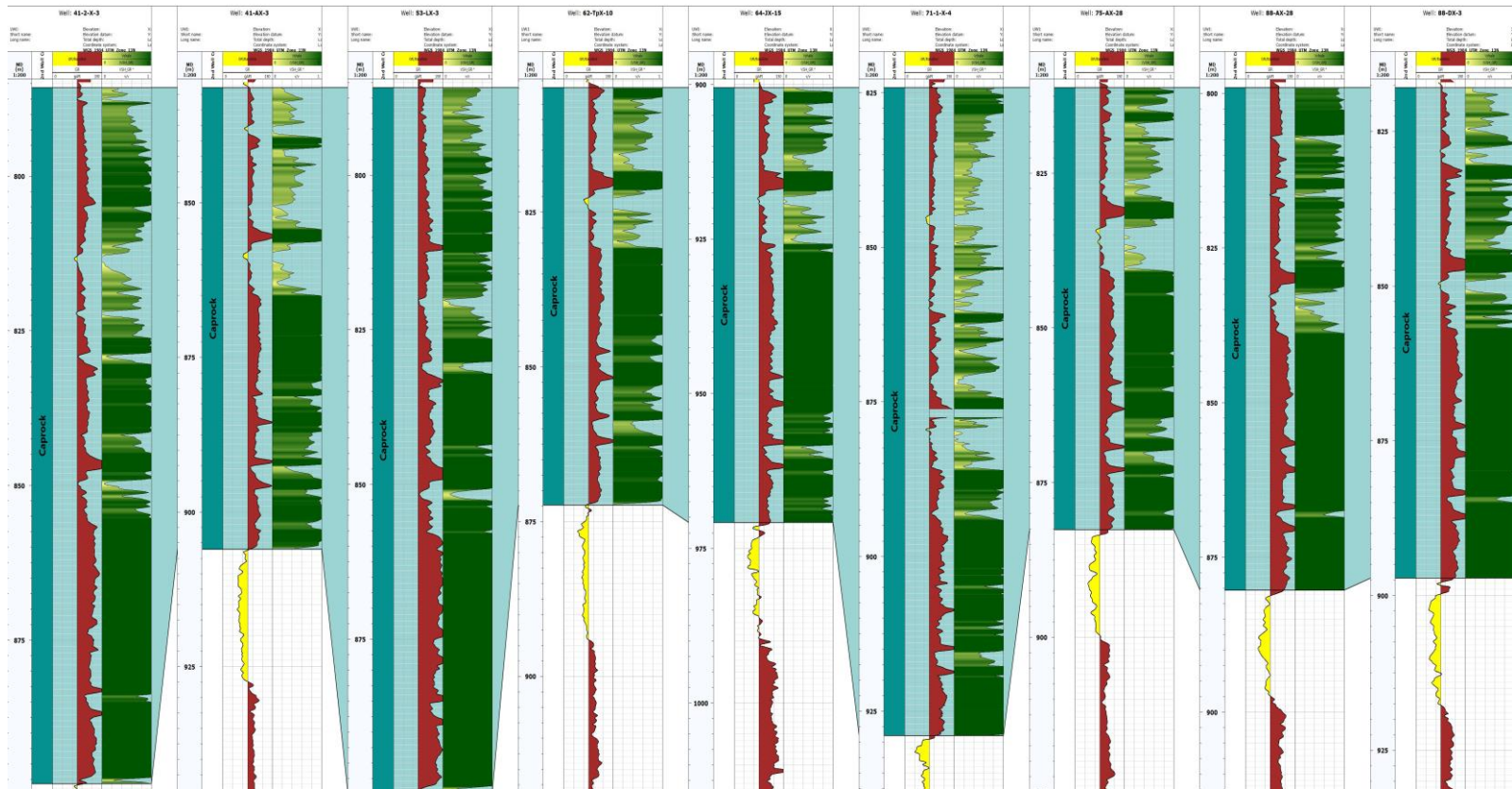


Figure 3. 2 - Shale volume calculation for the wells from left to right: 41-2-X-3, 41-AX-3, 53-LX-3, 62-TPX-10, 64-JX-15, 71-1-X-4, 75-AX-28, 88-AX-28, 88-DX-3

APPENDIX 4 – TOTAL AND EFFECTIVE POROSITY

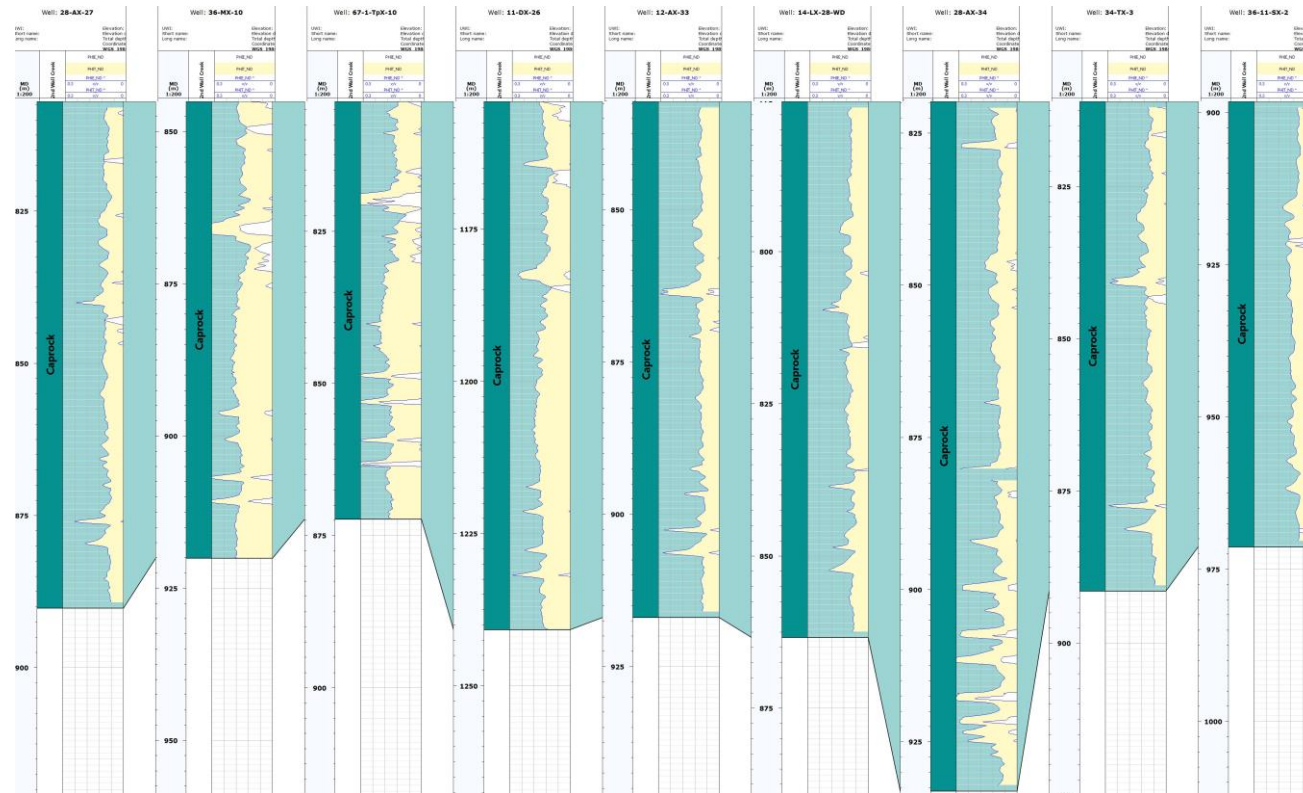


Figure 4. 1- Total and effective porosity for the wells from left to right: 28-AX-27, 36-MX-10, 67-1-TPX-10, 11-DX-26, 12-AX-33, 14-LX-28-WD, 28-AX-34, 34-TX-3, 36-11-SX-

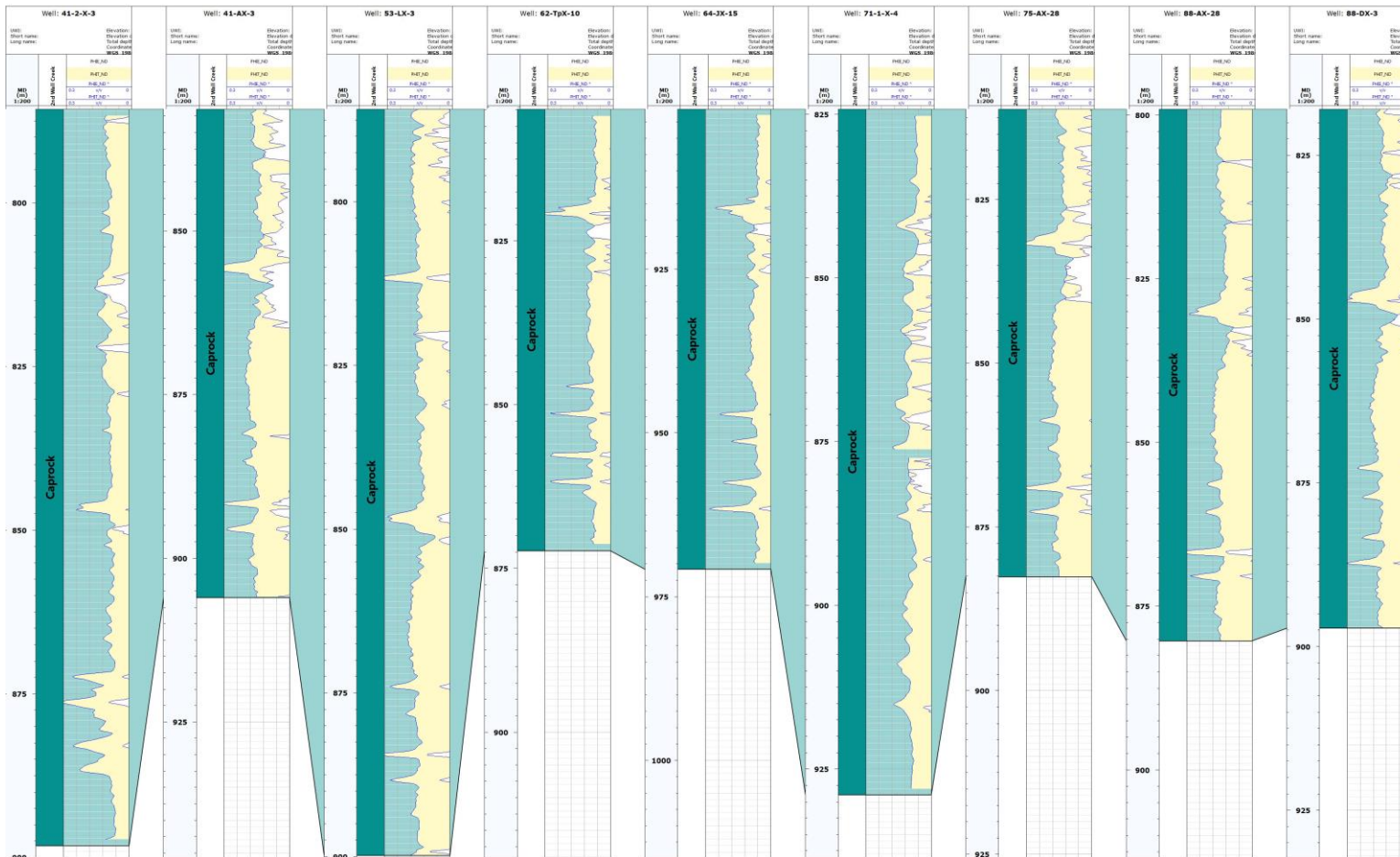


Figure 4. 2 - Total and effective porosity for the wells from left to right: 41-2-X-3, 41-AX-3, 53-LX-3, 62-TPX-10, 64-JX-15, 71-1-X-4, 75-AX-28, 88-AX-28, 88-DX-3

APPENDIX 5 – WATER SATURATION

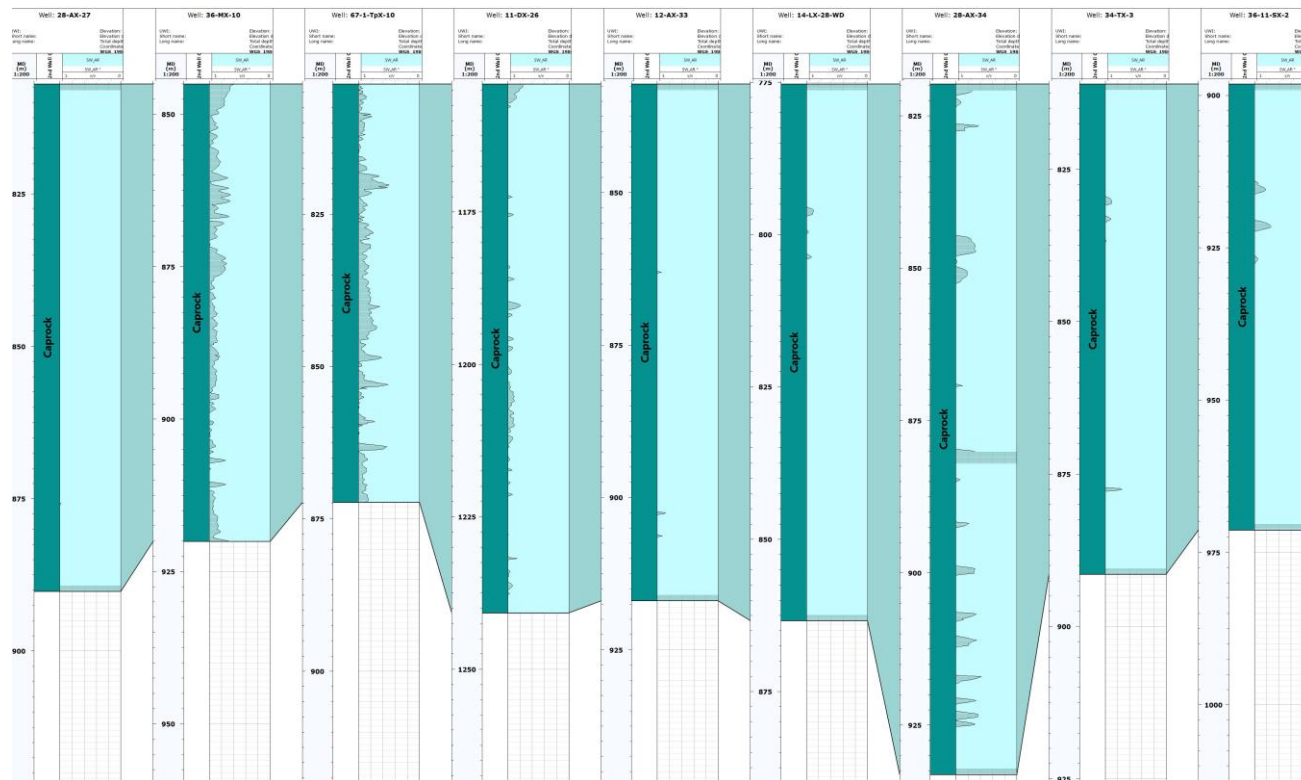


Figure 5. 1 - Water saturation for the wells from left to right: 28-AX-27, 36-MX-10, 67-1-TPX-10, 11-DX-26, 12-AX-33, 14-LX-28-WD, 28-AX-34, 34-TX-3, 36-11-SX-2

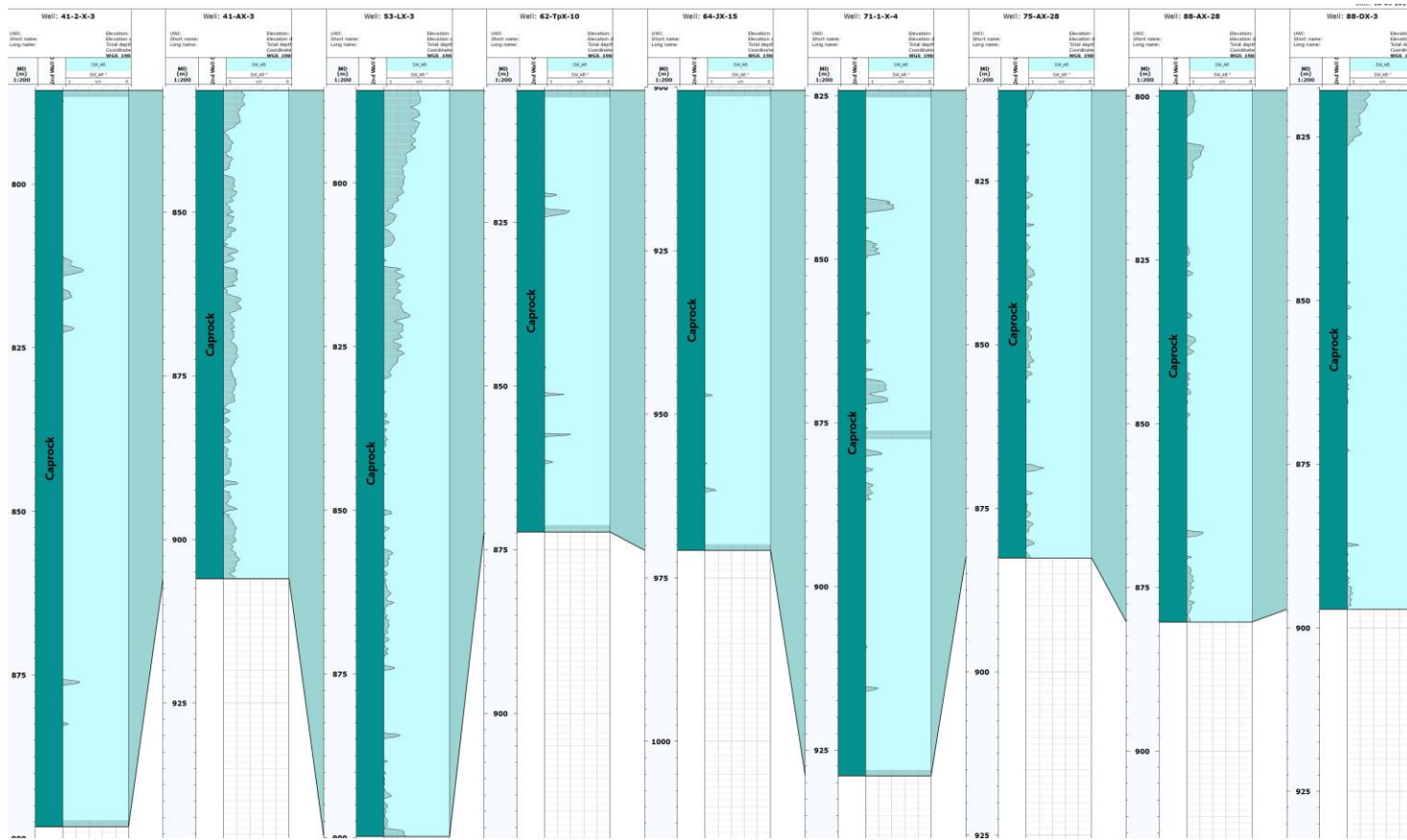


Figure 5. 2 - Water saturation for the wells from left to right: 41-2-X-3, 41-AX-3, 53-LX-3, 62-TPX-10, 64-JX-15, 71-1-X-4, 75-AX-28, 88-AX-28, 88-DX-3

APPENDIX 6 – MINERALOGY

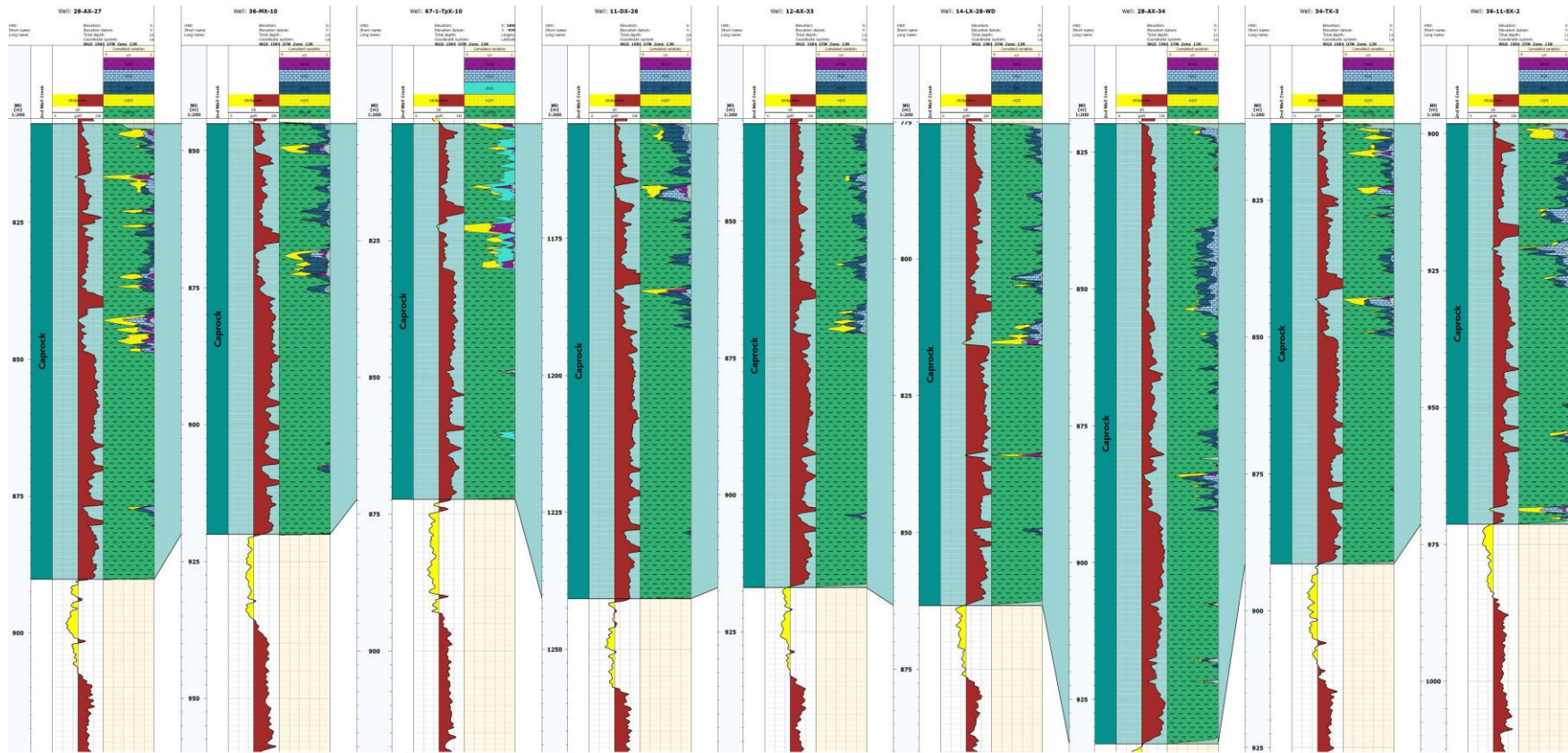


Figure 6. 1- Mineralogy for the wells from left to right: 28-AX-27, 36-MX-10, 67-1-TPX-10, 11-DX-26, 12-AX-33, 14-LX-28-WD, 28-AX-34, 34-TX-3, 36-11-SX-2

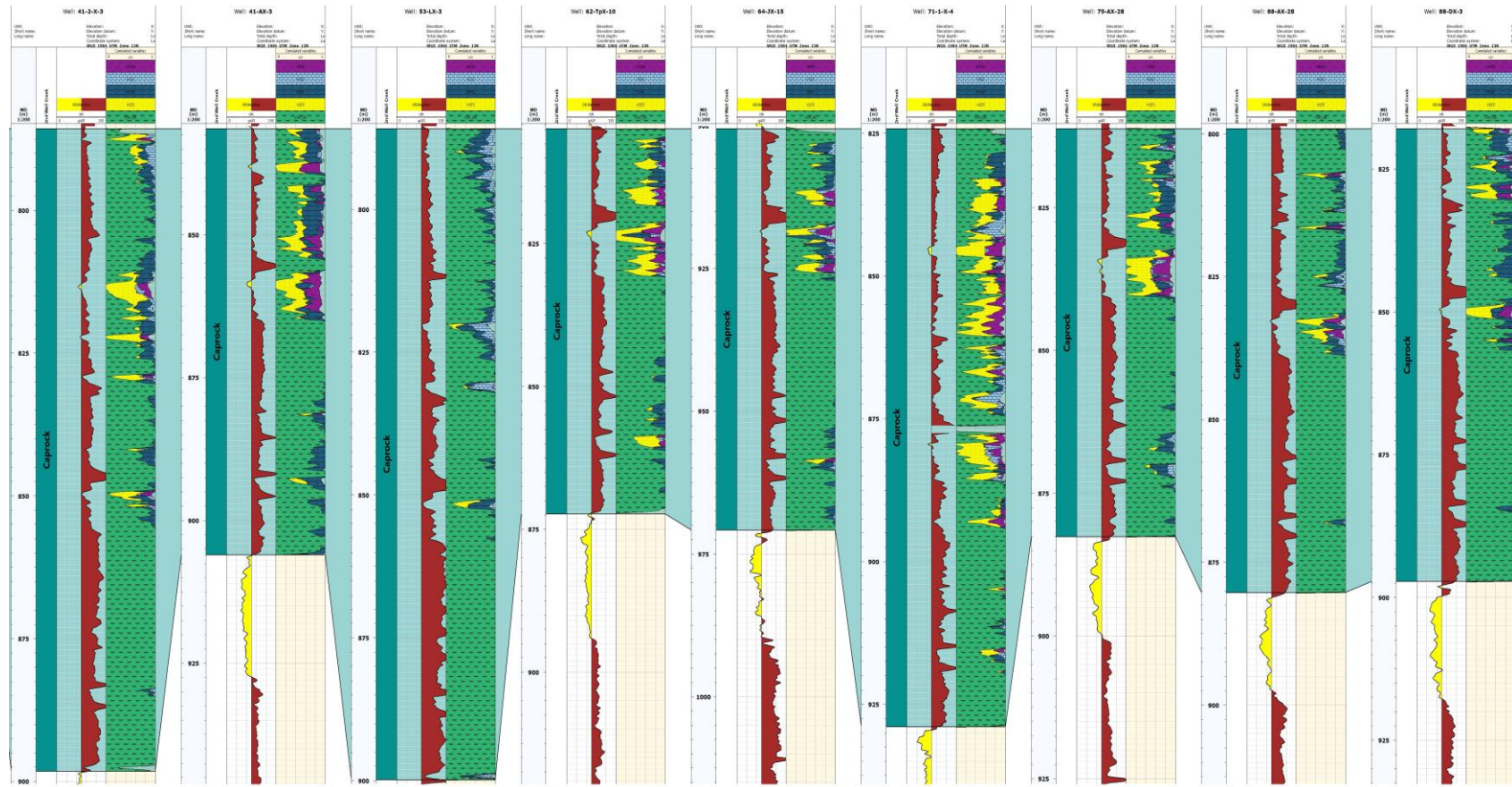


Figure 6. 2 - Mineralogy for the wells from left to right: 41-2-X-3, 41-AX-3, 53-LX-3, 62-TPX-10, 64-JX-15, 71-1-X-4, 75-AX-28, 88-AX-28, 88-DX-3

APPENDIX 7 – ACOUSTIC PROPERTIES



Figure 7.1 - Acoustic Properties for the wells from left to right: 28-AX-27, 36-MX-10, 67-1-TPX-10, 11-DX-26, 12-AX-33, 14-LX-28-WD, 28-AX-34, 34-TX-3, 36-11-SX-2

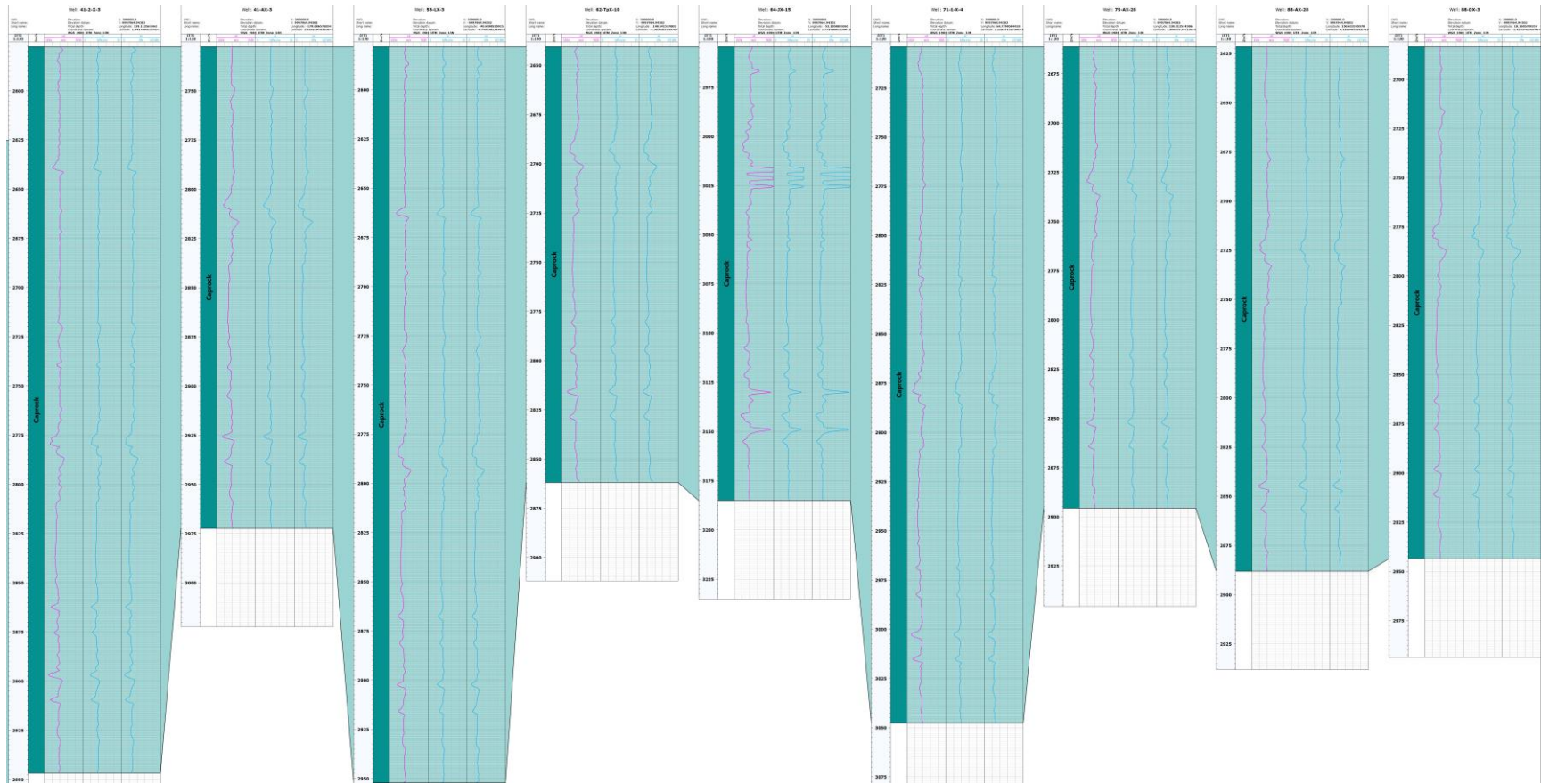


Figure 7.2 - Acoustic Properties for the wells from left to right: 41-2-X-3, 41-AX-3, 53-LX-3, 62-TPX-10, 64-JX-15, 71-1-X-4, 75-AX-28, 88-AX-28, 88-DX-3

APPENDIX 8 – SHEAR VELOCITY

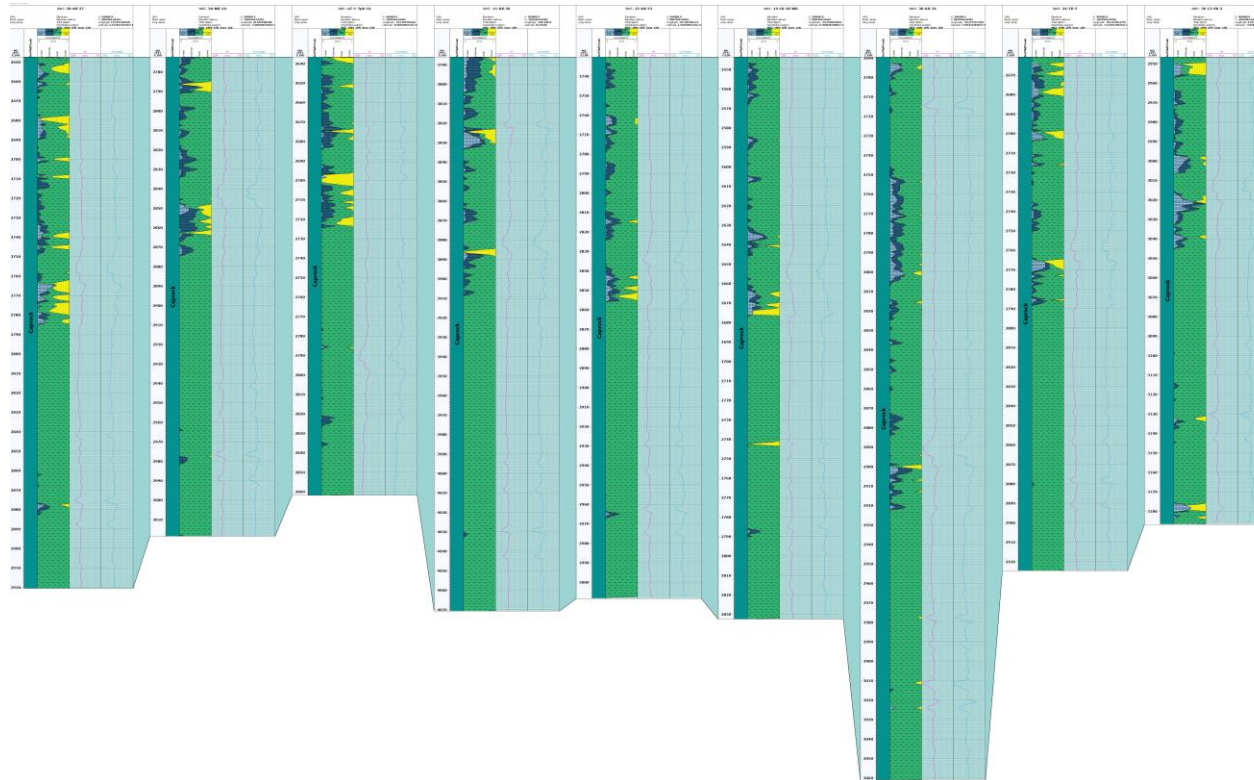


Figure 8. 1 - Shear velocity for the wells from left to right: 28-AX-27, 36-MX-10, 67-1-TPX-10, 11-DX-26, 12-AX-33, 14-LX-28-WD, 28-AX-34, 34-TX-3, 36-11-SX-2

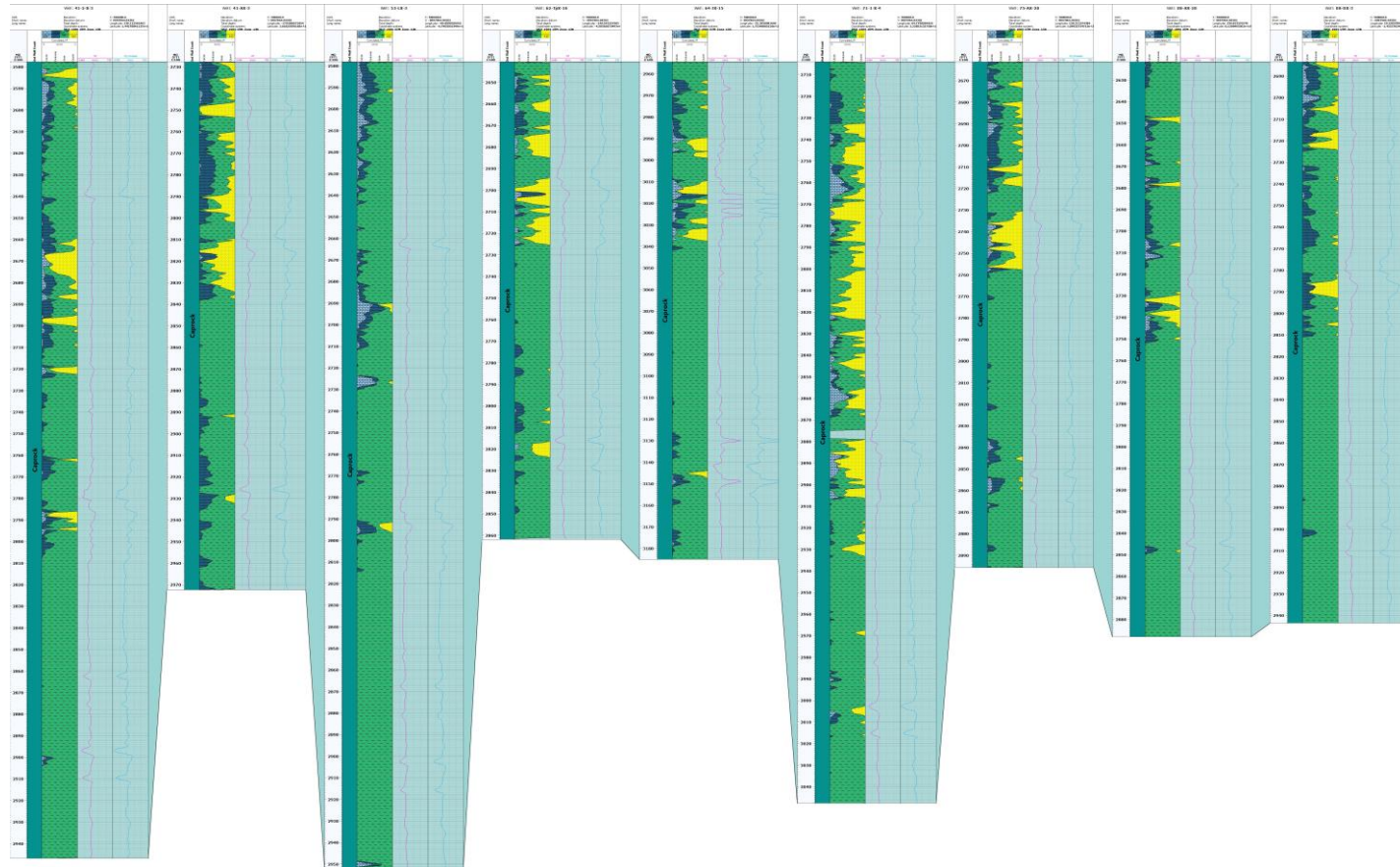


Figure 8. 2 – Shear velocity for the wells from left to right: 41-2-X-3, 41-AX-3, 53-LX-3, 62-TPX-10, 64-JX-15, 71-1-X-4, 75-AX-28, 88-AX-28, 88-DX-3

APPENDIX 9 – PORE PRESSURE

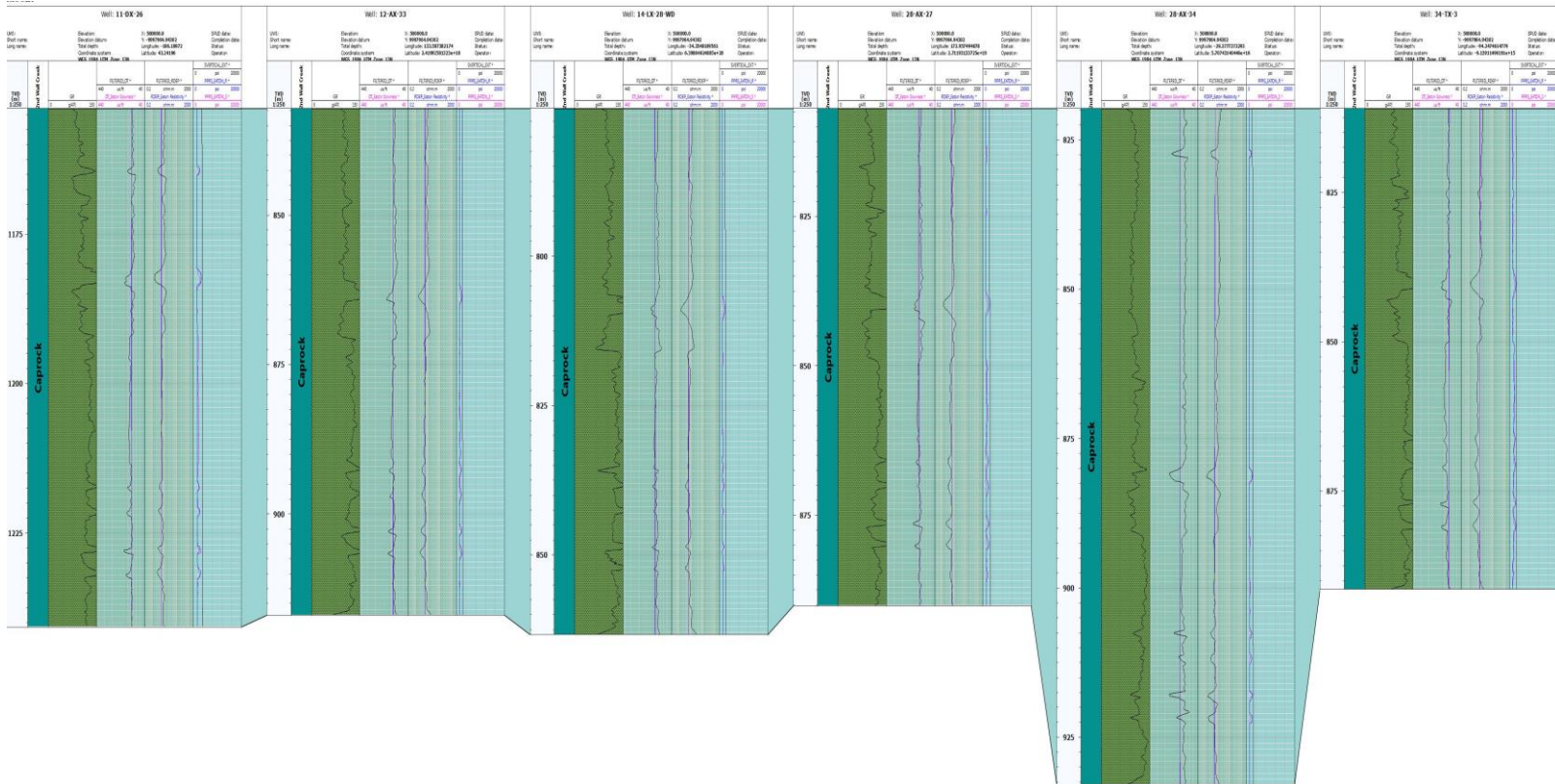


Figure 9. 1 - Pore pressure for the wells from left to right: 11-DX-26, 12-AX-33, 14-LX-28-WD, 28-AX-27, 28-AX-34, 34-TX-3

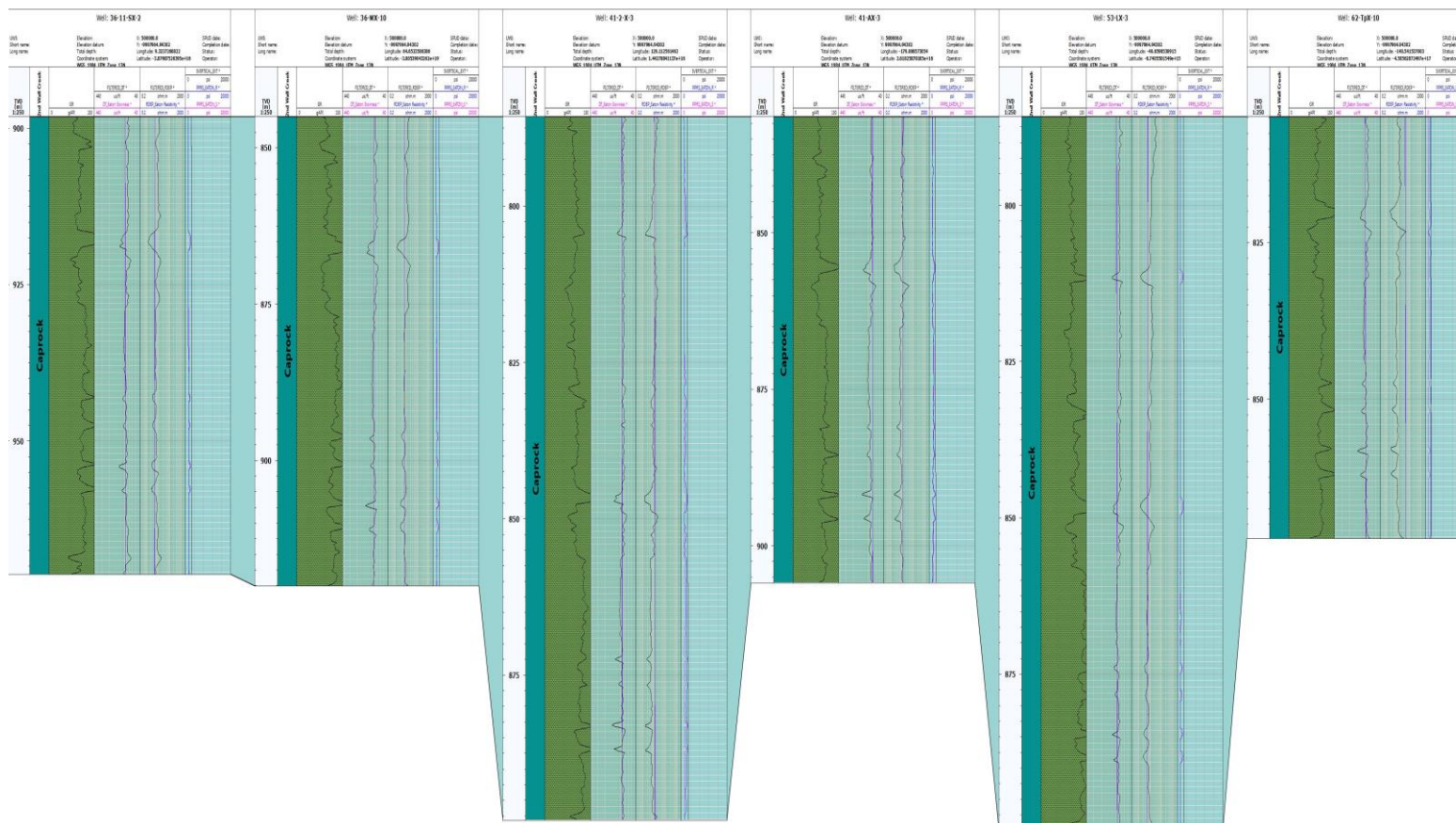


Figure 9.2 - Pore pressure for the wells from left to right: 36-11-SX-2, 36-MX-10, 41-2-X-3, 41-AX-3, 53-LX-3, 62-TpX-10

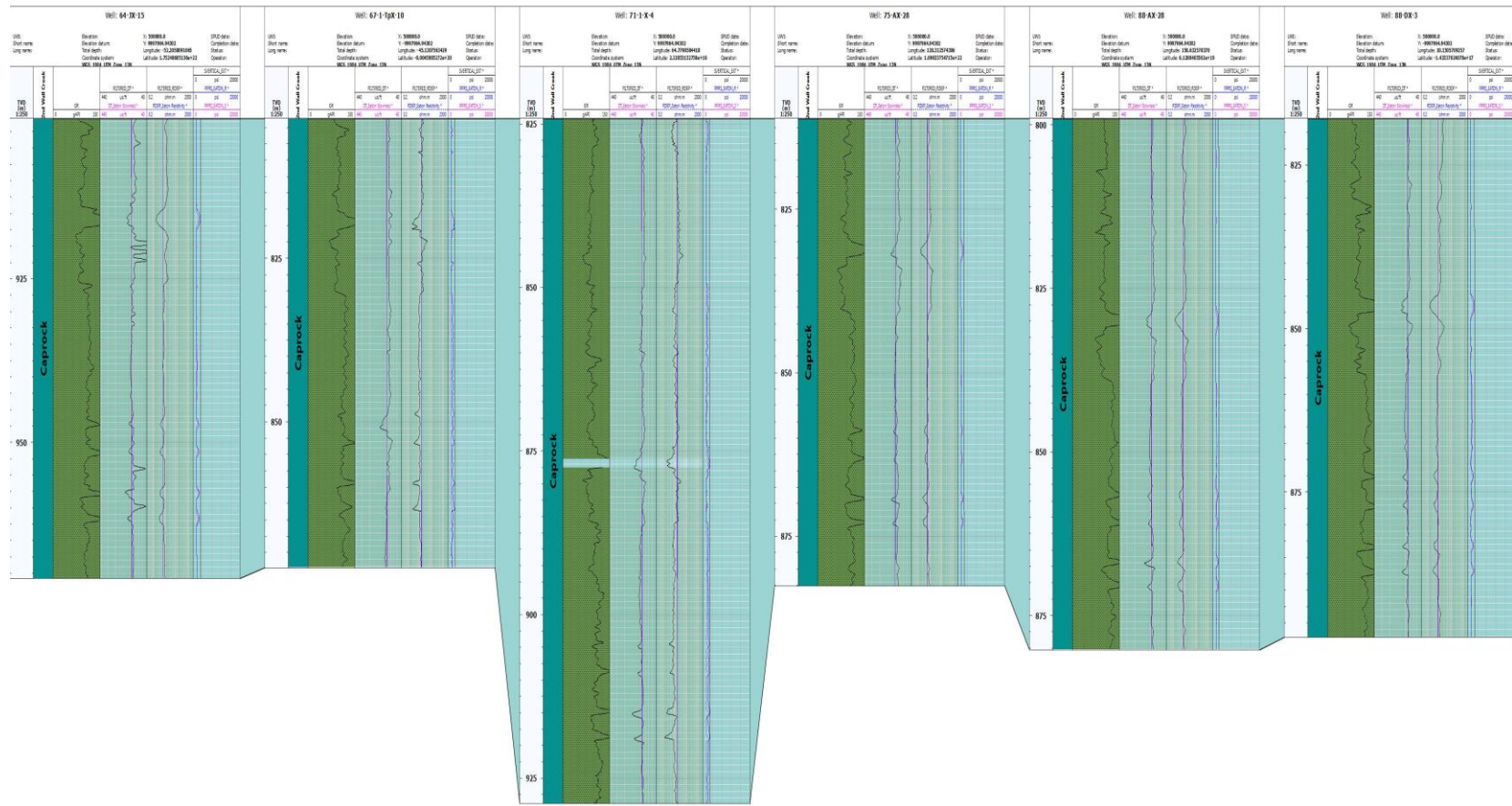


Figure 9.3 - Pore pressure for the wells from left to right: 64-JX-15, 67-1-TpX-10,71-1-X-4,75,AX-28,88-AX-28,88-DX-3

APPENDIX 10 – IPSOM RESULTS AND DYNAMIC ELASTIC PROPERTIES

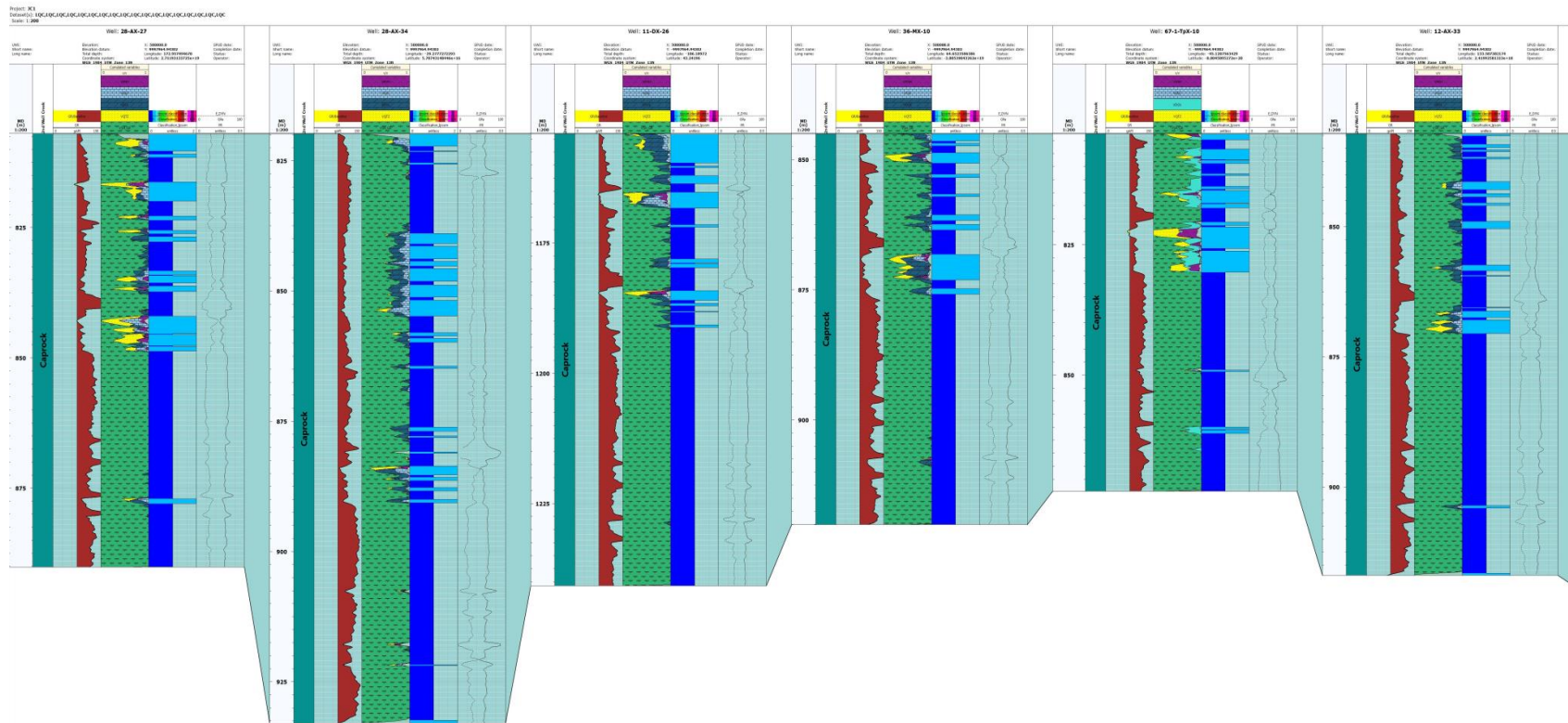


Figure 10. 1 - IPSOM results and dynamic elastic properties for the wells from left to right: 28-AX-27, 36-MX-10, 67-1-TPX-10, 11-DX-26, 12-AX-33

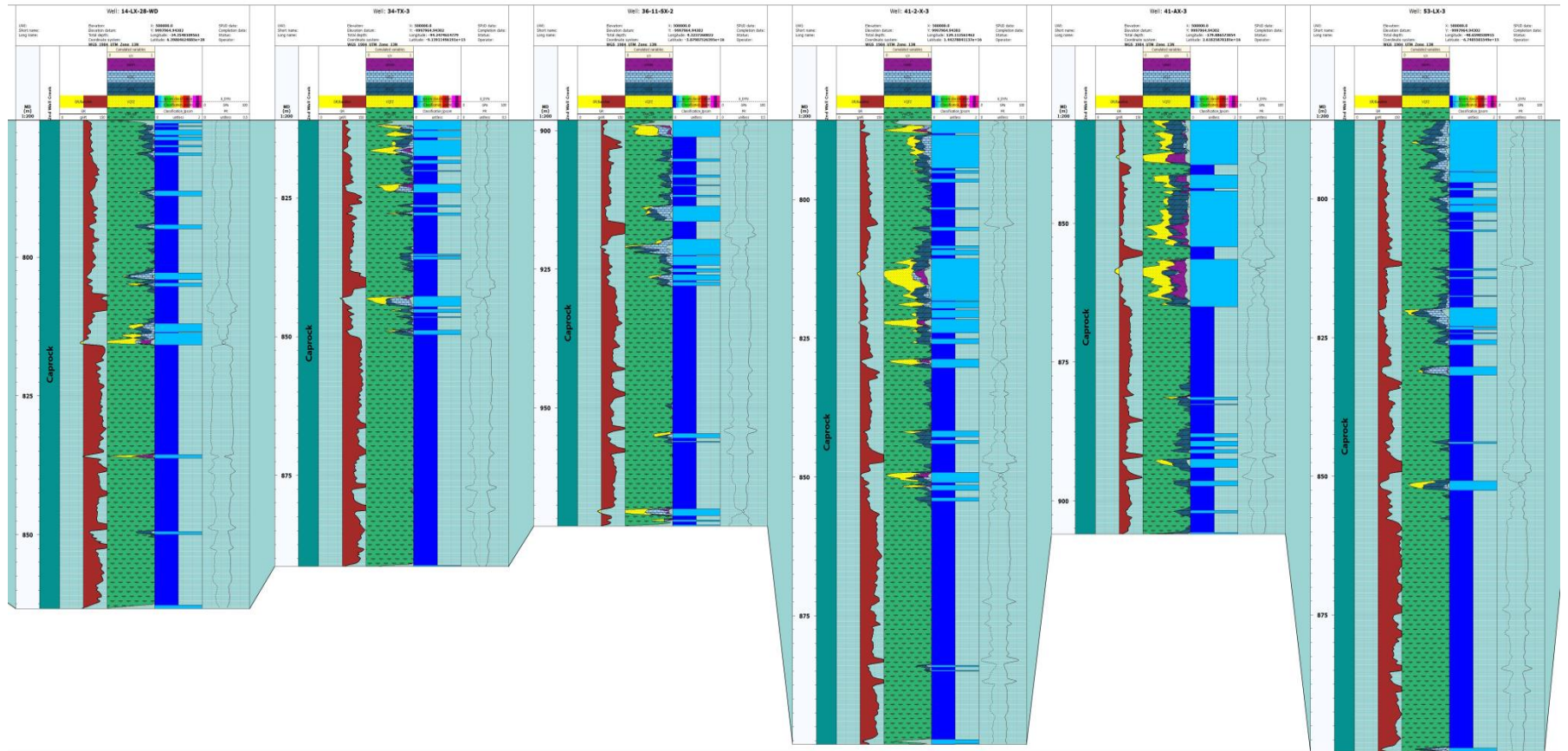


Figure 10. 2 - IPSOM results and dynamic elastic properties for the wells from left to right: 14-LX-28-WD,28-AX-27,28-AX,34-TX-3, 41-2-X-3, 41-AX-3, 53-LX-3

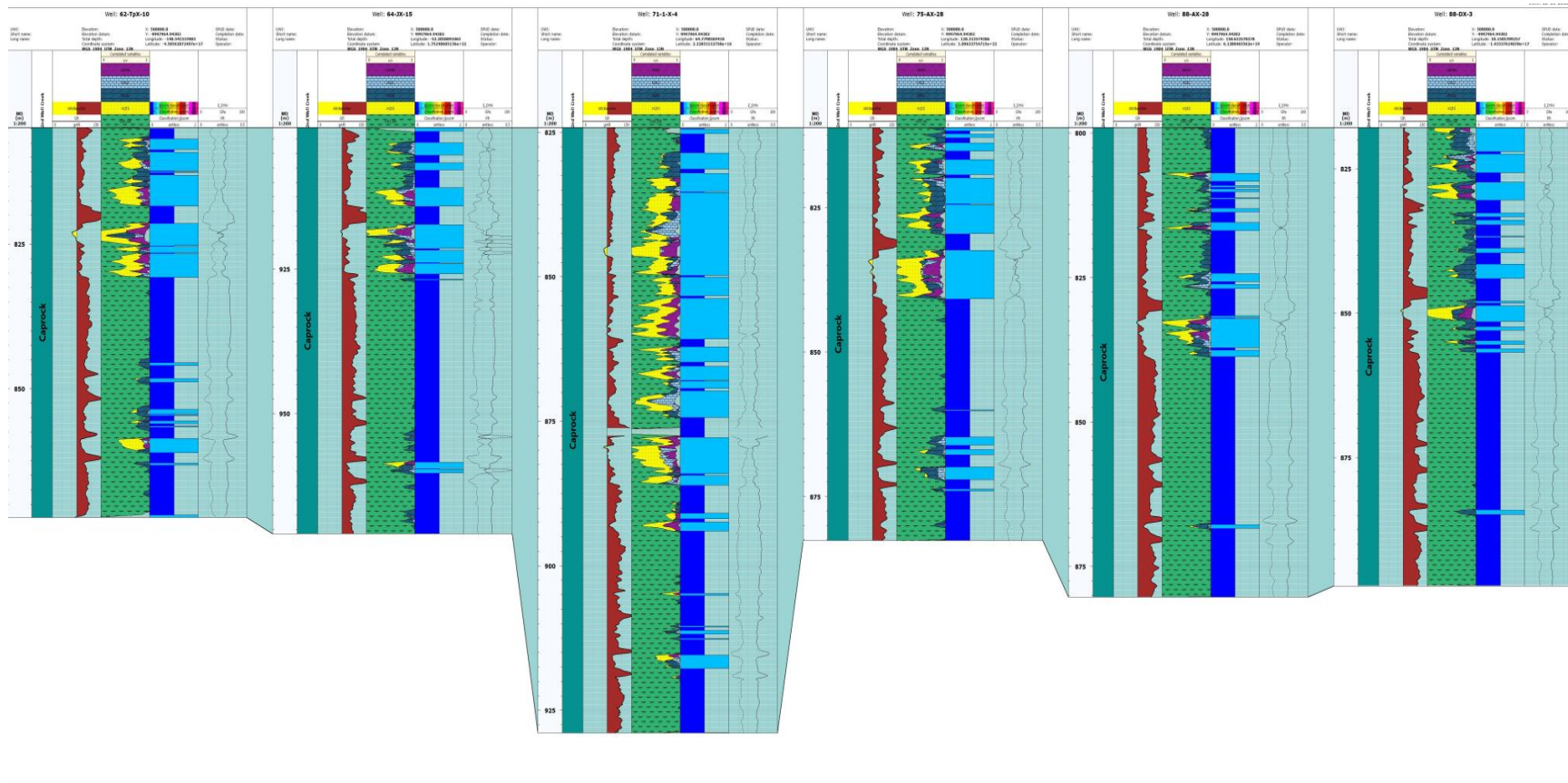


Figure 10. 3 - IPSOM results and dynamic elastic properties for the wells from left to right: 62-TPX-10, 64-JX-15, 71-1-X-4, 75-AX-28, 88-AX-28, 88-DX-3

APPENDIX 11 – IPSOM PIE-CHARTS

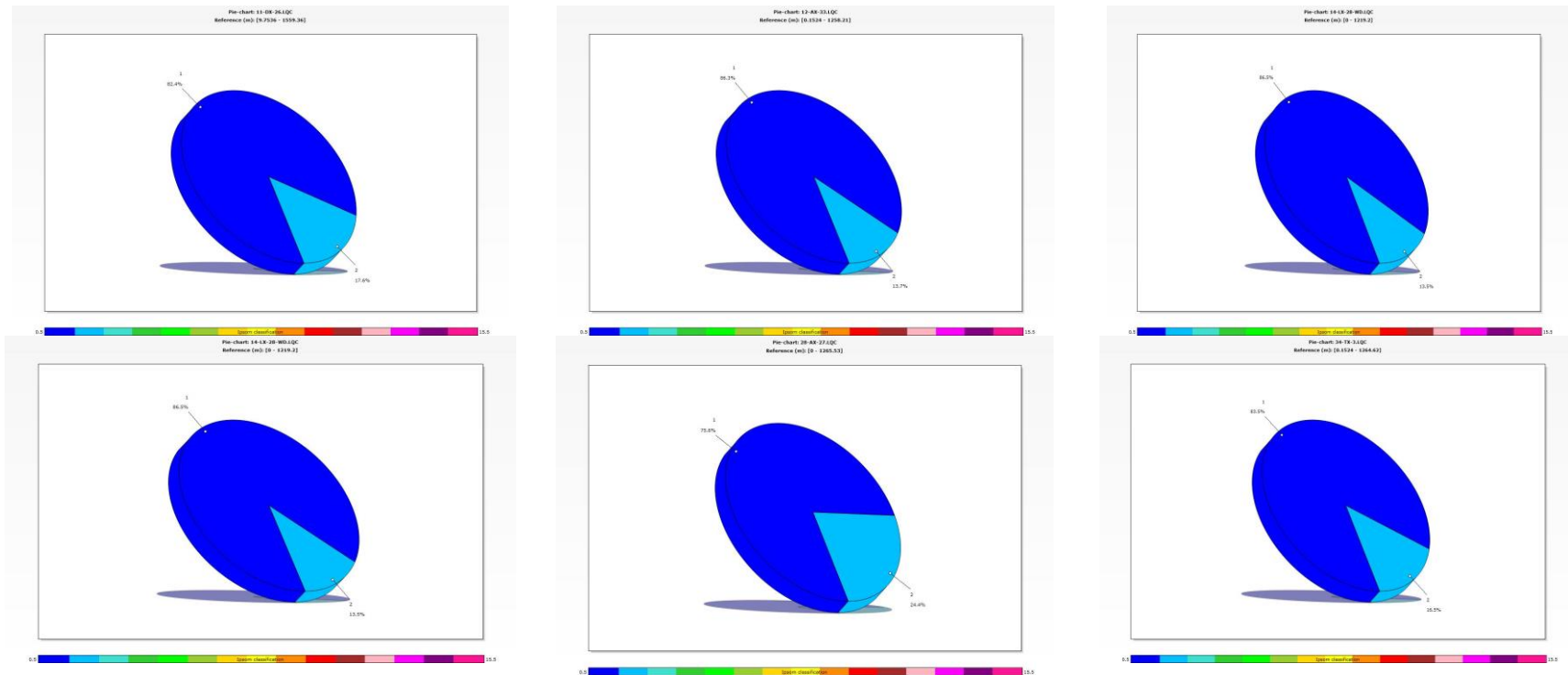


Figure 11. 1 - Pie-charts for the wells from le - ft to right: 11-DX-26, 12-AX-33, 14-LX-28-WD, 28-AX-27, 28-AX, 34-TX-3

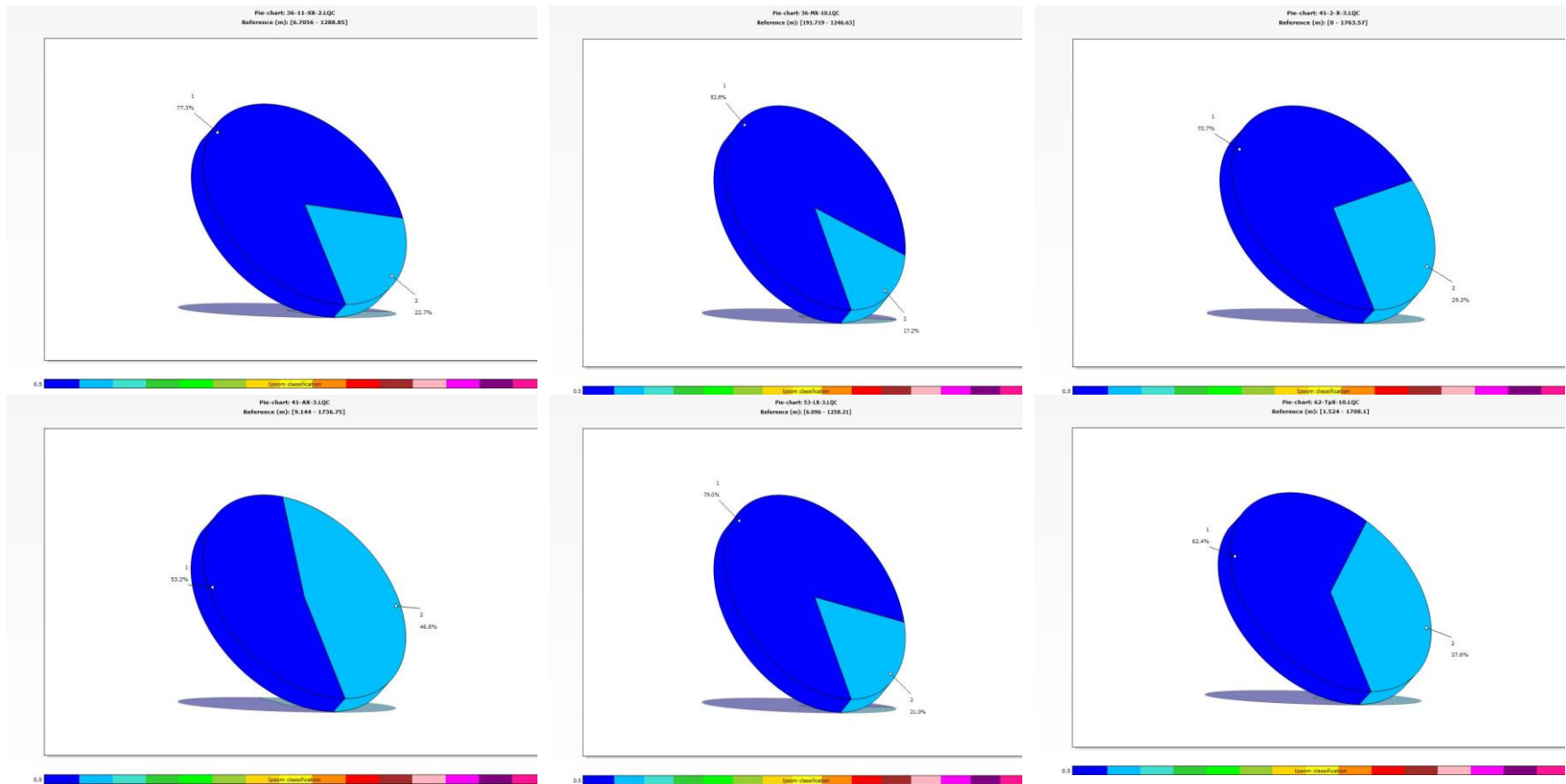


Figure 11. 2 - Pie-charts for the wells from left to right: 36-11-SX-2, 36-MX-10, 41-2-X-3,41-AX-3,53-LX-3,62-TpX-10

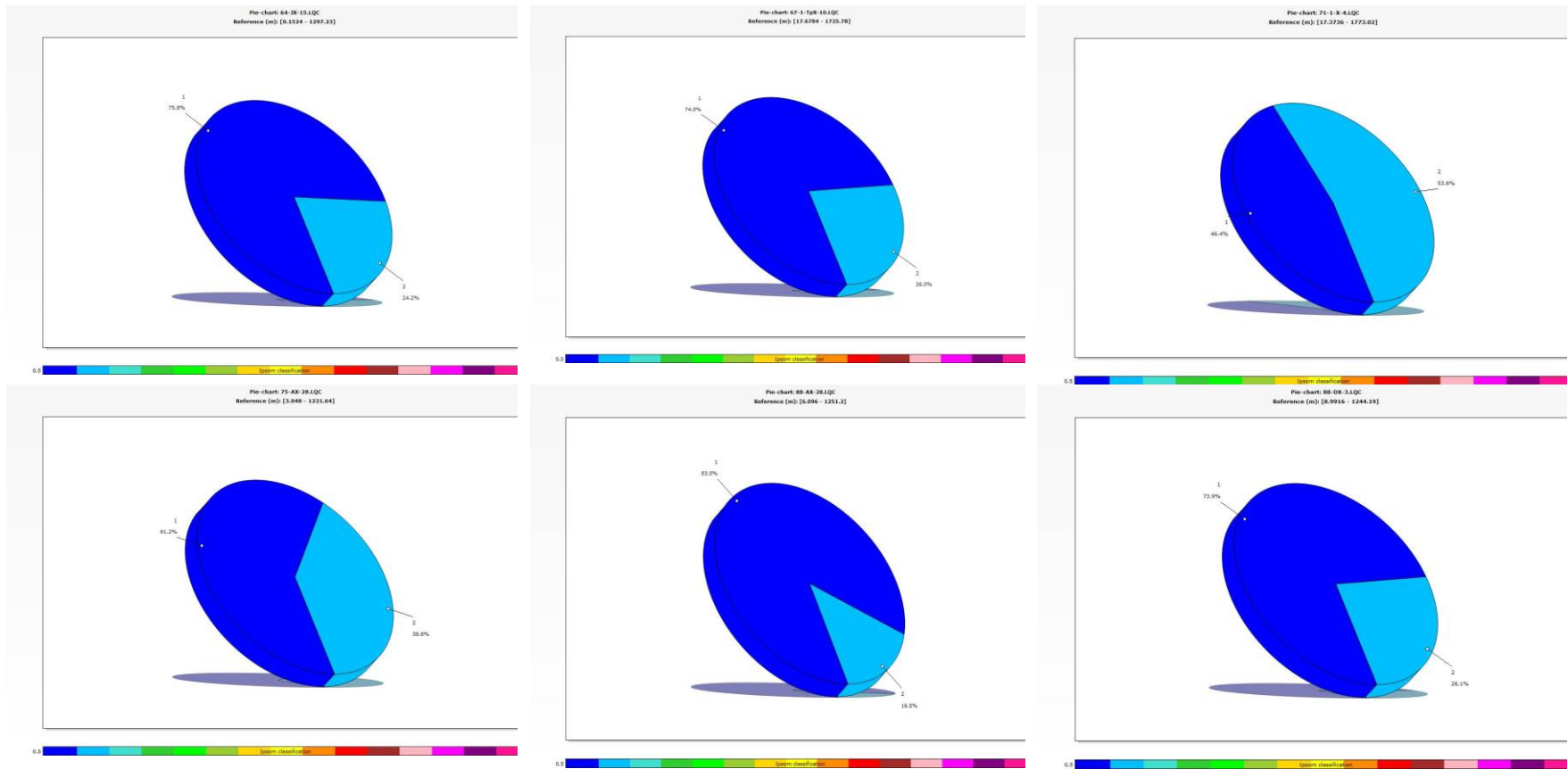


Figure 11. 3 - Pie-charts for the wells from left to right: 64-JX-15, 67-1-TpX-10,71-1-X-4,75-AX-28,88-AX-28,88-DX-3

APPENDIX 12 – BRITTLE INDEX

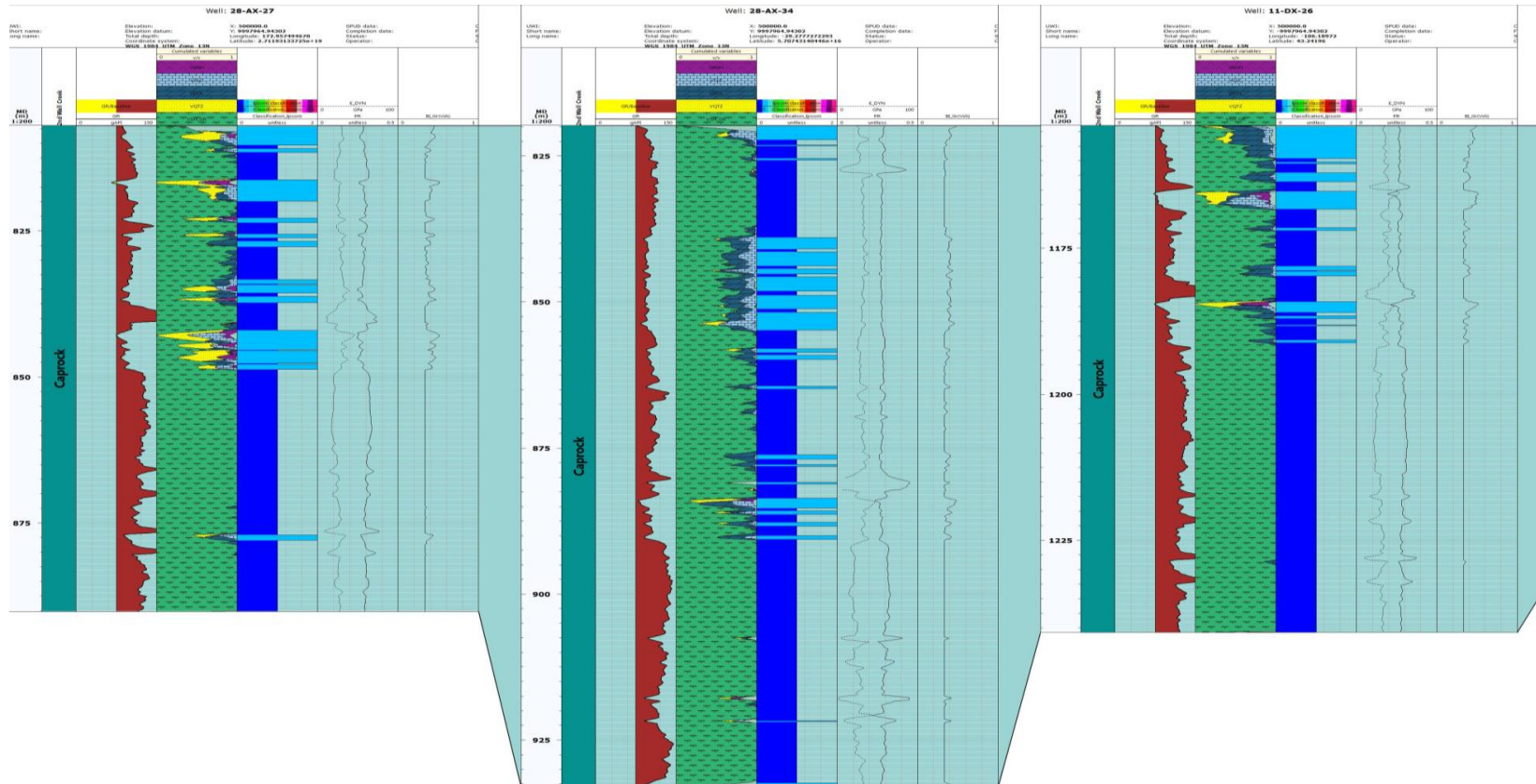


Figure 12. 1 – Brittle index for the wells from left to right: 28-AX-27, 28-AX-34, 11-DX-26

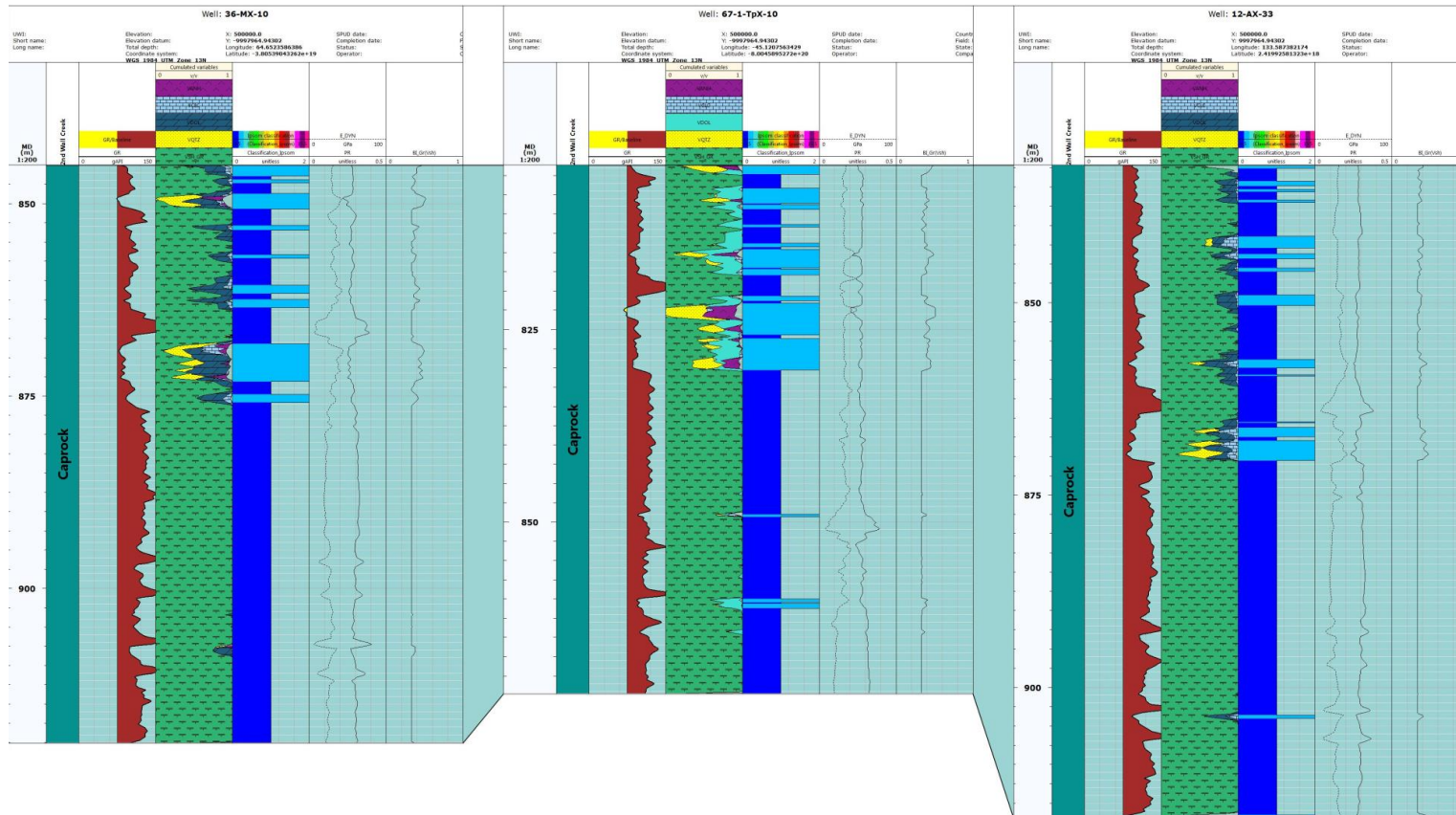


Figure 12. 2 – Brittleness index for the wells from left to right: 36-MX-10, 67-1-TpX-10, 12-AX-33

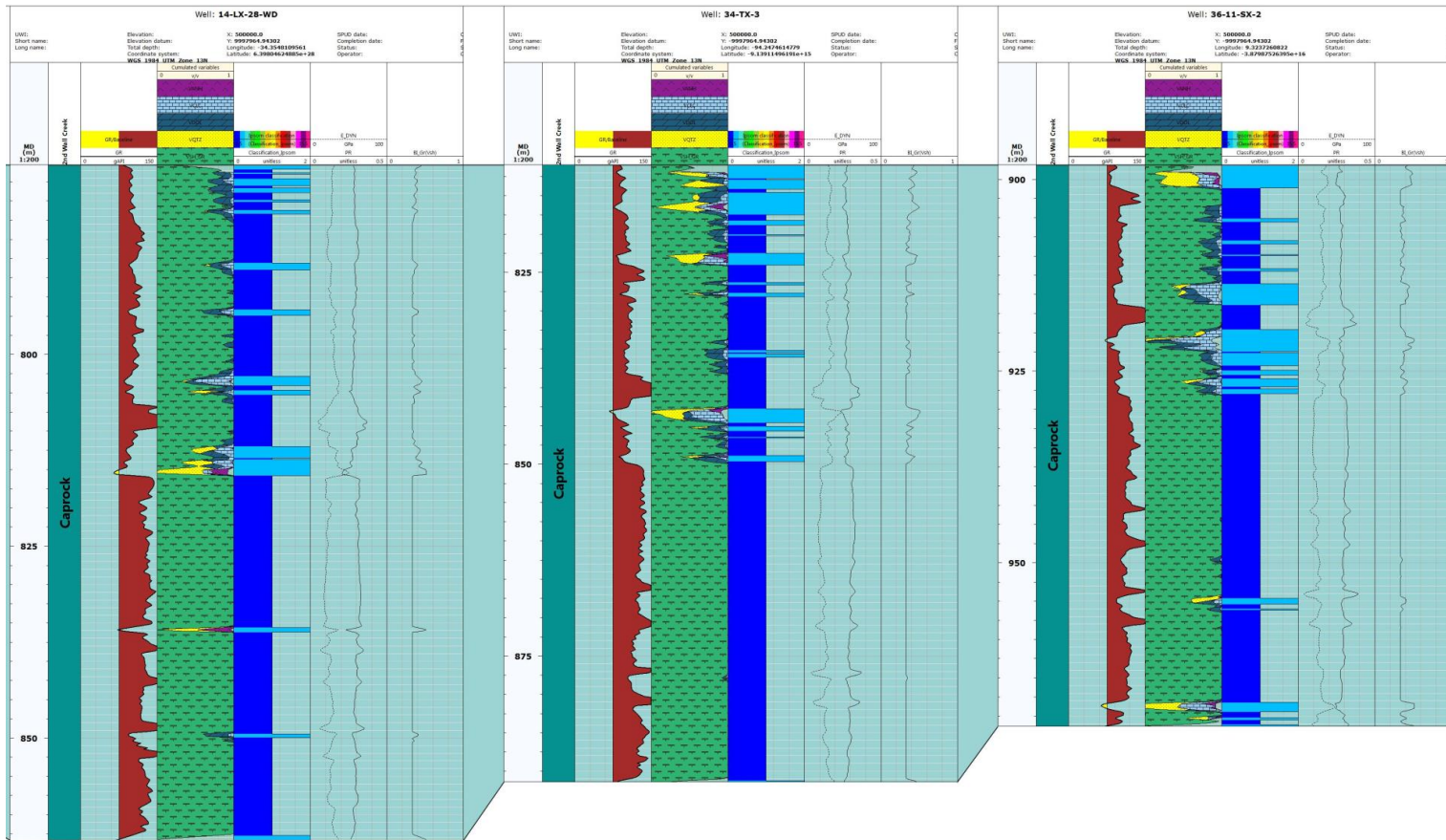


Figure 12. 3 – Brittle index for the wells from left to right: 14-LX-28-WD, 34-TX-3, 36-11-SX-2

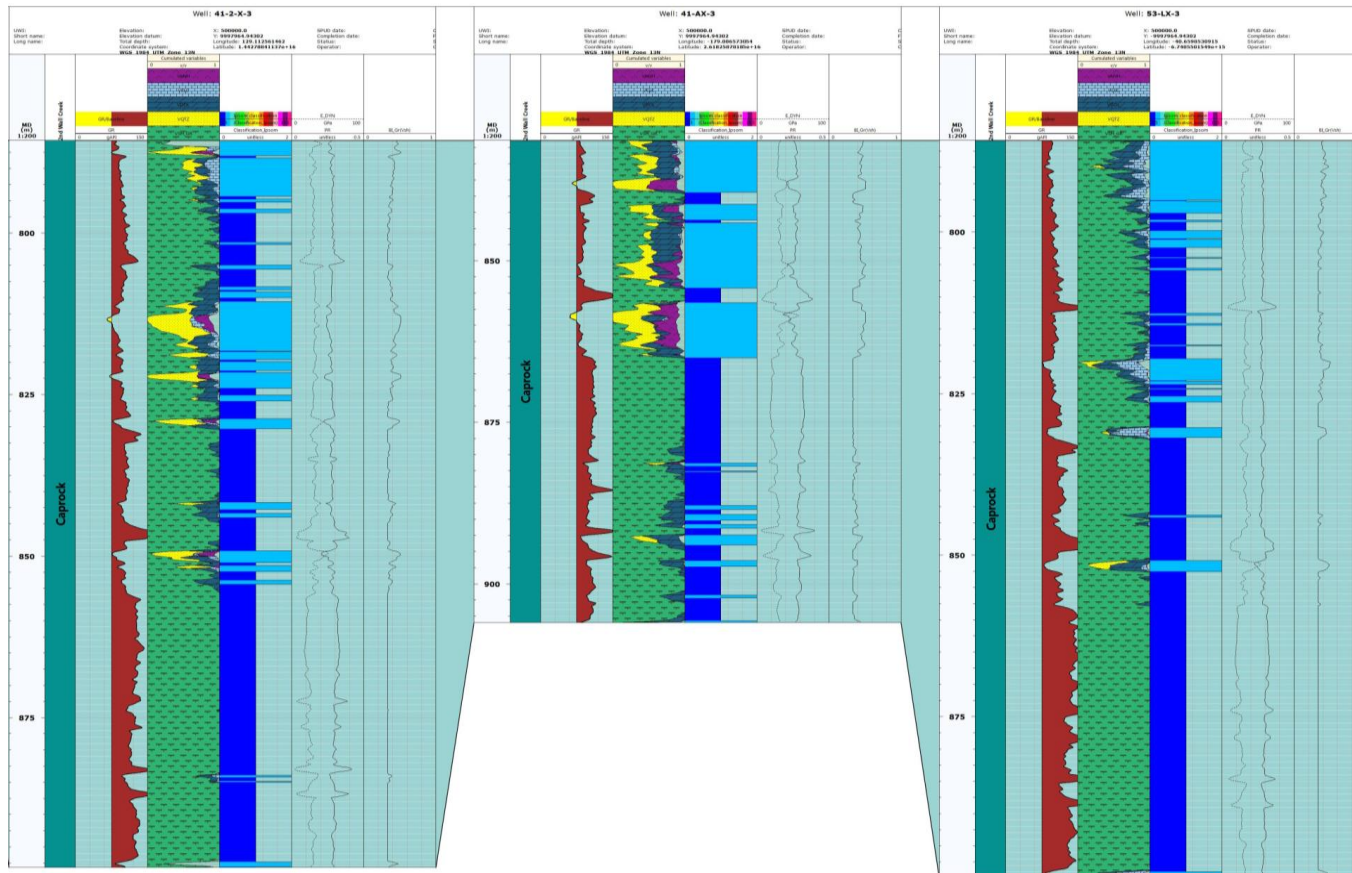


Figure 12. 4 – Brittle index for the wells from left to right:41-2-X-3,41-AX-3,53-LX-3

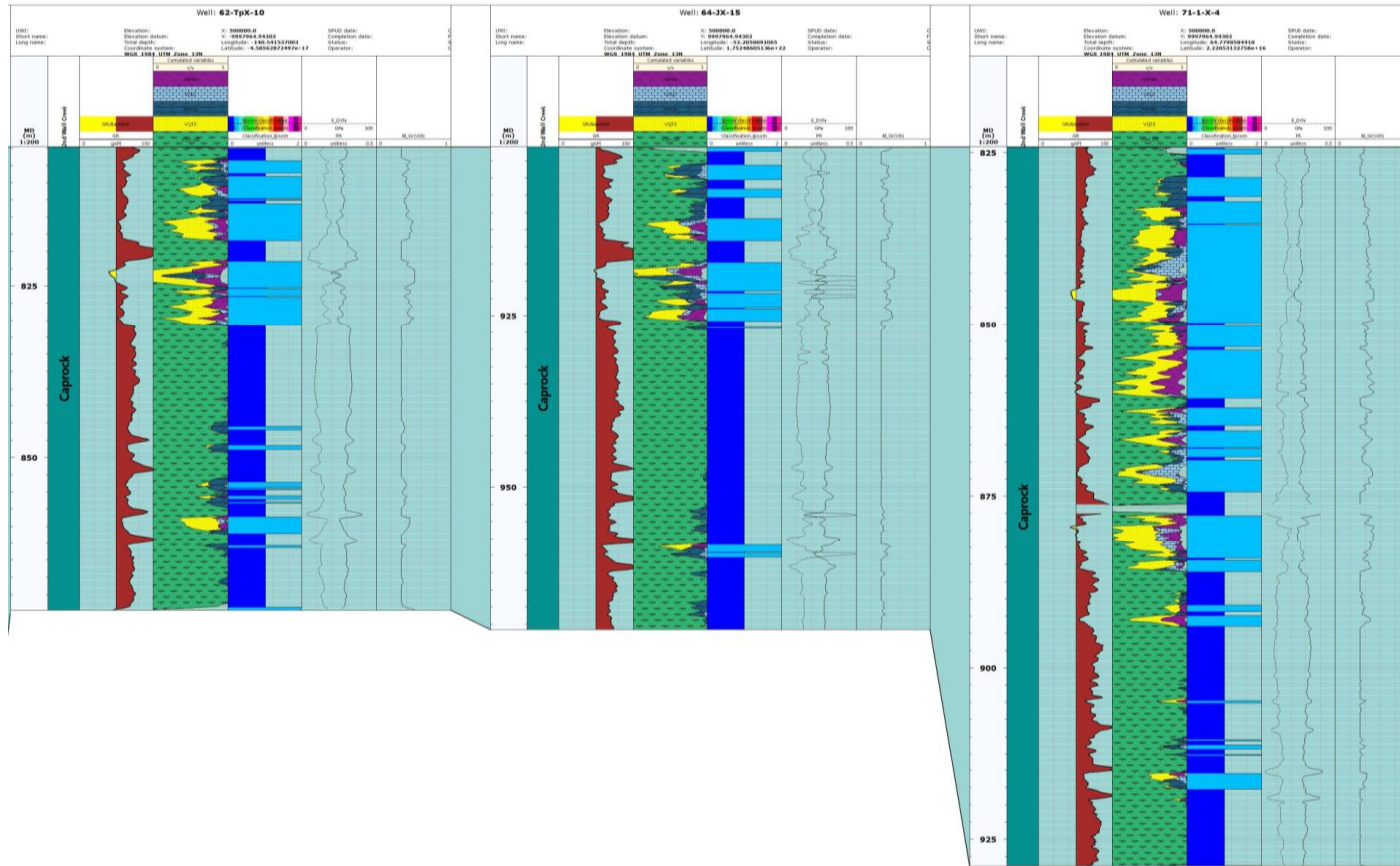


Figure 12. 5 – Brittle index for the wells from left to right: 62-TpX-10, 64-JX-15, 71-1-X-4

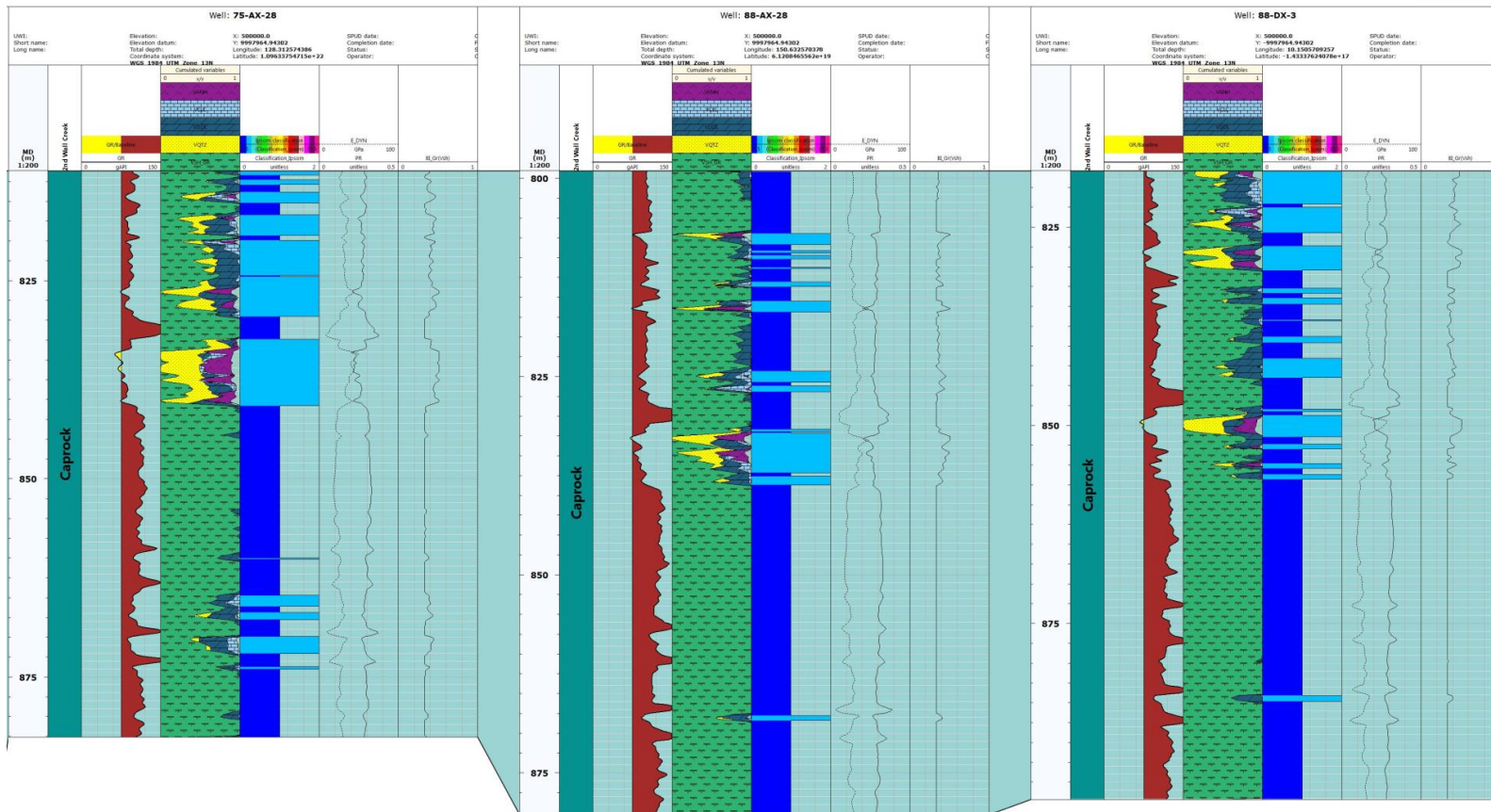


Figure 12. 6 – Brittleness index for the wells from left to right: 75-AX-28,88-AX-28,88-DX-3